

Artificial Brownian motors: Controlling transport on the nanoscale

Peter Hänggi^{1,2,*} and Fabio Marchesoni^{3,4,†}

¹*Institut für Physik, Universität Augsburg, Universitätsstr. 1, D-86135 Augsburg, Germany*

²*Department of Physics and Centre for Computational Science and Engineering, National University of Singapore, Singapore 117542*

³*Dipartimento di Fisica, Università di Camerino, I-62032 Camerino, Italy*

⁴*School of Physics, Korea Institute for Advanced Study, Seoul 130-722, Korea*

(Dated: September 24, 2008)

In systems possessing spatial or dynamical symmetry breaking, Brownian motion combined with unbiased external input signals, deterministic or random, alike, can assist directed motion of particles at the submicron scales. In such cases, one speaks of “Brownian motors”. In this review the constructive role of Brownian motion is exemplified for various physical and technological setups, which are inspired by the cell molecular machinery: working principles and characteristics of stylized devices are discussed to show how fluctuations, either thermal or extrinsic, can be used to control diffusive particle transport. Recent experimental demonstrations of this concept are surveyed with particular attention to transport in artificial, i.e. non-biological nanopores and optical traps, where single particle currents have been first measured. Much emphasis is given to two- and three-dimensional devices containing many interacting particles of one or more species; for this class of artificial motors, noise rectification results also from the interplay of particle Brownian motion and geometric constraints. Recently, selective control and optimization of the transport of interacting colloidal particles and magnetic vortices have been successfully achieved, thus leading to the new generation of microfluidic and superconducting devices presented hereby. The field has recently been enriched with impressive experimental achievements in building artificial Brownian motor devices that even operate within the quantum domain by harvesting quantum Brownian motion. Sundry akin topics include activities aimed at noise-assisted shuttling other degrees of freedom such as charge, spin or even heat and the assembly of chemical synthetic molecular motors. Our survey ends with a perspective for future roadways and potential new applications.

PACS numbers: 05.60.-k, 47.61.-k, 81.07.-b, 85.25.-j, 85.35.-p, 87.16.-b

Contents

I. INTRODUCTION	2	2. Vibrated ratchets	17
1. Artificial nanodevices	3		
2. Brownian motors	3		
II. SINGLE-PARTICLE TRANSPORT	5	III. TRANSPORT IN NANOPORES	18
A. Symmetric substrates	5	A. Ion pumps	18
1. dc drive	5	B. Artificial nanopores	19
2. ac drive	6	C. Chain translocation	20
3. Diffusion peak	7	D. Toward a next generation of mass rectifiers	21
4. Single-file diffusion	7	1. Zeolites	21
B. Rectification of asymmetric processes	7	2. Nanotubes	22
C. Nonlinear mechanisms	8	IV. COLD ATOMS IN OPTICAL LATTICES	22
1. Harmonic mixing	8	A. Bi-harmonic driving	23
2. Gating	9	B. Multi-frequency driving	23
3. Noise induced transport	10	C. More cold atom devices	24
D. Brownian motors	11	V. COLLECTIVE TRANSPORT	25
1. Rocked ratchets	11	A. Asymmetric 1D geometries	25
2. Pulsated ratchets	13	1. Boundary effects	25
3. Correlation ratchets	14	2. Asymmetric patterns of symmetric traps	26
4. Further asymmetry effects	15	B. 2D lattices of asymmetric traps	26
E. Efficiency and control issues	16	C. Binary mixtures	28
1. Optimization	16	VI. MICROFLUIDICS	29
		A. Transporting colloids	29
		B. Transporting condensed phases	31
		C. Granular flows	31
		VII. SUPERCONDUCTING DEVICES	33
		A. Fluxon channels	34
		B. Fluxon rectification in 2D arrays	36
		C. Anisotropic fluxon rectifiers	38
		VIII. QUANTUM DEVICES	39
		A. Quantum dissipative Brownian transport	39

*Electronic address: peter.hanggi@physik.uni-augsburg.de

†Electronic address: fabio.marchesoni@pg.infn.it

B. Josephson Brownian motors	40
1. Classical regime	40
2. Quantum regime	41
C. Quantum dot ratchets	42
D. Coherent quantum ratchets	43
1. Quantum ratchets from molecular wires	44
2. Hamiltonian quantum ratchet for cold atoms	44
IX. SUNDRY TOPICS	45
A. Pumping of charge, spin and heat	45
B. Synthetic molecular motors and machines	45
X. CONCLUDING REMARKS	46
Acknowledgments	47
References	48

I. INTRODUCTION

Over the past two decades advances in microscopy and microscale control have allowed scientists and engineers to delve into the workings of the biological matter. One century after Kelvin's death, today's researchers aim to explain how the engines of life actually work by stretching thermodynamics beyond its 19th-century limits (Haw, 2007).

Carnot realized that all engines transform energy from one form into another with a maximum possible efficiency that does not depend on the technology developed or on the fuel utilized, but rather on fundamental quantities such as heat and temperature. Kelvin and Clausius came up with two "rules of the engine", later known as the first two laws of thermodynamics. The first law states that energy cannot be destroyed or created but only transformed; the second law sets fundamental limitations to what energy transformation can achieve in practical terms. Just as the first law was centered on the notion of energy (from Greek for "work capability"), the second law revolved around the new concept of entropy (a term coined by Clausius also from Greek for "change capability").¹ When expressed in such terms, the second law states that entropy cannot decrease during any spontaneous or natural process. Notably, within the whole, virtual manufactory of all natural processes the first law takes on the role of an account clerk, keeping track of all energy changes, while the second law takes on the role of the director, determining the direction and action of all processes.

The fathers of thermodynamics developed their laws having in mind macroscopic systems that they could describe in terms of state (i.e., average) quantities such as

pressure and temperature, a reasonable assumption when dealing with the monster steam engines of the Victorian industry. A typical protein, however, is a few nanometers in size and consists of just a few tens of thousands of atoms. As a consequence the movements of a protein engine are swamped by the fluctuations resulting from the Brownian motion of its surroundings, which causes the energy of any its part to fluctuate continually in units of kT , with k denoting the Boltzmann constant and T the temperature. The effects of such energy fluctuations were brilliantly demonstrated by Yanagida's group (Nishiyama *et al.*, 2002, 2001), who observed kinesin molecules climbing the cytoskeletal track in a judgering motion made up of random hesitations, jumps and even backward steps. Similar results have been reported for a host of protein engines. The key question in modern thermodynamics is therefore how far energy fluctuations drive micro- and nano-engines beyond the limits of macroscopic laws.

A revealing experiment was performed recently by Bustamante *et al.* (2005), who first stretched a single RNA molecule, by optically tugging at a tiny plastic bead attached to one end, and then released the bead to study the effect of random energy fluctuations on the molecule recovery process. By repeating many identical stretching cycles, these authors found that the molecule "relaxation path" was different every time. In fact, the bead was drawing useful energy from the thermal motion of the suspension fluid and transforming it into motion. However, by averaging over increasingly longer bead trajectories that is, approaching a macroscopic situation, Bustamante *et al.* (2005) were able to reconcile their findings with the second law. These results lead to the conclusion that the straightforward extension of the second law to microscopic systems was ungranted; individual small systems do evolve under *inherently nonequilibrium conditions*.

However, a decade ago Jarzynski (1997) showed that the demarcation line between equilibrium and non-equilibrium processes is not always as clear cut as we were used to think. Imagining a microscopic single molecule process, Jarzynski evaluated not the simple average of the change of the (random) work of the underlying perturbed nanosystem, as it was pulled away from equilibrium according to an arbitrary protocol of forcing, but rather the average of the *exponential* of that tailored nonequilibrium work. Remarkably, such a quantity turned out to be the same as for an adiabatically slow version of the same process, and most remarkably, equals the exponential of the system's equilibrium free energy change. This result, also experimentally demonstrated by Bustamante *et al.* (2005), came as much of a surprise because it meant that information about macroscopic equilibrium was somehow buried inside individual, randomly fluctuating microscopic systems far from equilibrium, see also (Crooks, 1999; Gallavotti and Cohen, 1995; Jarzynski, 2007; Talkner *et al.*, 2008, 2007).

There is an additional limitation of 19th-century ther-

¹ Rudolf Julius Emanuel Clausius throughout his life allegedly preferred the German word "Verwandlungswert" rather than "entropy", although his colleagues suggested him to choose a name for his new thermodynamic quantity "S" (his chosen symbol for labeling "entropy", possibly in honor of "S"adi Carnot) that sounded as close as possible to the word "energy".

modynamics that is potentially even more significant in the design and operation of engines at the sub-micron scales. Kelvin's thermodynamics was based on the simplifying notion of an isolated system. The laws of macroscopic thermodynamics therefore apply only to systems that are either separated from their environment or coupled to it under controlled operating conditions, that is, measured in terms of the state variables of the system itself. However, at variance with a cylinder inside a steam engine, protein engines *do not (cannot) work in isolation*.

Very much on the footsteps of the 19th-century scientists and engineers, modern experimenters have probed the proteins that play a crucial role in the cell individually by feeding them with energy by injecting some chemical fuel "by hand" (e.g., ATP molecules) or exerting mechanical actions of some sort (Astumian, 1997; Bustamante *et al.*, 2005). In their natural setting, however, life engines are just parts of a closely interconnected functional web that keeps a cell alive. The great challenge of systems biology is therefore to put our understanding of isolated life engines back into the real world of the cell.

1. Artificial nanodevices

Nanotechnology has been intricately linked with biological systems since its inception. Fascinated by the complexity and smallness of the cell, Feynman (1960) challenged the scientific community to "make a thing very small which does what we want". In his visionary response, Drexler (1992) proposed to focus on protein synthesis as a pathway for creating nanoscale devices. Both Feynman and Drexler's propositions have been met with much skepticism as accurate manipulations at the nanoscale were deemed impossible. However, in view of the recent advances in systems biology (Gross, 1999), cellular mechanisms are now being cited as the key proof of the nanotechnological viability of devices with atomic precision. In spite of their established complementarity, a fundamental difference between systems biology and nanotechnology is their ultimate goal. Systems biology aims to uncover the fundamental operation of the cell in an effort to predict the exact response to specific stimuli and genetic variations, whereas nanotechnology is chiefly concerned with useful design.

Manufacturing nanodevices through positional assembly and self-assembly of biological components available at the cellular level is the goal of the so-called biomimetic approach – as opposed to the inorganic approach aimed at fabricating nanomechanical devices in hard, inorganic materials (e.g., using modern lithographic techniques, atomic force and scanning tunneling microscopy, etc). Nature has already proven that it is possible to engineer complex machines on the nanoscale; there is an existing framework of working components manufactured by Nature than can be used as a guide to develop our own *biology inspired* nanodevices. It is also true that the molecular machinery still outperforms anything that can

be artificially manufactured by many orders of magnitude. Nevertheless, inorganic nanodevices are attracting growing interest as a viable option due to their potential simplicity and robustness, without forgetting that inorganic nanodevices may provide additional experimental access to the molecular machinery itself.

With this review the authors intend to pursue further the inorganic approach to nanodevices, based on three main assumptions: (1) That, in view of the most recent developments on nonequilibrium thermodynamics, the science of nanodevices, regardless of the fabrication technique, is inseparable from the thermodynamics of microscopic engines (Hänggi *et al.*, 2005); (2) That the fabrication techniques on the nanoscales become more and more performing following the trend of the last two decades; (3) That a better understanding of the molecular machinery can help devise and implement new transport and control mechanisms for biology inspired nanodevices. In other words, we bet on a two-way cross-fertilization between the biomimetic and the inorganic approach.

2. Brownian motors

Nature provided microorganisms, with characteristic sizes of about 10^{-5} m, with a variety of self-propulsion mechanisms, all of which pertain to motion induced by cyclic shape changes. During one such cycle the configuration changes follow an asymmetric sequence, where one half cycle does not simply retrace the other half, in order to circumvent the absence of hydrodynamic inertia at the microscales, i.e., for low Reynolds numbers (Purcell, 1977). A typical example are motile bacteria that "swim" in a suspension fluid by rotating or waving their flagella (Astumian, 2007; Astumian and Hänggi, 2002). As anticipated above, a further complication arises when the moving parts of a (sub)micron-engine have molecular dimensions of 10^{-8} m or so. In that case, diffusion caused by Brownian motion competes with self-propelled motion. For example, a molecular motor mechanism becomes superior if at room temperature, and in a medium with viscosity close to that of water, a bacterium needs more time to diffuse a body length than it does to swim the same distance. A passive diffusive mechanism operating alone simply becomes inefficient.

A solution common to most cell machinery is to have molecular motors operating on a track that constrains the motion to essentially one dimension along a periodic sequence of wells and barriers. The energy barriers significantly suppress the diffusion, while thermal noise plays a constructive role by providing a mechanism, thermal activation (Hänggi *et al.*, 1990), by which motors can escape over the barriers. The energy necessary for directed motion is supplied by *asymmetrically* raising and lowering the barriers and wells, either via an external time-dependent modulation (e.g., due to the coupling with other motors) or by energy input from a nonequi-

librium source such as a chemical reaction, like the ATP hydrolysis. Thus, in agreement with the reasoning underlying the analysis² of the Smoluchowski-Feynman stylized ratchet engine (Feynman *et al.*, 1963; Smoluchowski, 1912), under appropriate nonequilibrium conditions, structural anisotropy can sustain directed motion. Such a device clearly does not violate the second law of thermodynamics because the very presence of nonequilibrium renders inoperative those limiting (thermal equilibrium) restrictions.

In the case of a bacterium, as for any ordinary heat engine, the relevant state variables, namely, its position and the phase of the flagellum stroke, always cycle through one and the same periodic time sequence; the two variables are tightly coupled and almost synchronized. In clear contrast to this familiar scenario, the state variables of molecular motors are often loosely coupled due to the prominent action of fluctuations, a salient feature nicely captured by Hänggi who originally coined the term *Brownian motors* in the feature (Bartussek and Hänggi, 1995).³

Important hallmarks of any genuine Brownian motor are (Astumian and Hänggi, 2002; Hänggi *et al.*, 2005): (i) The presence of some amount of (not necessarily thermal) noise. The intricate interplay among nonlinearity, noise-activated escape dynamics and non-equilibrium driving implies that, generally, not even the direction of transport is *a priori* predictable; (ii) Some sort of symmetry-breaking supplemented by temporal periodicity (typically via an unbiased, non-equilibrium forcing), if a cyclically operating device is involved. Therefore, not every small ratchet device falls under the category of Brownian motors. This holds true especially if the governing transport principle is deterministic, like in mechanical ratchet devices of macro- or mesoscopic size.

The following prescriptions should be observed when designing an efficient Brownian motor: (a) Spatial and temporal periodicity critically affect rectification; (b) All acting forces and gradients must vanish after averaging over space, time, and statistical ensembles; (c) Random forces (of thermal, non-thermal, or even deterministic origin) assume a prominent role; (d) Detailed balance symmetry, ruling thermal equilibrium dynamics, must be broken by operating the device away from thermal equilibrium; (e) A symmetry-breaking mechanism must apply. There exist several possibilities to induce symmetry-breaking. First, the spatial inversion symmetry of the

periodic system itself may be broken intrinsically; that is, already in the absence of non-equilibrium perturbations. This is the most common situation and typically involves a type of periodic, asymmetric ratchet potential. A second option consists in the use of an unbiased driving force (deterministic or stochastic, alike) possessing non-vanishing, higher order odd time-correlations. Yet a third possibility arises via collective effects in coupled, perfectly symmetric non-equilibrium systems, namely in the form of spontaneous symmetry breaking. Note that in the latter two cases we speak of a Brownian motor dynamics even though a ratchet potential is not necessarily involved.

The reasoning of using unbiased thermal fluctuations and/or unbiased nonequilibrium perturbations to drive directed motion of particles and alike has seen several rediscoveries since the visionary works by Marian von Smoluchowski (1912) and Richard P. Feynman *et al.* (1963). From a historic perspective, the theme of directed transport and Brownian motors was put into the limelight of the statistical and biological physics research with the appearance of several ground-breaking works, both theoretical and experimental, which appeared during the (1992-1994) period. Most notably, Ajdari and Prost (1992); Astumian and Bier (1994); Bartussek *et al.* (1994); Chauwin *et al.* (1994); Doering *et al.* (1994); Magnasco (1993); Millonas and Dykman (1994); Prost *et al.* (1994); Rousselet *et al.* (1994) helped ignite a tumultuous activity in this topical area which kept growing until the present days. The readers may deepen their historical insight by consulting earlier introductory reports such as those published by Astumian (1997); Astumian and Hänggi (2002); Hänggi and Bartussek (1996); Hänggi *et al.* (2005); Jülicher *et al.* (1997); Reimann (2002); Reimann and Hänggi (2002).

This review focuses on the recent advances in the science of non-biological, *artificial* Brownian motors.

In contrast to those reviews and feature articles mentioned above, which beautifully cover the rich variety of possible Brownian motor scenarios and working principles, our focus in this review is on non-biological, *artificial*, mostly, solid state based Brownian motors. In this spirit the authors have attempted to present a comprehensive overview of the present status of this field, including newest theory developments, most compelling experimental demonstrations, and first successful technological applications. Some closely related topics, such as the engineering of synthetic molecular motors and nanomachines based on chemical species, are only briefly discussed herein because comprehensive, up-to-date reviews have been published recently by research groups very active in that area (Balzani *et al.*, 2006; Kay *et al.*, 2007; Kottas *et al.*, 2005).

² Note in this context also the insightful examination of Feynman's analysis by Parrondo and Espanol (1996).

³ The notion of "molecular motor" is reserved within this review for motors specifying biological, intracellular transport. Likewise, the notion of "Brownian ratchet" or "thermal ratchet" is reserved for the operating principle of protein translocation processes. The latter term seemingly has been introduced by Simon *et al.* (1992) to describe isothermal trapping of Brownian particles to drive protein translocation, see also in Wang and Oster (2002).

II. SINGLE-PARTICLE TRANSPORT

Signal rectification schemes in the absence of noise have been known since long ago, especially in the electrical engineering literature. However, rectification in a nanodevices cannot ignore fluctuations and Brownian motion, in particular. New experiments on both biological and artificial devices showed how noise rectification can actually be utilized to effectively control particle transport on the small scales. By now, noise rectification has become one of the most promising techniques for powering micro- and nanodevices.

In order to set the stage, in the next subsection we first consider the case of systems where rectification cannot occur. In the following subsections we then single out all ingredients that do make rectification possible.

Let us consider a Brownian particle with mass m , coordinate $x(t)$, and friction coefficient γ in one dimension, subjected to an external static force F and thermal noise $\xi(t)$. The corresponding stochastic dynamics is described by the inertial Langevin equation

$$m\ddot{x} = -V'(x) - m\gamma\dot{x} + F + \xi(t), \quad (1)$$

where $V(x)$ is a periodic potential with period L , namely $V(x+L) = V(x)$, and $'$ indicates the differentiation with respect to x and \dot{x} the differentiation with respect to time t . Thermal fluctuations are modeled by a stationary Gaussian noise of vanishing mean, $\langle \xi(t) \rangle = 0$, satisfying the fluctuation-dissipation relation

$$\langle \xi(t)\xi(0) \rangle = 2D_p\delta(t), \quad (2)$$

where the momentum-diffusion strength reads $D_p = m\gamma kT$, with k denoting the Boltzmann constant, and T is the temperature of an equilibrium heat bath.

In extremely small systems, particle dynamics and fluctuations occurring in biological and liquid environments are often described well by the *overdamped* limit of Eq. (1), – for an illustrative discussion of this fact see the account given by Purcell (1977)–, in terms of a the massless Langevin equation, which is driven by a position-diffusion $D_x = kT/(m\gamma) \equiv D$, i.e.,

$$\dot{x} = -V'(x) + F + \xi(t), \quad (3)$$

with a corresponding noise correlation

$$\langle \xi(t)\xi(0) \rangle = 2D\delta(t). \quad (4)$$

In this overdamped regime, the inertia term $m\ddot{x}$ can be dropped altogether with respect to the friction term $-m\gamma\dot{x}$ (Smoluchowski approximation). Here $m\gamma$ has been scaled to unity for convenience, i.e., $D \equiv kT$.

In the absence of an external bias, i.e. $F = 0$, the equilibrium stochastic mechanism in Eq. (1) cannot sustain a non-zero stationary current, i.e., $\langle \dot{x}(t) \rangle = 0$, no matter what $V(x)$. This can be readily proven upon solving the corresponding Fokker-Planck equation with periodic boundary conditions (Mel'nikov, 1991; Risken, 1984).

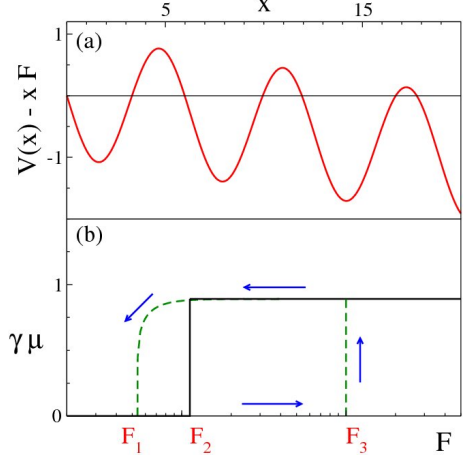


FIG. 1 (Color online) (a) Tilted periodic potential of Eq. (5), $V(x) - xF$, with $F = 0.1$; (b) Locked-to-running transitions. The thresholds F_1 and F_3 of the hysteretic loop (dashed curves) and the zero temperature step at F_2 (solid curve) are marked explicitly. Parameter values: $m = V_0 = 1$, i.e. $F_3 = 1$, and $\gamma = 0.03$.

A. Symmetric substrates

Let us consider first the case when the periodic substrate with the potential $V(x)$ is symmetric under reflection, that is $V(x - x_0) = V(-x + x_0)$ for certain x_0 with $x_0 \leq x_0 < L$. The most studied example is the symmetric washboard potential (Risken, 1984)

$$V(x) = -V_0 \sin(2\pi x/L), \quad (5)$$

displayed in presence of a static tilt-force F in Fig. 1a. The particle mobility $\mu(F) \equiv \langle \dot{x} \rangle / F$ is symmetric for $F \rightarrow -F$, namely, $\mu(F) = \mu(-F)$. For this reason in this section we restrict ourselves to $F \geq 0$.

1. dc drive

The Brownian motion, Eq. (1), in the washboard potential, Eq. (5), is detailed in Risken (1984) textbook. To make contact with Risken's notation one must rewrite Eq. (1) in terms of the rescaled quantities $x \rightarrow \frac{2\pi}{L}x$, $F \rightarrow \frac{2\pi}{L}\frac{F}{m}$, and $T \rightarrow (\frac{2\pi}{L})^2\frac{T}{m}$, so that

$$\ddot{x} = -\gamma\dot{x} + \omega_0^2 \cos x + F + \xi(t). \quad (6)$$

The angular frequency $\omega_0 = (2\pi/L)\sqrt{V_0/m}$ characterizes the oscillating motion of the particle at the bottom of the potential wells. To reconcile Eq. (6) with Eq. (1) for the potential in Eq. (5), it suffices to scale $m = 1$ and $L = 2\pi$, as assumed throughout this section, unless stated otherwise.

The dynamics of Eq. (6) is characterized by random switches occurring either between two locked states, dwelling a well minimum, or switches between a locked

state with zero average velocity and a (downhill) running state with a finite, average asymptotic velocity $\langle \dot{x} \rangle = F/\gamma$. In terms of mobility, locked and running states correspond to $\gamma\mu = 0$ and $\gamma\mu = 1$, respectively.

In the overdamped regime, Eq. (3), the particle is trapped most of the time at a local minimum of the tilted substrate as long as $F \leq F_3 = \omega_0^2$; for $F > F_3$ there exist no such minima and the particle runs in the F direction with average speed approaching F/γ . This behavior is described quantitatively by the mobility formula (Risken, 1984):

$$\mu(F) = \frac{L}{\langle t(L, F) \rangle F}, \quad (7)$$

where $\langle t(L, F) \rangle$, the mean first-passage time of the particle across a substrate unit cell in the F direction, can be computed explicitly for any choice of $V(x)$ (Hänggi *et al.*, 1990).

In the underdamped regime $\gamma \ll \omega_0$ the locked-to-running transition depends crucially on the presence of noise, no matter how weak. In the *noiseless* case, $\xi(t) \equiv 0$, the average speed of a Brownian particle with coordinate $x(t)$ depends on the initial conditions according to the hysteretic cycle illustrated in Fig. 1b: The transition from the locked to the running state occurs on raising F above F_3 (depinning threshold), while the opposite transition takes place on lowering F below $F_1 = (4/\pi)\gamma\omega_0$ (repinning threshold). Of course, for sufficiently large values of γ , say, in the damped regime with $\gamma > \gamma_0 = (\pi/4)\omega_0$, the distinction between F_1 and F_3 becomes meaningless; the locked-to-running transition occurs at $F = F_3$, no matter what the initial conditions.

At zero temperature, $T = 0+$, we have a totally different scenario, as the *stationary* dynamics of $x(t)$ is controlled by one threshold $F_2 = 3.3576 \dots \gamma\omega_0$, only (Risken, 1984): For $F < F_2$ the Brownian particle remains trapped in one potential well; for $F > F_2$ it falls down the tilted washboard potential with speed close to F/γ . At the threshold F_2 the quantity $\gamma\mu$ jumps from zero to (very close to) one, stepwise (Fig. 1b). Note that, at variance with F_3 , F_2 indicates a dynamical transition occurring in the presence of a relatively small tilt. Nevertheless, at low damping, switches between locked and running states correspond to long forward particle jumps, which can span over many substrate unit cells L ; the distributions of the relevant jump lengths exhibit persistent non-exponential tails (Borromeo and Marchesoni, 2000; Costantini and Marchesoni, 1999; Ferrando *et al.*, 1995; Pollak *et al.*, 1993; Shushin, 2002).

For finite but low temperatures, $kT \ll V_0$, the transition from the locked to the running state is continuous but still confined within a narrow neighborhood of F_2 ; the relevant locked-to-running transition threshold F_{th} is numerically identifiable with high accuracy as a convex function of γ ; F_2 and F_3 are respectively the $\gamma \rightarrow 0$ and $\gamma \rightarrow \infty$ asymptotes of the numerical curve $F_{\text{th}}(\gamma)$ (Risken, 1984).

2. ac drive

Suppose now that the external force $F(t)$ acting on the unit-mass Brownian particle is periodic in time. The simplest case possible is represented by a *noiseless* particle, $\xi(t) \equiv 0$, moving on a sinusoidal potential, Eq. (5), under the action of a harmonic force

$$F(t) = A_1 \cos(\Omega_1 t + \phi_1). \quad (8)$$

The wide class of devices thus modeled may be assimilated to a damped-driven pendulum operated at zero noise level, a chaotic system investigated at depth in the 1980s (Baker and Gollub, 1990). The dynamics of a massive particle in a sinusoidal potential was reproduced in terms of a climbing-sine map (Geisel and Nierwetberg, 1982; Grossmann and Fujisaka, 1982): Running orbits, leading to a spontaneous symmetry breaking, can be either periodic or diffusive, depending on the value of the map control parameter (viz. the amplitude of the sine term). The phase-space portrait of the actual damped-driven pendulum was computed by Huberman *et al.* (1980), who revealed the existence of delocalized strange attractors with an intricate structure on all scales, later recognized to be fractal objects (Baker and Gollub, 1990). This means that, despite the global reflection symmetry of the dynamics in Eqs. (1) and (8), for sufficiently small γ the particle drifts either to the right or to the left, depending on the initial conditions, but with equal probability in phase-space.

Coupling the particle to a heat bath, no matter how low the temperature, changes this scenario completely. The action of the noise source $\xi(t)$ amounts to scrambling the initial conditions, which therefore must be averaged on. As a consequence, trajectories to the right and to the left compensate one another and the symmetry is restored: No Brownian drift is expected in the zero temperature limit.

A system symmetry can be broken by adding a dc component A_0 to the external force,

$$F(t) = A_0 + A_1 \cos(\Omega_1 t + \phi_1). \quad (9)$$

The most evident effect of such a periodic drive is the appearance of hysteresis loops (Borromeo *et al.*, 1999) in the parametric curves of the mobility $\mu(t)$ versus $F(t)$. For $\Omega_1 \ll \omega_0$ and $A_0 \ll F_{\text{th}}$, the mobility hysteresis loop is centered on the static mobility curve $\mu(A_0)$ and traversed counterclockwise; with decreasing Ω_1 , its major axis approaches the tangent to the curve $\mu(A_0)$. Hysteresis loops have been observed even for Ω_1 much smaller than the relevant Kramers rate, the smallest relaxation rate in the unperturbed stationary process of Eq. (6) with $F = 0$. The area encircled by the hysteretic loops is maximum for $A_0 \simeq F_{\text{th}}$, that is close to the transition jump. Even more interestingly, it exhibits a resonant dependence on both the forcing frequency and the temperature, thus pointing to a dynamical stochastic resonance (Gammaitoni *et al.*, 1998) mechanism between

locked and running states (Borromeo and Marchesoni, 2000).

Finally, Machura *et al.* (2007a) showed that under special conditions, involving small Brownian motion at temperature T and appropriate relaxation constants $\gamma \lesssim \Omega_1 \lesssim \omega_0$, the damped process in Eq. (6) occasionally exhibits the phenomenon of absolute negative mobility: The ac cycle averaged drift velocity $\langle \dot{x} \rangle$ may be oriented against the dc bias A_0 , as the result of a delicate interplay of chaotic and stochastic dynamics. This observation was corroborated theoretically by Speer *et al.* (2007) and Kostur *et al.* (2008) and experimentally by Nagel *et al.* (2008). Yet, another artificial Brownian motor system where this phenomenon can likely be validated experimentally are cold atoms dwelling in periodic optical lattices.

3. Diffusion peak

Diffusive transport of particles or, more generally, small objects is a ubiquitous feature of physical and chemical reaction systems (Burada *et al.*, 2009). Directed Brownian motor transport is typically controlled both by the fluctuation statistics of the jittering objects and the phase space available to their dynamics. For example, as the particle in Eq. (6) drifts with average speed $\langle \dot{x} \rangle$ in the direction of the external force F , the random switches between locked and running state cause a spatial dispersion of the particle around its average position. The corresponding *normal* diffusion constant,

$$D(F) = \lim_{t \rightarrow \infty} \frac{\langle x(t)^2 \rangle - \langle x(t) \rangle^2}{2t}, \quad (10)$$

was computed numerically as a function of F at constant temperature by Costantini and Marchesoni (1999). A peak in the curves of D versus F is detectable in the vicinity of the transition threshold F_{th} , irrespective of the value of γ . In particular, at low damping, where $F_{\text{th}} \simeq F_2$, and low temperature, $kT \ll \omega_0^2$, the peak of D at $F = F_2$ is very pronounced; on increasing the damping, the diffusion peak eventually shrinks down to just a bump corresponding to the threshold $F_{\text{th}} \simeq F_3$. In any case, in an appropriate neighborhood of F_{th} the diffusion constant can grow larger than Einstein's diffusion constant for the free Brownian motion in one dimension, $D_0 = kT/\gamma$. On increasing T the diffusion peak eventually disappears, no matter what γ .

A refined analytical formula for the diffusion peak was obtained by Reimann and collaborators who regarded the locked-to-running transition in the overdamped regime as a renewal process, that is (Reimann *et al.*, 2001, 2002):

$$D(F) = \frac{L^2}{2} \frac{\langle t^2(L, F) \rangle - \langle t(L, F) \rangle^2}{\langle t(L, F) \rangle^3}, \quad (11)$$

where the n -th moments of the first passage time, $\langle t^n(L, F) \rangle$, can be computed explicitly. For $F \rightarrow 0$, Eq. (11) reproduces the zero-bias identity $D/D_0 = \gamma\mu$ (Festa and d'Agliano, 1978).

4. Single-file diffusion

When a gas of particles is confined to a linear path, an individual particle cannot diffuse past its neighbors. This constrained 1D geometry is often called a "single-file", or Jepsen gas (Harris, 1974; Jepsen, 1965). Let us consider a file of N indistinguishable, unit-mass Brownian particles moving on a tilted sinusoidal substrate in Eq. (6) of length L . If the particle interaction is hard-core (zero radius), the file constituents can be labeled according to a given ordered sequence and the long-time diffusion of an individual particle gets strongly suppressed. In early studies (Harris, 1974; Jepsen, 1965; Lebowitz and Percus, 1967; Levitt, 1973; Marchesoni and Taloni, 2006) the mean square displacement of a single particle in the thermodynamic limit ($L, N \rightarrow \infty$ with constant density $\rho = N/L$) was calculated analytically. Those results were generalized to the diffusion of a single-file of driven Brownian particles on a periodic substrate by Taloni and Marchesoni (2006) who derived the subdiffusive law

$$\lim_{t \rightarrow \infty} [\langle x(t)^2 \rangle - \langle x(t) \rangle^2] = \frac{2}{\rho} \sqrt{\frac{D(F)t}{\pi}}, \quad (12)$$

with $D(F)$ given in Eq. (11). This result applies to any choice of the substrate potential $V(x)$ (Burada *et al.*, 2009) and to the transport of composite objects (Heinsalu *et al.*, 2008), as well. Excess diffusion peaks have been obtained experimentally in the context of particle transport in quasi-1D systems (Sec. III).

B. Rectification of asymmetric processes

Stochastic transport across a device surely can be induced by applying a macroscopic gradient, like a force or a temperature difference. However, under many practical circumstances this is no viable option: (a) Current induced by macroscopic gradients are rarely selective; (b) A target particle that carries no charge or dipole, can hardly be manipulated by means of an external field of force; (c) External controls, including powering, critically overburden the design of a small device. Ideally, the optimal solution would be a self-propelled device that operates by rectifying environmental signals. In the quest for rectification mechanisms of easy implementation, we will start from the symmetric dynamics of Eq. (1) and add the minimal ingredients needed to induce and control particle transport.

If $V(x)$ is symmetric under reflection, the only way to induce a drift of the Brownian particle consists in driving it by means of a non-symmetric force $F(t)$, either deterministic or random (Astumian and Hänggi, 2002; Chialvo *et al.*, 1997; Hänggi *et al.*, 1996; Luczka *et al.*, 1995; Reimann and Hänggi, 2002). Here, "symmetric" means that all force moments are invariant under sign reversal $F \rightarrow -F$. Note that the condition of a vanishing dc component, $\lim_{t \rightarrow \infty} \frac{1}{t} \int_0^t F(s) ds = 0$, would not be

sufficient. For instance, a bi-harmonic signal with commensurate frequencies and arbitrary phase constants, although zero-mean valued, is in general nonsymmetric.

On the contrary, particles in an asymmetric potential can drift on average in one direction even when all perturbing forces or gradients are symmetric. However, as pointed out in Sec. II.D, to achieve directed transport in such a class of devices, the external perturbation is required to be at least time-correlated, like in the presence of a non-Markovian noise source (correlation ratchets) or a time periodic drive (rocked and pulsated ratchets).

The interplay of time and space asymmetry in the operation of a Brownian motor has been established on firmer mathematical grounds by Yevtushenko *et al.* (2001) and by Reimann (2001). Let us slightly generalize the overdamped dynamics in Eq. (3) to incorporate the case of time dependent substrates, that is

$$\dot{x} = -V'[x, F_2(t)] + F_1(t) + \xi(t). \quad (13)$$

The potential $V[x, F_2(t)]$ is termed supersymmetric (Jung and Hänggi, 1991; Marchesoni *et al.*, 1988) if, for an appropriate choice of the x and t origins,

$$-V[x, F_2(t)] = V[x + L/2, F_2(-t)]. \quad (14)$$

Analogously, the additive drive $F_1(t)$ is supersymmetric if for an appropriate t origin,

$$-F_1(t) = F_1(-t). \quad (15)$$

Should $F_i(t)$, with $i = 1, 2$, be stationary noises, clearly no restriction can be set on the t origin; the equalities in Eq. (14) and in Eq. (15) must then hold in a statistical sense, meaning that the two terms of each equality must be statistically indistinguishable.

Let us consider now the time reversed process $z(t) = x(-t) + L/2$. By definition, $\langle \dot{z} \rangle = -\langle \dot{x} \rangle$, whereas, on simultaneously imposing the supersymmetry conditions (14) and (15), the Langevin equation (13) yields $\langle \dot{z} \rangle = \langle \dot{x} \rangle$; hence, $\langle \dot{x} \rangle = 0$. As a consequence, a nonzero rectification current requires that either the substrate or the additive drive (or both) are *non-supersymmetric*.

We remark that the above theorem has been proven only for zero-mass particles, that is, when the Smoluchowski regime $m\ddot{x} = 0$ applies. In the presence of inertia, instead, rectification may occur, under very special conditions, also in fully supersymmetric devices, as shown lately by Machura *et al.* (2007a) for a rocked cosine potential.

C. Nonlinear mechanisms

In this Section we review transport on symmetric substrates driven by asymmetric forces. The rectification mechanisms outlined below can be traced back to the *nonlinear* nature of the substrate; for this reason, at variance with Brownian motors, they work also, if not more effectively, in the absence of noise.

We remind the reader that these mechanisms have been introduced and demonstrated experimentally in the most diverse fields of physics and engineering. Direct applications to various categories of artificial nanodevices will be discussed in the subsequent sections.

1. Harmonic mixing

A charged particle spatially confined by a nonlinear force is capable of mixing two alternating input electric fields of angular frequencies Ω_1 and Ω_2 , its response containing all possible higher harmonics of Ω_1 and Ω_2 . For commensurate input frequencies, i.e., $\Omega_1/\Omega_2 = n/m$ with n and m coprime integer numbers, the output contains a dc component, too (Schneider and Seeger, 1966); harmonic mixing thus induces a rectification effect of the $(n+m)$ -th order in the dynamical parameters of the system (Goychuk and Hänggi, 1998; Marchesoni, 1986).

Let us consider the overdamped stochastic dynamics of Eq. (3) in the potential of Eq. (5), driven by the bi-harmonic force

$$F(t) = A_1 \cos(\Omega_1 t + \phi_1) + A_2 \cos(\Omega_2 t + \phi_2) \quad (16)$$

Let the two harmonic components of $F(t)$ be commensurate with one another, meaning that Ω_1, Ω_2 are integer-valued multiples of a fundamental frequency Ω_0 , i.e., $\Omega_1 = n\Omega_0$ and $\Omega_2 = m\Omega_0$. For small amplitudes and low frequencies of the drive in Eq. (16), a simple expansion of the mobility function, Eq. (7), in powers of $F(t)$, yields, after time averaging, the following approximate expression for the non-vanishing dc component of the particle velocity:

$$\langle \dot{x} \rangle = 2\bar{\mu} \frac{m+n}{m! n!} \left(\frac{A_1}{2}\right)^m \left(\frac{A_2}{2}\right)^n \cos(\Delta_{m,n}), \quad (17)$$

where $\bar{\mu}$ is the positive $(n+m-1)$ -th derivative of $\mu(F)$ at $F = 0$, $\Delta_{m,n} = n\phi_2 - m\phi_1$, and $m+n$ is an odd number. Harmonic mixing currents $j = \langle \dot{x} \rangle/L$ clearly result from a spontaneous symmetry breaking mechanism: indeed, averaging j over ϕ_1 or ϕ_2 would eliminate the effect completely. This is true under any regime of temperature and forcing, as proven by means of standard perturbation techniques (Breymayer and Wonneberger, 1981; Marchesoni, 1986). In particular, rectification of two small commensurate driving signals, $A_1, A_2 \ll \omega_0^2$, is a noise assisted process and, therefore, is strongly suppressed for $kT \ll \omega_0^2$, when $\bar{\mu}$ decays exponentially to zero (Risken, 1984). Moreover, we anticipate that accounting for finite inertia effects requires introducing in Eq. (17) an additional damping and frequency dependent phase-lag, as discussed in Sec. IV.A.

In all calculations of $\langle \dot{x} \rangle$, including Eq. (17), the reflection symmetry of $V(x)$ plays no significant role; rectification via harmonic mixing is caused solely by the *nonlinearity* of the substrate. However, it must be noticed,

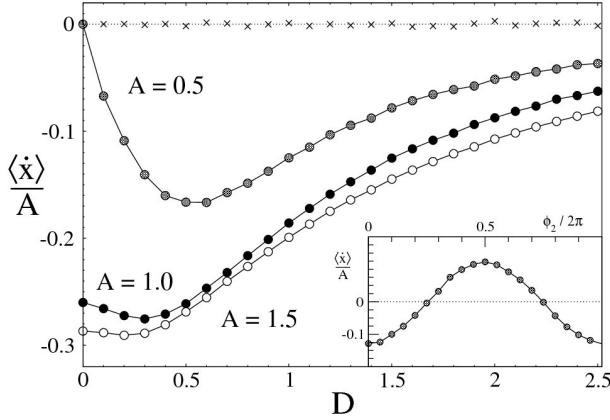


FIG. 2 Gating mechanism. Equation (19) has been simulated numerically for $\Omega_1 = \Omega_2 = 0.01$, $\phi_1 = \phi_2 = 0$, $A_1 = A_2 = A$, and $V(x) = \omega_0^2(1 - \cos x)$ with $\omega_0 = 1$; the net velocity $\langle \dot{x} \rangle$ has been plotted versus $D = kT$ for different amplitudes A . For a comparison we show $\langle \dot{x} \rangle$ versus D for $\Omega_1 = 0.01$, $\Omega_2/\Omega_1 = \sqrt{2}$ and $A = 0.5$ (crosses). Inset: $\langle \dot{x} \rangle$ versus ϕ_2 for $\phi_1 = 0$, $A = 0.5$, and $D = 1$. Note the resonant behavior of $\langle \dot{x} \rangle$ for subthreshold drives, $A < 1$, where a low noise level enhances rectification; increasing D for $A > 1$ degrades the rectification effect.

that a symmetric nonlinear device cannot mix rectangular waveforms, like

$$F(t) = A_1 \text{sgn}[\cos(\Omega_1 t + \phi_1)] + A_2 \text{sgn}[\cos(\Omega_2 t + \phi_2)], \quad (18)$$

with $A_1, A_2 \geq 0$ and $\text{sgn}[\dots]$ denoting the sign of $[\dots]$ (Savel'ev *et al.*, 2004a; Savel'ev *et al.*, 2004). As shown in Sec. II.D.4, *asymmetric* devices do not exhibit this peculiarity. Moreover, we underscore that for incommensurate frequencies, Ω_1/Ω_2 not a rational number, harmonic mixing takes place only in the presence of spatial asymmetry, as reported in Sec. II.D.4.

For practical applications, any commensuration condition, like $\Omega_1/\Omega_2 = n/m$ for harmonic mixing (but see also Secs. II.C.2 and II.D.4) is affected by an uncertainty that is inverse proportional to the observation time, i.e., the code running time for numerical simulations or the data recording time for real experiments. As such time is necessarily finite, only a limited number of commensuration spikes can be actually detected.

We conclude by reminding that the notion of harmonic mixing has been introduced long ago, e.g., to interpret the output of certain charge wave density experiments (Schneider and Seeger, 1966) and to design laser ring gyroscopes (Chow *et al.*, 1985) and annular Josephson junctions (Ustinov *et al.*, 2004); applications in the context of nano-particle transport is more recent (see Secs. II.C.3 and IV).

2. Gating

A periodically-driven Brownian motion can also be rectified by modulating the amplitude of the substrate potential $V(x)$. Let us specialize the overdamped dynamics in Eq. (13) as follows:

$$\dot{x} = -V'(x)[1 + F_2(t)] + F_1(t) + \xi(t) \quad (19)$$

To avoid interference with possible harmonic mixing effects we follow the prescription of Sec. II.C.1, namely we take $F_i(t) = A_i \text{sgn}[\cos(\Omega_i t + \phi_i)]$, $i = 1, 2$, with $A_1 > 0$ and $0 < A_2 < 1$. Mixing of the additive $F_1(t)$ and the multiplicative signal $F_2(t)$ provides a control mechanism of potential interest in device design.

In the adiabatic limit, the Brownian particle moves cyclicly back and forth subjected to opposite dc forces with amplitude A_1 ; the substrate potential $V(x, t) = V(x)[1 + F_2(t)]$ switches, in turn, periodically between the two symmetric configurations $V_{\pm}(x) = V(x)(1 \pm A_2)$. The relevant mobilities $\mu_{\pm}(A_1)$ can be easily related to the static mobility function $\mu(A)$ for the tilted potential $V(x)$ studied in Fig. 1, namely (Savel'ev *et al.*, 2004a; Savel'ev *et al.*, 2004)

$$\mu_{\pm}(A_1) = (1 \pm A_2) \mu \left[\frac{A_1}{1 \pm A_2} \right], \quad (20)$$

with $T \rightarrow T/(1 \pm A_2)$.

In particular, for any pair of commensurate frequencies Ω_1 and Ω_2 such that $\Omega_2/\Omega_1 = (2m-1)/(2n-1)$ (with m, n positive integers), the net particle velocity mediated over an integer number of cycles of both $F_1(t)$ and $F_2(t)$ can be cast in the form

$$\langle \dot{x} \rangle = -\frac{(-1)^{m+n} A_1}{(2m-1)(2n-1)} \Delta\mu(A_1, A_2) p(\Delta_{n,m}), \quad (21)$$

where $\Delta\mu(A_1, A_2) = \mu_{-}(A_1) - \mu_{+}(A_1)$ and $p(\Delta_{n,m}) \equiv |\pi - \Delta_{n,m}|/\pi - 0.5$ is a modulation factor with $\Delta_{n,m} = (2n-1)\phi_2 - (2m-1)\phi_1, \text{mod}(2\pi)$. Note that for different choices of the ratio Ω_2/Ω_1 , no induced drift is predicted (see Fig. 2).

As a consequence, a relatively small modulation of the sinusoidal potential amplitude at low temperatures results in a net transport current as illustrated in Fig. 2. Let us consider the simplest possible case, $\Omega_1 = \Omega_2$ and $\phi_1 = \phi_2$: As the ac drive points to the right, the amplitude of $V(x, t)$ is set at its maximum value $\omega_0^2(1 + A_2)$; at low temperatures the Brownian particle can hardly overcome the substrate barriers within a half ac-drive period π/Ω_1 . In the subsequent half period $F_1(t)$ switches to the left, while the potential amplitude drops to its minimum value $\omega_0^2(1 - A_2)$: The particle has a better chance to escape a potential well to the left than to the right, thus inducing a negative current with maximum intensity for Ω_1 of the order of the Kramers rate (resonant activation (Borromeo and Marchesoni, 2004)). Of course, amplitude and sign of the net current may be controlled via the modulation parameters A_2 and ϕ_2 , too (see inset of Fig. 2).

3. Noise induced transport

Induced transport in the symmetric dynamics can be achieved also by employing two *correlated* noisy signals.

(i) *Noise mixing.* Borromeo and Marchesoni (2004) showed that the gating process in Eq. (19) can be driven also by two stationary, zero-mean valued Gaussian noises, $F_i(t) = \eta_i(t)$ with $i = 1, 2$. The two random drives may be cross- and auto-correlated with

$$\langle \eta_i(t) \eta_j(0) \rangle = \sqrt{Q_i Q_j} \frac{\lambda_{ij}}{\tau_{ij}} \exp\left(-\frac{|t|}{\tau_{ij}}\right), \quad i, j = 1, 2. \quad (22)$$

Without loss of generality, one sets $\lambda_{11} = \lambda_{22} = 1$ and $\lambda_{12} = \lambda_{21} = \lambda$, and to avoid technical complications, $\tau_{ij} \equiv \tau$. Of course $\tau \rightarrow 0$ corresponds to taking the white noise limit of $\eta_i(t)$, Eq. (4). The parameter λ characterizes the cross-correlation of the two signals; in particular, $\lambda = 0$: independent signals; $\lambda = 1$: identical signals, $\eta_2(t) \equiv \eta_1(t)$; $\lambda = -1$: signals with reversed sign, $\eta_2(t) \equiv -\eta_1(t)$. Two such signals may have been generated by a unique noise source and then partially de-correlated through different transmission or coupling mechanisms.

In the white noise limit, $\tau \rightarrow 0$, the Fokker-Planck equation associated with the process of Eqs. (19) and (22) admits of a stationary solution in closed form. Non-vanishing values of $\langle \dot{x} \rangle$ for $\lambda \neq 0$ are the signature of a stochastic symmetry breaking due to *nonlinear noise mixing*; the sign of λ , similarly to the relative phase $\Delta_{m,n}$ in the gating set-up of Sec. II.C.2, determines the direction of the particle drift. The interpretation of this result is straightforward. Let us consider, for instance, the case of the symmetric potential in Eq. (5), rocked and pulsated by the same signal, i.e., $\eta_1(t) = \eta_2(t)$: For $\lambda = 1$, when pushed to the left ($\eta_i < 0$), the Brownian particle encounters lower substrate barriers than when pushed to the right ($\eta_i > 0$), hence the negative average drift current detected by means of numerical simulation (Borromeo *et al.*, 2006; Borromeo and Marchesoni, 2005b).

The magnitude of the induced current is controlled by the correlation time τ (Borromeo and Marchesoni, 2005b). While one can easily estimate $\langle \dot{x} \rangle$ for $\lambda \neq 0$ and $\tau = 0$ (white noise (Risken, 1984)) or $\tau \rightarrow \infty$ (strongly correlated noise (Hänggi *et al.*, 1989)), the intermediate τ values are accessible solely through numerical simulation. In Fig. 3(a) we report $\langle \dot{x} \rangle$ versus τ for different noise intensities: the two sets of curves at Q and Q/τ fixed, illustrate well the noise mixing effect for $\tau \rightarrow 0$ and $\tau \rightarrow \infty$, respectively.

(ii) *Noise recycling.* If the noises $\eta_i(t)$ are generated by the same source and then coupled to the diffusing particle through different paths, it may well happen that they are simply delayed in time. Under stationary conditions, we can assume that $\eta_2(t) = \eta_1(t - \tau_d)$, with $\eta_i(t)$ given in Eq. (22) and, for simplicity, $\lambda = 0$. In the notation of Refs. (Borromeo *et al.*, 2006; Borromeo and Marchesoni, 2007b), $\eta_1(t)$ represents the primary noise source and

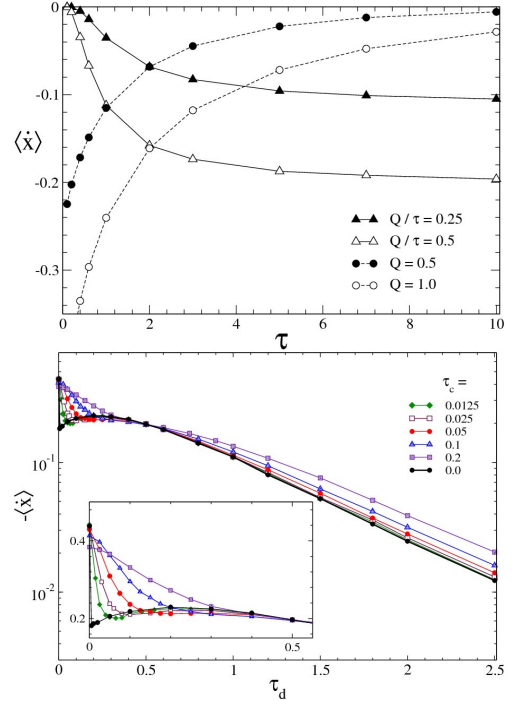


FIG. 3 (Color online) Equation (19), with $F_i(t) = \eta_i(t)$, $i = 1, 2$, and $V(x) = -\sin x$, has been simulated numerically; the noises $\eta_i(t)$, Eq. (22), have same strength, $Q_1 = Q_2 = Q$. After Borromeo and Marchesoni (2005b): (a) Nonlinear noise mixing: Characteristics curve $\langle \dot{x} \rangle - \tau$ for different intensities Q of the noises and $\lambda = 1$; $D = 0.1$. (b) Noise recycling: Characteristics curve $\langle \dot{x} \rangle - \tau_d$, where τ_d is the relative time delay of η_i (see text). Data are for different τ and $Q = 1$; $D = 0$, see in Borromeo *et al.* (2006).

$\eta_2(t)$ a recycled noise to be used as a control signal.

By the same argument as for noise mixing, we expect that the Brownian dynamics gets rectified to the left with negative velocity $\langle \dot{x}(\tau_d) \rangle$. Note that: $\langle \dot{x}(-\tau_d) \rangle = \langle \dot{x}(\tau_d) \rangle$ and $\langle \dot{x}(\tau_d) \rangle \rightarrow -\langle \dot{x}(\tau_d) \rangle$, upon changing the relative signs of η_i . The dependence of the characteristic curve $\langle \dot{x}(\tau_d) \rangle$ on the time constants τ_d and τ displayed in Fig. 3(b), is important in view of practical applications. Indeed, in many circumstances, it would be extremely difficult to recycle a control signal $\eta_2(t)$ so that $\tau_d \ll \tau$; stated otherwise, measuring $\langle \dot{x}(0) \rangle$ requires a certain degree of experimental sophistication. On the contrary, if we agree to work on the resonant tail of its response curve $|\langle \dot{x}(\tau_d) \rangle|$, a noise controlled rectification device can be operated with less effort; its net output current may be not the highest for $\tau_d > \tau$, but is still appreciable and, more importantly, stable against the accidental floating of the time constant τ_d .

In this sense both schemes discussed in this section are a simple-minded attempt at implementing the operation of a Maxwell's daemon: The ideal device we set up is intended to gauge the primary random signal η_1 at the sampling time t and, depending on the sign of each reading, to lower or raise the gate barriers accordingly at a later

time $t + \tau_d$, i.e., open or close the trap door. The rectifying power of such a daemon is far from optimal; lacking the dexterity of Maxwell's "gate-keeper" (Leff and Rex, 2003; Maruyama *et al.*, 2008), it only works "in average" like an automaton.

D. Brownian motors

As detailed in Sec. II.B, a necessary condition for the rectification of symmetric signals, random or periodic in time, alike, is the spatial asymmetry of the substrate. Rectification devices involving asymmetric substrates are termed *ratchets*. In most such devices, however, noise (no matter what its source, i.e. stochastic, or chaotic, or thermal) plays a non-negligible, or even the dominant role. Under such conditions one speaks of Brownian motors (Astumian, 1997; Astumian and Hänggi, 2002; Bartussek and Hänggi, 1995; Hänggi and Bartussek, 1996; Hänggi *et al.*, 2005, 2002; Kay *et al.*, 2007; Linke, 2002; Reimann *et al.*, 1996). The label Brownian motor should not be abused to refer to all small ratchet-like devices. For instance, the rocked ratchets of Sec. II.D.1 work quite differently in the presence or in the absence of noise, whereas the pulsated and correlation ratchets (sometimes also referred to as "stochastic" ratchets) of Secs. II.D.2 and II.D.3 work only in the presence of noise.

The hallmarks of genuine Brownian motors are listed in Sec. I. In this Section we discuss in detail noise rectification and directed transport on asymmetric periodic substrates and potentials. We caution the reader that: (1) Strict periodicity is not a requirement for the operation of a Brownian motor. The ratchet system may contain small amounts of disorder (Harms and Lipowsky, 1997; Kafri and Nelson, 2005; Martinez and Chacon, 2008; Popescu *et al.*, 2000) or even be non-periodic (Marchesoni, 1997); (2) Spatial asymmetry can also result as a collective effect, for instance, in the extended systems consisting of interacting, symmetric dynamical components, introduced in Sec. V.

The archetypal model of ratchet substrates in 1D is the double-sine potential proposed by Bartussek *et al.* (1994)

$$V(x) = -V_0 \left[\sin\left(\frac{2\pi x}{L}\right) + \frac{1}{4} \sin\left(\frac{4\pi x}{L}\right) \right], \quad (23)$$

or, in the rescaled units of Eq. (6), $V(x) = -\omega_0^2[\sin x + \frac{1}{4} \sin(2x)]$. In the sketch of Fig. 4, the barriers are skewed to the right with ratchet length $l_+ > l_-$. A Brownian particle with Langevin equation (1) moving on such a substrate is characterized by an asymmetric mobility function, $\mu(F) \neq \mu(-F)$; as the particle mobility depends now not only on the amplitude, but also on the orientation of the drive F , symmetric substrate perturbations are expected to induce a net current in either direction.

Broadly speaking, ratchet devices fall into three categories depending on how the applied perturbation couples to the substrate asymmetry.

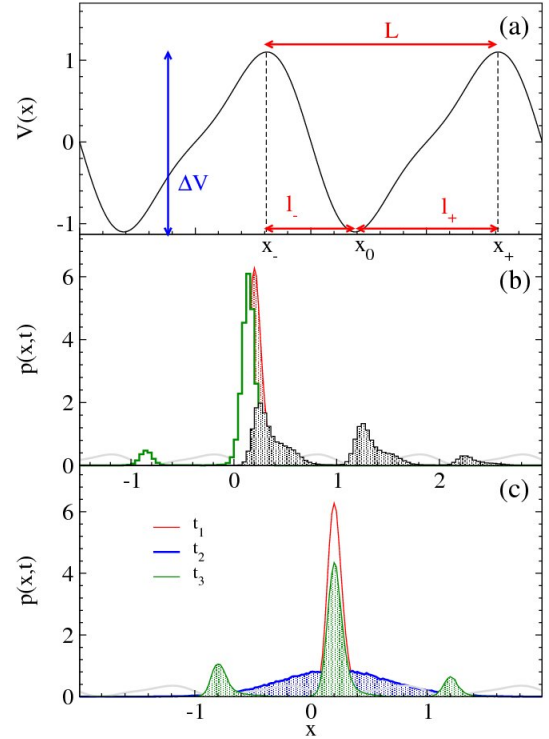


FIG. 4 (Color online) Ratchet mechanism. (a) Sketch of the potential in Eq. (23) with $L = 1$ and $V_0 = L/2\pi$. The three consecutive extremal points, $x_- = -0.19$, $x_0 = 0.19$ and $x_+ = 0.81$, define a potential well; the barrier height is $\Delta V = V(x_\pm) - V(x_0) \simeq 0.35$ and its asymmetry is quantified by the difference $l_+ - l_-$ with $l_\pm = |x_\pm - x_0|$. The curvature of the potential at the bottom of the well is $\bar{\omega}_0^2 = (3\sqrt{3}/2)\omega_0^2 \simeq 10.1$. (b) Rocket ratchet. Probability density $p(x,t)$ for a Brownian particle initially centered around $x = 0$ (red) and then driven for $t = 10$ by a dc force $A_0 = -0.5$ (green) and 0.5 (grey). The backward displacement is strongly suppressed, hence the positive natural orientation of this ratchet. (c) Pulsated ratchet. The ratchet potential is switched "on" and "off" periodically with $t^{\text{on}} = 1$, $t^{\text{off}} = 3$ and $T_2 = t^{\text{on}} + t^{\text{off}}$ (see text). The particle, initially set at $x = x_0$, relaxes first in the starting well during t^{on} (curve 1, red, $t_1 = t^{\text{on}}$), then diffuses symmetrically only driven by noise for t^{off} (curve 2, blue, $t_2 = T_2$), and finally gets retrapped in the neighboring wells as the next cycle begins (curve 3, green, $t_3 = T_2 + t^{\text{on}}$). As the left side peak of $p(x,t_3)$ is more pronounced than the right peak, the natural orientation of this ratchet is negative. In the simulations of (b) and (c) the ratchet potential $V(x)$ is the same as in (a) (also drawn to guide the eye) and the intensity of the noise in Eq. (4) is $D = 0.1\Delta V$. Courtesy of Marcello Borromeo.

1. Rocked ratchets

Let us consider first, for simplicity, the Langevin equation (3) with the sinusoidal drive of Eq. (8). When applied to the reflection-symmetric sine potential of Eq. (5), $F(t)$ breaks instantaneously the symmetry of the potential by tilting it to the right for $F(t) > 0$, and to the left for $F(t) < 0$. However, due to the spatio-

temporal symmetry of the process, $V(x) = V(-x)$ and $F(t) = F(-t)$, over one drive cycle, $T_1 = 2\pi/\Omega_1$, the drift to the right and to the left compensate one another: the net current is null. When placed in the double-sine potential of Eq. (23), instead, an overdamped particle is apparently more movable to the right than to the left. Indeed, depinning occurs at $F = F_{3R} = 3/4$ and $F = -F_{3L}$ for $F(t)$ oriented respectively to the right and to the left; moreover from the asymmetry condition $l_+ > l_-$ follows immediately the inequality $F_{3R} < F_{3L}$. The depinning thresholds of the potential of Eq. (23) in the rescaled units of Eq. (6) are $F_{3R} = 3/4$ and $F_{3L} = 3/2$.

If the forcing frequency Ω_1 is taken much smaller than all the intrawell relaxation constants, $\omega_0^2 T_1 \gg 1$ and $T_1 \gg \langle t(L, 0) \rangle$, than the net transport current can be computed in the adiabatic approximation by averaging the instantaneous velocity $\dot{x}(t) = \mu[F(t)]F(t)$, see Eq. (7), over one forcing cycle, that is (Bartussek *et al.*, 1994; Borromeo *et al.*, 2002)

$$j \equiv \frac{\langle \dot{x} \rangle}{L} = \frac{1}{T_1} \int_0^{T_1} \frac{\text{sgn}[F(s)]}{\langle t[L, F(s)] \rangle} ds. \quad (24)$$

The adiabatic current in Eq. (24) is positive definite, as the natural ratchet direction is defined by the choice $F_{3R} < F_{3L}$. However, its range of validity is restricted to extremely low temperatures T and drive frequencies Ω_1 . On raising Ω_1 , the rectification current develops a more complicated dependence on the noise intensity D and the drive amplitude A_1 , as proven by the numerical simulations reported in panels (a)-(c) of Fig. 5. This is due to the fact that for forcing periods T_1 shorter than the mean first-passage time $\langle t(L, 0) \rangle$, the driven particle oscillations span over fewer substrate cells. A few properties of the rocked ratchet current in Fig. 5 are remarkable:

- (a) At finite temperature, the maximum rectification effect occurs right in the adiabatic regime, $\Omega_1 \rightarrow 0$, and with natural orientation, panels (a) and (b);
- (b) For $\Omega_1 > \omega_0$, the drive and the interwell oscillations may combine to reverse the current orientation. Such *current inversions* are restricted to select D and A_1 ranges, but never in the absence of noise, panel (a) and (b);
- (c) In the noiseless regime, $T \equiv 0$, the incommensuration between forced oscillation amplitude and substrate periodicity causes the quantized locking structure of panel (c). Such a structure disappears either in the limit $\Omega_1 \rightarrow 0$, as the forced oscillation amplitude grows infinitely large, or in the presence of noise, when, due to randomness, the finer steps for $A_1 > F_{3L}$ merge into the broad oscillations of panel (b);
- (d) As the temperature vanishes, the adiabatic current in Eq. (24) gets suppressed for $A_1 < F_{3R}$ and enhanced elsewhere [see Fig. 8(a)]. For $F_{3R} < A_1 < F_{3L}$ the particle can only move to the right, so that j grows almost linearly with A_1 , while for $A_1 > F_{3L}$ the particle can drift in both directions, thus making j decrease.

Rectifiers, like a rocked ratchet, can work against an

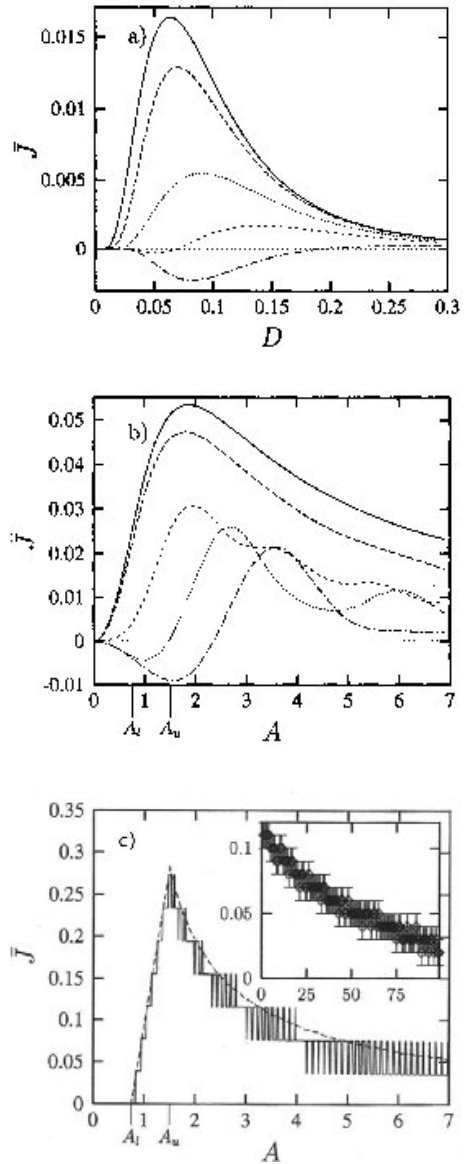


FIG. 5 Rocked ratchet. Rectification current j versus the noise intensity D , see Eq. (4), panel (a), and versus ac modulation strength $A \equiv A_1$, panels (b) and (c) for the ratchet potential in Eq. (23) with $L = 1$. The relevant simulation parameters are: (a) $A_1 = 0.5$ and $\Omega_1 = 0.01, 1, 2.5, 4$ and 7 (top to bottom); (b) $D = 0.1$ and $\Omega_1 = 0.01, 1, 4$ and 7 (top to bottom). In both panels (a) and (b) the solid line for $\Omega_1 = 0.01$ coincides with the adiabatic limit in Eq. (24); (c) deterministic regime with $D = 0$, and $\Omega_1 = 0.01$ (dashed line) and 0.25 (solid line). After Bartussek *et al.* (1994).

external dc drive. On adding a dc component A_0 to the sinusoidal force, namely, on applying the drive (9) instead of (8), we can determine the value of A_0 , termed *stopping force*, such that for a certain choice of the other perturbation parameters, A_1 , Ω_1 and D , the net current vanishes.

Rocked ratchets with massive particles exhibit strong

inertial effects also capable of reversing their current. A noiseless inertial rocked ratchet is naturally subject to developing chaotic dynamics; indeed, its current turns out to be extremely sensitive to the initial conditions (Borromeo *et al.*, 2002; Jung *et al.*, 1996; Machura *et al.*, 2007a; Mateos, 2000, 2003). However, an appropriate noise level suffices to stabilize the rectification properties of an inertial ratchet and makes it a useful device with potential applications in science and technology (Machura *et al.*, 2004b; Marchesoni *et al.*, 2006a).

In the notation of Sec. II.A.1, slightly generalized to account for the asymmetry of the potential in Eq. (23), we define two additional pairs of thresholds, besides the depinning thresholds $F_{3R,L}$: the repinning thresholds $F_{1R,L}$ and the underdamped transition thresholds $F_{2R,L}$, with $F_{iR} < F_{iL}$ for $i = 1, 2, 3$ [the suffix R, L denoting the orientation of the drive]. Under the adiabatic condition $\Omega_1 \ll \gamma, \omega_0$, the following approximations have been obtained in Borromeo *et al.* (2002); Marchesoni *et al.* (2006a):

(a) in the zero-temperature limit, $T \rightarrow 0$:

$$\begin{aligned} j(A_1) &= j_R(A_1), & F_{2R} < A_1 < F_{2L} \\ &= j_R(A_1) - j_L(A_1) & A_1 > F_{2L} \end{aligned} \quad (25)$$

and $j(A_1) = 0$ for $A_1 < F_{2R}$. The right/left current components are $j_{R,L}(A_1) = 2\sqrt{A_1^2 - F_{2R,L}^2}/(\pi\gamma L)$.

(b) in the noiseless regime, $T \equiv 0$:

$$\begin{aligned} j(A_1) &= j_R(A_1), & F_{3R} < A_1 < F_{3L} \\ &= j_R(A_1) - j_L(A_1), & A_1 > F_{3L} \end{aligned} \quad (26)$$

and $j(A_1) = 0$ for $A_1 < F_{3R}$. Here, $j_{R,L}(A_1) = [\sqrt{A_1^2 - F_{1R,L}^2} + \sqrt{A_1^2 - F_{3R,L}^2}]/(\pi\gamma L)$. Note that $j(A_1)$ in Eq. (26) is discontinuous at the depinning thresholds $F_{3R,L}$ as expected for the response curve of any underdamped rocked ratchet operated in the deterministic regime (see Sec. II.A.1).

2. Pulsated ratchets

Let us consider now the overdamped process of Eq. (19) with $F_1(t) = 0$ and $F_2(t) = A_2 \text{sgn}[\cos(\Omega_2 t + \phi_2)]$. As discussed in Sec. II.C.2, modulating the amplitude of a symmetric potential $V(x)$ in the presence of an uncorrelated, time-symmetric perturbation $\xi(t)$ does not suffice to induce rectification. This state of affair changes when $F_2(t)$ couples, instead, to an asymmetric substrate, like our reference ratchet potential (23). For the sake of simplicity, we set $A_2 = 1$, so that the effective substrate potential $[1 + F_2(t)]V(x)$ appears to switch on and off at every half period $T_2/2 = \pi/\Omega_2$. The interplay between time modulation and spatial asymmetry generates a non-zero drift current, which, at low (but not too low!) frequencies, is oriented in the positive direction. Devices operated under similar conditions are termed *pulsated ratchets*.

Rectification by a pulsated ratchet can be explained qualitatively by looking at the cartoon of Fig. 6. The probability density of a particle initially placed at the bottom of a potential well (top), is mostly confined to that well, as long as $T_2/2$ is not exceedingly longer than the escape time $\langle t(L, 0) \rangle$, which is the case at low temperatures. When, during the following half cycle, the substrate is switched off (middle), the particle, still subject to noise, diffuses freely with Einstein's constant D and, for $T_2 \gg L^2/D$, its probability density approaches a Gaussian spanning over many a unit cell. By switching on again, the substrate cuts such a probability density into smaller peaks of different size, one for each well surrounding the initial one. For potential barriers skewed like in figure, $l_+ > l_-$, wells on the right are expected to be more populated than wells on the left, hence a positive net current. This is also the case of the potential in Eq. (23), which has positive natural orientation when pulsated, and negative orientation when rocked. The mechanism illustrated in Fig. 6 can work even in the presence of dc force, $F_1(t) = A_0$, pointing in the opposite direction, $A_0 < 0$. Such an upward directed motion is clearly powered by the thermal fluctuations $\xi(t)$.

The directed particle current is clearly bound to vanish in the adiabatic limit, $\Omega_2 \rightarrow 0$, when thermal equilibrium is approached. A similar conclusion holds true for very fast substrate modulations, $\Omega_2 \gg \omega_0^2$ (in rescaled units). In perturbation analysis (Savel'ev *et al.*, 2004c), one finds the noteworthy result that the current decays to zero in both asymptotic regimes remarkably fast, namely like Ω_2^2 in the slow modulation limit, and Ω_2^2 , in the fast modulation limit respectively. Moreover, for intermediate modulation frequencies, the current in a pulsated ratchet is generally not oriented in its natural direction; current inversions are possible when the forcing frequency matches some intrinsic relaxation rate of the process.

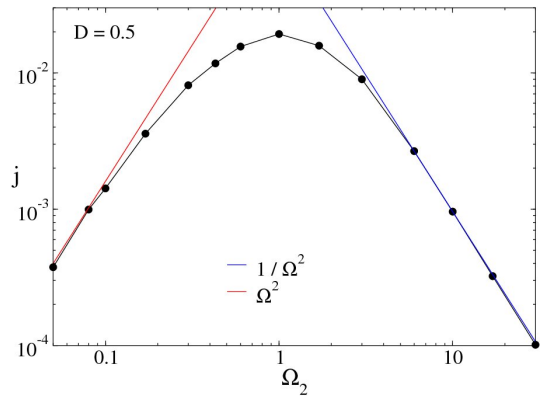


FIG. 6 (Color online) Pulsated ratchet. Rectification current $j = \langle \dot{x} \rangle$ versus Ω_2 (dimensionless units), for the ratchet potential of Eq. (23) with $L = 2\pi$ and $V_0 = 1$. Other simulation parameters are: $A_2 = 0.8$ and $D = 0.5$. The low frequency Ω_2^2 , and high frequency, Ω_2^{-2} asymptotic limits are denoted by straight lines. Courtesy of Marcello Borromeo.

Finally, pulsated ratchets can be operated under very

general amplitude modulations $F_2(t)$, as well. This ratchet effect proved robust with respect to (a) modifications of the potential shape (Reimann, 2002); (b) changes in the switching sequence. A generic discrete modulation signal $F_2(t)$ is characterized by different residence times, namely, t_{on} in the “on” state, $+A_2$, and t_{off} in the “off” state, $-A_2$, respectively. For periodic modulations, $t_{\text{on}} + t_{\text{off}} = T_2$ defines the so-called duty cycle of the device (Ajdari and Prost, 1992; Bug and Berne, 1987); for random modulations, instead, t_{on} and t_{off} must be interpreted as the average residence times in the respective “on”, “off” state (Astumian and Bier, 1994; Faucheux *et al.*, 1995). In both cases the modulation is asymmetric for $t_{\text{on}} \neq t_{\text{off}}$; (c) replacement of pulsed with flashing substrates. The substrate is made switch, either periodically or randomly in time, among two or more discrete configurations, which do not result from the amplitude modulation of a unique substrate profile (Borromeo and Marchesoni, 1998; Chen, 1997; Gorman *et al.*, 1996; Lee *et al.*, 2004). The rectification process is controlled by the spatial asymmetry of the single substrate configurations or by the temporal asymmetry of the switching sequence, or by a combination of both; (d) modulation of the temperature (Bao, 1999; Reimann *et al.*, 1996). Modulating the intensity of the ambient noise $\xi(t)$ or its coupling to the device, corresponds to introducing the time dependent temperature $T(t) = [1 + F_2(t)]T$, for an appropriate control signal $F_2(t)$ with amplitude smaller than one. Pulsating the potential amplitude V_0 or the temperature T yield very similar rectification effects, being the net current of a pulsed ratchet mostly controlled by the barrier-to-noise ratio; (e) the addition of constant or spatially modulated damping terms (Luchsinger (2000); Suzuki and Munakata (2003); see also Reimann (2002)). Inertial effects make the rectification mechanism sensitive to the particle mass, so that selective transport and segregation of mixed species becomes possible (Derényi and Ajdari, 1996; Derényi and Vicsek, 1995).

3. Correlation ratchets

To better understand the role of asymmetry in the rectification of a nonequilibrium process, we consider now an overdamped Brownian particle with Langevin equation (3) diffusing in the ratchet potential of Eq. (23) subject to a zero-mean, colored Gaussian noise $F \equiv \eta(t)$, with

$$\langle \eta(t)\eta(0) \rangle = \frac{Q}{\tau} \exp\left(-\frac{|t|}{\tau}\right). \quad (27)$$

The substrate asymmetry is capable *per se* of rectifying the correlated fluctuation $\eta(t)$, even in the absence of external modulations or thermal noise. The early prediction of this transport effect, based on simple perturbation arguments (Bartussek *et al.*, 1994; Doering *et al.*, 1994; Luczka *et al.*, 1995; Magnasco, 1993; Millonas and Dykman, 1994), kindled a widespread interest in the thermodynamics of molecular motors. A more sophisticated

path-integral analysis (Bartussek *et al.*, 1996) led later to the following low-noise estimates of the correlation ratchet current:

(a) in the weak color limit, $\omega_0^2\tau \ll 1$,

$$j(\tau) = j_+(\tau) - j_-(\tau), \quad (28)$$

where $j_{\pm}(\tau) = r_K \exp[-\tau^2 Q c_{\pm}/(D + Q)^2]$ and r_K is the equilibrium Kramers rate for the particle to exit a potential well through one side, $r_K = \bar{\omega}_0 \omega_{\pm} \exp[-\Delta V/(D + Q)]/(2\pi)$. Here, x_0 and x_{\pm} are the extremal points of $V(x)$ defined as in Fig. 4; $\bar{\omega}_0^2 = V''(x_0)$, $\omega_{\pm}^2 = |V''(x_{\pm})|$, and $c_{\pm} = \int_{x_0}^{x_{\pm}} [V''(x)]V'(x)dx$;

(b) in the strong color limit, $\tau \rightarrow \infty$,

$$j(\tau) = j_0 \left[1 - \exp\left(-\frac{QL}{2D^2\tau}(l_+ - l_-)\right) \right], \quad (29)$$

where j_0 is a positive definite constant. Equation (28) can be regarded as the difference of two exit currents $j_{\pm}(\tau)$, respectively through x_+ (forward) and x_- (backward), in the presence of colored noise (Millonas and Dykman, 1994).

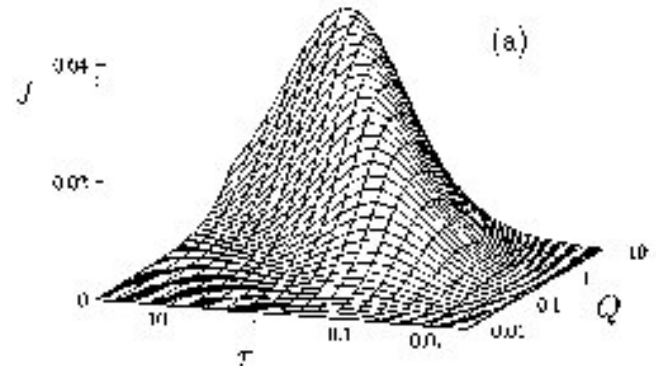


FIG. 7 Correlation ratchet. Rectification current j versus τ and Q for $D = 0.1$. The parameters of the ratchet potential, Eq. (23), are as in Fig. 4. More data can be found in Bartussek *et al.* (1996).

The orientation of the current of a correlation ratchet is extremely sensitive to the substrate geometry. In the strong color limit, the condition $(l_+ - l_-) > 0$ between the two ratchet lengths guarantees that the current is positive, no matter what the choice of $V(x)$; all correlation ratchets work in the natural direction of the corresponding rocked ratchet.

In the weak color limit, the current in Eq. (28) has the same sign as the difference $c_- - c_+ = \int_0^L [V''(x)]V'(x)dx$, which, in turn, depends on the detailed profile of $V(x)$, regardless of $\text{sgn}[l_+ - l_-]$. Numerical simulation of correlation ratchets with potential given in Eq. (23), confirmed that, consistently with the inequality $c_- - c_+ > 0$, $j(\tau)$ is positive definite, as illustrated in Fig. 7; as $j(\tau \rightarrow 0) = j(\tau \rightarrow \infty) = 0$, optimal rectification is achieved for an intermediate noise correlation time, $\omega_0^2\tau \sim 1$. Modifying the potential profile, e.g., by adding

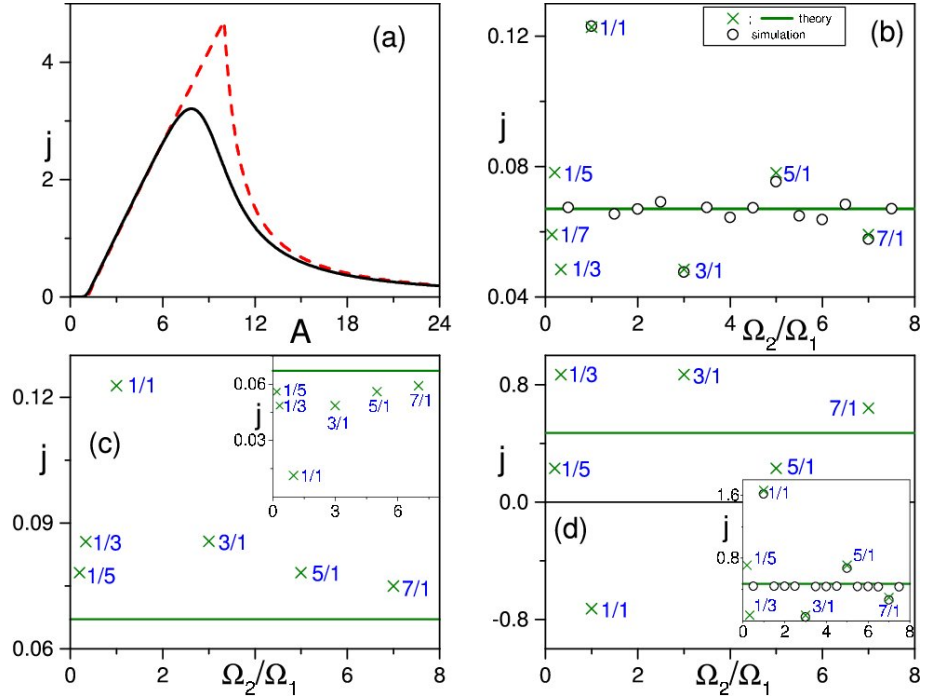


FIG. 8 (Color online) Net current in a piecewise linear potential with amplitude ΔV , driven by two rectangular waveforms, Eq. (18): (a) one-frequency rocked ratchet; (b), (c) harmonic mixing of Sec. II.C.1; (d) gating mechanism, Eq. (19). The ratchet potential is: $V(x) = x\Delta V/L_2$ for $-L_2 < x < 0$ and $V(x) = x\Delta V/L_1$ for $0 < x < L_1$, with $L_1 = 0.9$ and $L = 1$; $\Delta V = 1$ in (a)-(c) and $\Delta V = 2$ in (d). Panel (a): Response curve $j(A) \equiv \langle \dot{x} \rangle / L$ to a low-frequency rectangular force with amplitude A at zero temperature $D = 0$ (dashed curve), and low temperature $D/\Delta V = 0.05$ (solid curve). Panel (b): Numerical simulations for a doubly rocked ratchet with $\phi_1 = \phi_2 = \pi$ and $\Omega_1 = 0.01$ (open circles) versus adiabatic approximation, Eqs. (21) and (30) (green line and green crosses). The off-set j_{avg} , Eq. (30), is indicated by the green line; the spikes of Eq. (21) at some selected integer-valued odd harmonics are marked with green crosses (\times); Panel (c): Adiabatic approximation for $\phi_1 = \phi_2 = 3\pi/2$ (main panel) and $\phi_1 = 3\pi/2$, $\phi_2 = \pi/2$ (inset). In both cases $A_1 = 3$, $A_2 = 2$, $D = 0.6$; Panel (d): Numerical simulations versus adiabatic approximation, Eqs. (21) and (31), for a rocked-pulsated ratchet with $A_1 = 4$, $A_2 = 0.5$ and $\Omega_1 = 0.01$; noise level: $D = 0.4$. Main panel: $\phi_1 = \phi_2 = \pi$ (adiabatic approximation); inset: simulation (open circles) versus the fully adiabatic approximation (\times) for $\phi_1 = \pi$ and $\phi_2 = 0$. After Borromeo and Marchesoni (2005b).

an appropriate higher order Fourier component without changing $l_+ - l_-$, suffices to reverse the sign of $c_- - c_+$ and, thus, introduce at least one current inversion (Barussek *et al.*, 1996).

Correlation ratchets have the potential for technological applications to “noise harvesting”, rather than to nano-particle transport. The low current output and its extreme sensitivity to the substrate geometry and the particle mass (Lindner *et al.*, 1999; Marchesoni, 1998) makes the design and operation of correlation ratchets as mass rectifiers questionable. However, the asymmetry induced rectification of nonequilibrium fluctuations, no matter how efficient and hard to control, can be exploited by a small device to extract from its environment and store the power it needs to operate.

4. Further asymmetry effects

The rectification mechanisms introduced in Sec. II.C apply to any periodic substrate, independently of its spatial symmetry. In the presence of spatial asymmetry, the

relevant drift currents get modified as follows:

(i) *Current off-sets.* At variance with Secs. II.C.1 and II.C.2, two ac drives applied to an asymmetric device are expected to induce a net current $j_{\text{avg}} = \langle \dot{x} \rangle_{\text{avg}}$ also for incommensurate frequencies Ω_1 , Ω_2 . This is a mere ratchet effect that in most experiments is handled as a simple current off-set. This conclusion is apparent, for instance, in the case of low-frequency rectangular input waves, where the device output current can be expressed as a linear combination of two known ratchet currents (Savel'ev *et al.*, 2004a; Savel'ev *et al.*, 2004), namely:

(a) *Harmonic mixing current* (Sec. II.C.1). When the drive is a double rectangular wave, Eq. (18), j_{avg} can be regarded as the incoherent superposition of currents from two rocked ratchets driven by rectangular waves with amplitudes $A_1 + A_2$ and $|A_1 - A_2|$, respectively, i.e.

$$j_{\text{avg}} = \frac{1}{2} [j_0(|A_1 - A_2|) + j_0(A_1 + A_2)]; \quad (30)$$

(b) *Gating current* (Sec. II.C.2). The rocked-pulsated device of Eq. (19) can be regarded as the incoherent superposition of two ratchets with potentials $V_{\pm}(x) =$

$(1 \pm A_2)V(x)$, respectively, both rocked with amplitude A_1 ; hence

$$j_{\text{avg}} = \frac{1}{2}[j_+(A_1) + j_-(A_1)]. \quad (31)$$

In Eqs. (30) and (31) $j_{0,\pm}(A)$ are the net currents of Eq. (24) for a rocked ratchet driven by a rectangular wave with amplitude A and vanishing frequency, the suffixes 0, \pm referring to the regular, high/low amplitude potential configurations, $V(x)$ and $V_{\pm}(x)$.

(ii) *Asymmetry induced mixing.* As anticipated in Sec. II.C.1, a double rectangular wave is not capable of rectifying a Brownian particle in a symmetric potential, that is, $\langle \dot{x} \rangle = 0$ also under harmonic mixing conditions, $\Omega_2/\Omega_1 = m/n$ with m, n coprime integers and $m + n$ odd. This is no more the case if $V(x)$ is asymmetric. The non-zero odd moments of the process $x(t)$, determined by the substrate asymmetry, generate additional harmonic couplings of the “odd” harmonics of the drive, i.e., for $\Omega_2/\Omega_1 = (2m - 1)/(2n - 1)$ with $2m - 1$ and $2n - 1$ coprime, as shown in Fig. 8. The total rectification current, including both the incommensurate term of Eq. (30) and this new harmonic mixing spikes, was calculated analytically in Savel’ev *et al.* (2004a); Savel’ev *et al.* (2004):

$$j = j_{\text{avg}} - \frac{(-1)^{m+n} p(\Delta_{n,m})}{(2m - 1)(2n - 1)} j_{\text{odd}}, \quad (32)$$

where $p(\Delta_{n,m})$ is defined after Eq. (21) and $j_{\text{odd}} = \frac{1}{2}[j_0(|A_1 - A_2|) - j_0(A_1 + A_2)]$.

The competition between current off-set, item (i), and asymmetry induced spikes, item (ii), may cause surprising current reversals for special values of the driving frequencies, as observed in several experimental setups (cf. Secs. III, IV and VII.B). Moreover, replacing the rectangular waveform, Eq. (18), with a more conventional linear superposition of two sinusoids of the same frequency, Eq. (16), leads to an even more complicated interplay of nonlinearity and asymmetry induced harmonic mixing (Savel’ev *et al.*, 2004a). A special limit of bi-harmonically driven rocked ratchet is discussed in Sec. II.E.2.

A brilliant demonstration of the combination of harmonic mixing and asymmetry effects in the context of particle transport at the nanoscales, has been recently reported by Kalman *et al.* (2007), who managed to drive dilute ions through conical nanopores by applying a biharmonic rectangular voltage. Harmonic mixing and gating currents could be separated, as predicted by the theory, and the resulting commensuration effects are displayed in Fig. 9.

E. Efficiency and control issues

The analysis of Sec. II.D suggests that the output of a real ratchet device is hard to control experimentally, let alone to predict. As a matter of fact, if we use a ratchet

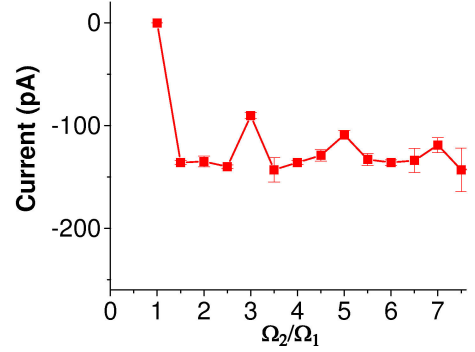


FIG. 9 (Color online) Net current through a single conical nanopore for the sum of two voltage signals applied across the pore, $0.5\text{sgn}[\sin(\Omega_1 t)] + 0.5\text{sgn}[\sin(\Omega_2 t + \pi)]$, with different Ω_2/Ω_1 . The measurements were taken in a 0.1M KCl solution at pH 8.0. For further details see Kalman *et al.* (2007).

to rectify an assigned signal, the only tunable variables are the temperature T , the damping constant γ (or the mass m), and the substrate profile $V(x)$. Under certain experimental circumstances these quantities may prove not directly accessible to this purpose or inconvenient to change. This is why control of particle transport in small devices sometimes requires introducing auxiliary signals, auxiliary particle species (Sec. V.C), or even the use of a feedback control scheme to optimize the Brownian motor current (Craig *et al.*, 2008a,b; Feito and Cao, 2007, 2008; Son *et al.*, 2008).

1. Optimization

The most common definition of efficiency for a loaded Brownian motor is

$$\eta_0 = \langle \dot{x} \rangle A_0 / \langle P \rangle_{\text{in}}, \quad (33)$$

where $\langle \dot{x} \rangle A_0$ is the average mechanical work done per unit of time against a working load A_0 and $\langle P \rangle_{\text{in}}$ is the average net power pumped into the system by the external drives, no matter how applied. The quantity η_0 has been interpreted in terms of macroscopic thermodynamics by Sekimoto (1998) (for further developments on issues of energetics and efficiency see also Parrondo and de Cisneros (2002)), and references therein. In their scheme, a ratchet operates like a Carnot cycle, where the lower temperature is determined by the thermal noise, Eqs. (2 and 4), and the higher temperature is related to the magnitude of the external modulation. Operating far from thermal equilibrium, the efficiency is typically smaller than the upper limit of a thermal reversibly operating Carnot cycle.

The ensuing question, whether a ratchet can be operated at the maximal Carnot efficiency, spurred an intense debate (see for a review, Sec. 6.9 in Reimann (2002)). The issue has been clarified by an analysis performed within the validity regime of the framework of linear irreversible thermodynamics by den Broeck (2007): The key

towards obtaining maximal Carnot efficiency for a Brownian motor is zero overall entropy production. This can be achieved by use of architectural constraints for which the (linear) Onsager matrix has a determinant equal to zero, implying vanishing (linear) irreversible heat fluxes. Maximizing efficiency subject to “maximum power” also leads to the same condition of a vanishing determinant of the Onsager matrix (i.e perfect coupling) (den Broeck, 2005), yielding the Curzon-Ahlborn limit (Curzon and Ahlborn, 1975), which in turn at small temperature difference just yields half the Carnot efficiency. For the archetype Smoluchowski-Feynman Brownian motor device (Feynman *et al.*, 1963; Smoluchowski, 1912) the efficiency at maximum power has recently been evaluated for different coupling schemes by Tu (2008): Interestingly enough, the typical upper bound set by Curzon and Ahlborn (1975) can then even be surpassed.

In spite of the combined efforts of theorists and experimenters, as of today the question remains unanswered. At present, ratchet devices operating under controllable experimental conditions hardly achieve an efficiency η_0 larger than a few percent.

On the other hand, definition (33) of efficiency is not always adequate to determine the optimal performance of a Brownian motor. Firstly, η_0 assumes that work is being done against a load A_0 , which is not always the case. For example, one clearly finds a vanishing efficiency whenever no load A_0 is present. Secondly, the only transport quantifier used in Eq. (33) is the drift velocity $\langle v \rangle$, whereas the fluctuations of $\dot{x}(t) = v(t)$, i.e., the variance $\sigma_v^2 = \langle v^2 \rangle - \langle v \rangle^2$, are also of practical importance. Note that in this Section we use $v(t)$ to denote the particle velocity in Eq. (6) as a proper stochastic process. If $\sigma_v > \langle v \rangle$, and even more so if $\sigma_v \gg \langle v \rangle$, the Brownian motor can possibly move for some time against its drift direction $\langle v \rangle$.

A load-independent rectification efficiency, η_r , has been introduced by Suzuki and Munakata (2003) and then generalized by Machura *et al.* (2004b). They computed η_r as the ratio of the dissipated power associated with the directed motion of the motor against both the friction and the load, and the input power from the time-periodic forcing. The result assumes the explicit form

$$\eta_r = \frac{\langle v \rangle (A_0 + \langle v \rangle)}{|\langle v^2 \rangle + \langle v \rangle A_0 - D_0|}, \quad (34)$$

where D_0 is the free diffusion coefficient of Sec. II.A.3. This definition holds evidently also for $A_0 = 0$, while numerical evidence indicates that $\langle v^2 \rangle \geq D_0$, consistently with the inequality $\eta_r \leq 1$. Note that the definition (34) assumes that $x(t)$ is a damped process with finite γ (no matter how large). In this way η_r accounts explicitly also for the power dissipated as velocity fluctuations during the rectification process; in particular, it increases upon decreasing σ_v . Machura *et al.* (2004b) noticed that, for a rocked ratchet, σ_v exhibits pronounced peaks in correspondence with the rectification thresholds $F_{3R,L}$ (large damping) and $F_{2R,L}$ (low damping), where the diffusion

coefficient also has a maximum (Sec. II.A.3). That lead to the general conclusion that transport by a Brownian motor can be optimized by operating away from activation thresholds, in regimes of large net currents, where the velocity fluctuations are intrinsically small.

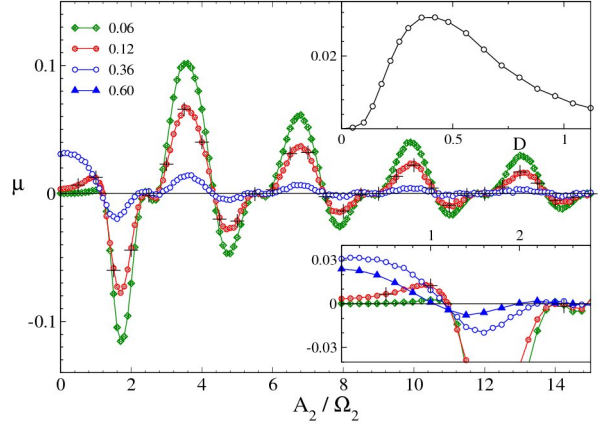


FIG. 10 (Color online) Mobility versus A_2/Ω_2 for a vibrated ratchet with $A_1 = 0.5$, $\Omega_1 = 0.01$, $\phi_1 = \phi_2 = 0$, and different values of the noise intensity D (see legend, main panel). All simulation data have been obtained for $\Omega_2 = 10$, but the black crosses where we set $D = 0.12$ and $\Omega_2 = 20$. Bottom inset: simulation data for μ as in the main panel with an additional curve at $D = 0.6$. Top inset: μ versus D for $A_2 = 0$, $A_1 = 0.5$, and $\Omega_1 = 0.01$; circles: simulation data; solid curve: adiabatic formula (11.44) in (Risken, 1984). After Borromeo and Marchesoni (2005a).

2. Vibrated ratchets

Besides the remarkable exceptions presented in Sec. IV, transport control in a rocked ratchet cannot be obtained experimentally by deforming the substrate potential “on demand”. As shown by Borromeo and Marchesoni (2005a), this goal can more easily be achieved by means of an external tunable signal. Let $V(x)$ be assigned a fixed profile, say, the standard double-sine in Eq. (23). The ratchet current can be still varied by injecting an additional control signal with frequency Ω_2 , that is, by replacing the harmonic drive in Eq. (8) with the bi-harmonic drive in Eq. (16); in the adiabatic regime $\Omega_2 \gg \Omega_1$ the system response is very different than in Sec. II.D.4. A rocked ratchet operated under such conditions is termed *vibrational ratchet*.

Following the perturbation approach of Baltanás *et al.* (2003); Bleckman (2000); Landa and McClintock (2000), the variable $x(t)$ in Eq. (3) can be separated as $x(t) \rightarrow x(t) + \psi(t)$: in the remainder of this Section $x(t)$ will represent a slowly time-modulated stochastic process and $\psi(t)$ the particle free spatial oscillation

$\psi(t) = \psi_0 \sin(\Omega_2 t + \phi_2)$, with $\psi_0 = A_2/\Omega_2$. On averaging out $\psi(t)$ over time, the Langevin equation for the slow reduced spatial variable $x(t)$ can be written as

$$\dot{x} = -\bar{V}'(x) + A_1 \cos(\Omega_1 t + \phi_1) + \xi(t), \quad (35)$$

where

$$\bar{V}(x) = -V_0 \left[J_0(\psi_0) \sin x + \frac{1}{4} J_0(2\psi_0) \sin 2x \right] \quad (36)$$

and $J_0(x)$ is the Bessel function of zero-th order. The symmetry of the effective vibrated potential (35) is restored if one of its Fourier components vanishes, namely for $A_2/\Omega_2 = \frac{1}{2}j_1, j_1, \frac{1}{2}j_2, \frac{1}{2}j_3, j_2, \frac{1}{2}j_4, \frac{1}{2}j_5, j_3, \dots$, where $j_1 = 2.405, j_2 = 5.520, j_3 = 8.654, j_4 = 11.79, j_5 = 14.93\dots$, are the ordered zeros of the function $J_0(x)$; correspondingly, the ratchet is expected to vanish, as confirmed by the simulation data displayed in Fig. 10.

Not all zeros of this sequence mark an inversion of the ratchet current. For instance, for $A_2/\Omega_2 < \frac{1}{2}j_1$ the current is oriented in the natural direction of the effective potential, Eq. (36); for $\frac{1}{2}j_1 < A_2/\Omega_2 < j_1$, the coefficient of $\sin 2x$ changes sign and so does the ratchet natural orientation, or polarity; on further increasing A_2/Ω_2 larger than j_1 , the sign of both Fourier coefficients in Eq. (36) become reversed: this is equivalent to turning $V(x)$ upside-down (beside slightly re-modulating its profile), so that the polarity of $\bar{V}(x)$ stays negative. Following this line of reasoning one predicts *double* zeros (i.e. no current inversions) at $\psi_0 = j_1, j_2, j_3, j_4, \dots$

This control technique can be easily applied to the transport of massive Brownian particles both in symmetric (Borromeo and Marchesoni, 2007a) – see inset of Fig. 10 – and asymmetric devices (Borromeo and Marchesoni, 2006). Likewise, the use of a delay in a feedback control signal (Craig *et al.*, 2008a,b; Feito and Cao, 2007, 2008; Son *et al.*, 2008) can, via synchronization mechanisms, efficiently improve the performance of Brownian motor currents; a scheme that as well can be implemented readily in experimental flashing ratchets (Craig *et al.*, 2008a).

III. TRANSPORT IN NANOPORES

Membranes in biology encase cells and their organelles and allow the compartmentalization of cellular processes, thereby operating far from thermal equilibrium, a condition that is essential to life. Membranes separate two phases by creating an active or passive barrier to the transport of matter between them. As a first classification, membranes can be divided into biological and artificial membranes. The latter term is applied to all membranes made by man with natural, possibly modified, materials and with synthetic materials (synthetic membranes). Synthetic membranes can be further divided into organic (made with polymers) and inorganic membranes (made with alumina, metals, etc.).

Transport across a membrane occurs through channels, or pores (Berezhkovskii *et al.*, 2003; Kolomeisky, 2007).

In several cases, the membrane transport properties must be regarded as a collective effect, where the function of an individual channel is influenced by the presence of (possibly diverse) neighboring channels. This is the case, for instance, of ion pumps (Im and Roux, 2002; Läuger, 1991) in cellular membranes (Sec. III.A) or for coupled ion channels which experience a common transmembrane voltage. Single molecule techniques, however, allow for the study and characterization of rectification properties of individual entities, such as single ion channels. Nowadays, synthetic membranes with assigned pore density and patterns are made commercially available. Moreover, by means of increasing sophisticated growth methods, irradiation (Fleischer *et al.*, 1975), and nanofabrication techniques (Dekker, 2007; Healy *et al.*, 2007; Li *et al.*, 2001; Storm *et al.*, 2003), the cross section of membrane pores can be modulated along their axis. As a result, transport in artificial ion channels fabricated from asymmetric single pores of the most diverse geometries has become accessible to experiments (Healy *et al.*, 2007; Siwy and Fuliński, 2004), see also in Sec. III.B.

In this Section we focus on devices where the size of the transported particles is comparable to the pore cross section. Transport in these devices can be analyzed in terms of the one-particle 1D mechanisms illustrated in Sec. II. Larger pores, commonly used to channel fluids (liquid or gaseous) or colloidal particles suspended in a fluid, are considered in Sec. VI in the context of microfluidic devices.

A. Ion pumps

As remarked already before, biology teaches us useful lessons that can guide us in the design of artificial Brownian motors. Biological membranes knowingly form lipophilic barriers and have embedded a diverse range of units which facilitate the selective movement of various ionic and polar segments, or the pumping of protons and electrons across channel like membrane openings. These biological nanodevices make typically use of electrochemical gradients that enable them to pump a species against its concentration gradient at the expense of yet another gradient. Such devices thereby convert nondirectional chemical energy, from the resource of the hydrolysis of adenosintriphosphate (ATP), into directed transport of charged species against electrochemical gradients.

Although many details of the underlying mechanism are far from being understood, these machines apparently make use of mechanisms that characterize the physics of Brownian motors (Astumian, 2007). A characteristic feature is that changes in the binding affinity at selective sites in the transmembrane region must be coupled to conformational changes which, in turn, control motion into the desired direction. Thus, in contrast to rocked or pulsated ratchets, where the particle-potential interaction acts globally along the whole periodic substrate landscape, the transport mechanism at work here can be

better described as an “information” ratchet (Astumian and Derényi, 1998; Parrondo and de Cisneros, 2002). Indeed, the effective potential bottlenecks to transduction of Brownian motion get modified locally according to the actual location of the transported unit; as a result, information gets transferred from the unit to the potential landscape. For example, this scheme can be used to model the pumping of Ca^{++} ions in Ca^{++} -ATPase (Xu *et al.*, 2002). Related schemes have been invoked also in the theoretical and experimental demonstration of pumping of Na^{+} - and K^{+} -ions via pulsed electric field fluctuations in Na- and K-ATPase (Freund and Schimansky-Geier, 1999; Tsong, 2002; Xie *et al.*, 1994), or for the operation of a catalytic wheel with help of a ratchet-like, electro-conformational coupling model (Rozenbaum *et al.*, 2004).

Yet another mechanism can be utilized to pump electrons in biomolecules. It involves nonadiabatic electron tunneling in combination with asymmetric, but non-biased, nonequilibrium fluctuations, as proposed by Goychuk (2006). The nonequilibrium fluctuations originate from either random binding of negatively charged ATP or externally applied asymmetric, but non-biased, electric stochastic fields. Likewise, unbiased nonequilibrium two-state fluctuations (telegraphic noise) can induce directional motion across an asymmetric biological nanopore, as numerically investigated for an aquaglyceroporin channel, where water and glycerol get transported by means of a rocked ratchet mechanism (Kosztin and Schulten, 2004).

Finally, we stress that in such realistic complex biological channels the physical implications of an externally applied control are often difficult to predict. This is due to the multi-facetted consequences any control action may have in terms of chemical variations, conformational changes, polarization effects, and the alike. Moreover, at variance with single-molecule type experiments, single channel recordings are not easily accessible when dealing with biological molecules. Nanopores of lesser complexity are thus synthetic nanopores which can be fabricated by use of bottom-down nanoscience techniques – the theme we review next.

B. Artificial nanopores

With the recent advances of track-etching (Fleischer *et al.*, 1975) and silicon technologies (Dekker, 2007; Li *et al.*, 2001; Storm *et al.*, 2003), charge transport in a single nanopore became experimentally accessible. This is a substantial leap forward with respect to ion pump and zeolite transport experiments, where experimental data are taken over a relatively high channel density. Fabricated nanopores in polymer films and silicon materials are being investigated in view of their potential applications as biomimetic systems, that is, for modeling biological channels, and as biosensors.

Siwy and coworkers (Constantin and Siwy, 2007; Siwy

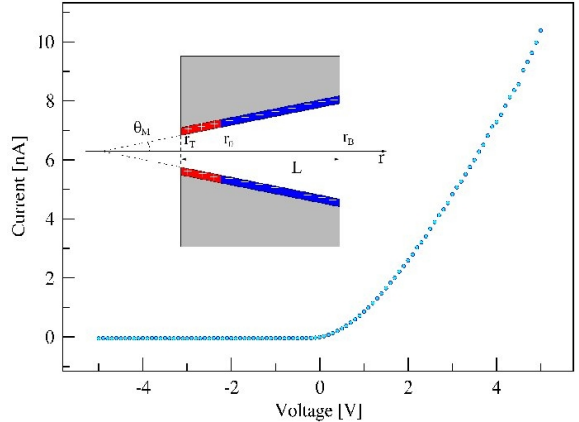


FIG. 11 (Color online) Ion current recorded experimentally by Constantin and Siwy (2007) at 0.1M KCl, $\text{pH} = 5.5$ through a single conical nanopore with diameters were 5 nm and 1000 nm, respectively. The pore rectification power is $\eta = 217$ at 5V. Inset: geometry of a conical nanopore with schematic representation of surface charge distribution creating a bipolar nanofluidic diode. Figure provided by Zuzanna Siwy.

et al., 2005; Siwy and Fuliński, 2002; Vlassiouk and Siwy, 2007) have recently prepared a nanofluidic diode, which had been predicted to rectify ion current in a similar way as a bipolar semiconductor diode rectifies electron current (Daigiji *et al.*, 2005). This diode is based on a *single* conically shaped nanopore track-etched in a polymer film with openings of several nm and 1 μm , respectively (see sketch in Fig. 11). The surface charge of the pore is patterned so that two regions of the pore with positive and negative surface charges create a sharp barrier called the transition zone. This nanofluidic diode is bipolar in character since both positively and negatively charged ions contribute to the measured current. Majumdar and coworkers (Karnik *et al.*, 2007) fabricated a similar nanofluidic diode with a sharp barrier between a positively charged and a neutral side of the pore. The presence of only one type of surface charge causes the latter device to be unipolar.

Ion rectification was achieved by applying a longitudinal ac voltage (Fig. 11); the system thus operate as a one-cell 1D rocked ratchet (Sec. II.D.1), where the spatial asymmetry is determined by the interaction of a single ion with the inhomogeneous charge distribution on the pore walls. The rectification power of the pore is defined as the ratio of the ionic currents recorded for positive and negative driving voltages, i.e., $\eta(V) = |I(V)|/|I(-V)|$. Of course, due to their asymmetric geometry, conical pores can rectify diffusing ions also for uniform wall-charge distributions (Siwy *et al.*, 2005); however, the corresponding η factor would be at least one order of magnitude smaller than reported here.

As a serious limitation of the present design, it is not possible to control the rectification power of a given conical nanopore without introducing changes to its built-in

electro-chemical potential. An alternate approach has been proposed by Kalman *et al.* (2007), where two superposed rectangular voltage signals of zero mean were used to control the net ion current through a nanopore of preassigned geometry. By changing the amplitude, frequency and relative phase of these signals these authors used the gating effect of Sec. II.C.2 to gain control over the orientation and the magnitude of ion flow through the pore. Their experimental data were found in excellent agreement with the theoretical prediction of Eq. (32). The magnitude of ion current variation achieved by asymmetric signal mixing was comparable with the incommensurate current off-set Eq. (30), which means that the nanopore diode could be operated disregarding the details of its intrinsic rectification power.

We conclude this Section on artificial nanopores anticipating that asymmetric micropores etched in silicon membranes also work as microfluidic ratchet pumps for suspended colloidal particles (Kettner *et al.*, 2000; Matthias and Müller, 2003). For instance, entropic effects on the rectification efficiency of the conical nanopores of Siwy and coworkers have been analyzed by Kosinska *et al.* (2008). However, in-pore diffusion in a liquid suspension requires a fully 3D analysis of the pumping mechanism, which sets the basis for the fabrication of more complicated ionic devices (van der Heyden *et al.*, 2004; Stein *et al.*, 2004). This category of devices is reviewed in Sec. VI.

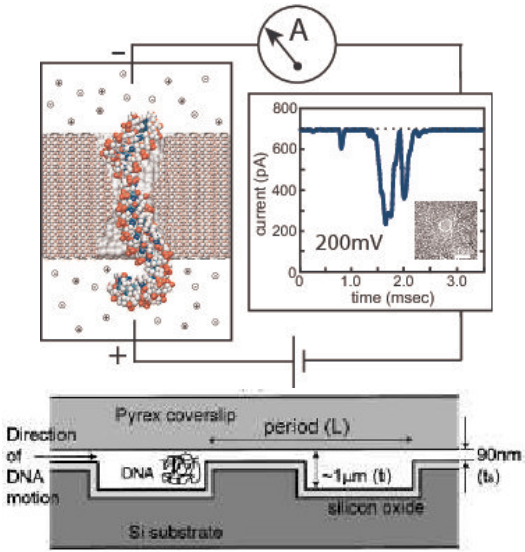


FIG. 12 (a) (Color online) Electric detection of individual DNA molecules with a nanopore. A constant voltage bias induces a steady-state ionic current through a single nanopore (left panel, from simulation); adding DNA to the negatively biased compartment causes transient reductions of the ionic current (right panel, from experiment). This reduced conductance is associated with the translocation of DNA through the pore, which partially blocks the ionic current. After Aksimentiev *et al.* (2004). (b) Schematic diagram of the entropic trap in Han *et al.* (1999).

C. Chain translocation

The opposite limit of composite objects passing through a much narrower opening is often called “translocation”. Using the experimental set-up sketched in Fig. 12(a), Kasianowicz *et al.* (1996) measured, for the first time, the blockage currents of single-stranded RNA and DNA electrophoretically driven through the a transmembrane pore. Recent developments of this technique demonstrated single nucleotide resolution for DNA hairpins (Ashkenasy *et al.*, 2005; Gerland *et al.*, 2004; Vercoutere *et al.*, 2003), thus raising the prospect of creating nanopore sensors capable of reading the nucleotide sequence directly from a DNA or RNA strand, see for recent comprehensive reviews (Healy, 2007; Movileanu, 2008; Zwolak and Di Ventra, 2008). Nowadays, translocation mechanisms are investigated in both protein channels (mainly the bacterial α -hemolysin pore (Kasianowicz *et al.*, 1996)) and synthetic pores. Both these approaches have advantages and disadvantages (Dekker, 2007; Healy, 2007). Protein channels can be engineered with almost angstrom precision, but the lipid membrane in which they may be incorporated is very mechanically unstable. Synthetic pores, on the other hand, offer robustness to the system, which allows to better characterize the physical aspects of translocation phenomena.

As a main difference with ion transport, the translocation of a long polymer molecule in a 1D device involves entropic effects, which become important when the opening cross section grows comparable with the radius of gyration, R_0 , of the polymer. These effects were predicted in (Arvanitidou and Hoagland, 1991) to account for the conformation changes a chain undergoes to move past a conduit constriction and, finally, observed by Han and Craighead (2000); Han *et al.* (1999) in an artificial channel. As a model pore-constriction system, these authors fabricated a channel consisting in a periodic sequence of regions of two different depths, as shown in Fig. 12(b). The thick regions were 1mm deep, i.e., comparable with the R_0 of the double stranded DNA molecules they used in their experiment, whereas the depth of the thin region, 90nm, was much smaller than R_0 .

The thick regions act like “entropic traps”, as the DNA molecules are entropically prevented from entering the thin regions. For the same reason, a chain caught in between two traps, tends to fall back into the trap that contains the most of it. In the presence of an external electric field, escape from a trap is initiated by the introduction of a small portion of DNA into an adjacent thin region, just enough to overcome the escaping activation barrier. This initiation process is local in nature, and the energy barrier does not depend on the total length of the trapped DNA molecule. Once a DNA molecule is in the transition state (once a proper length of “beachhead” is formed), it readily escapes the entropic trap, regardless of the length of the remaining molecule in the trap. Quite counter intuitively, Han and coworkers found that escape of DNA in longer entropic traps occurs faster than

in shorter ones.

A theoretical interpretation of these results was given by Park and Sung (1999), who treated the dynamics of a flexible polymer surmounting a 1D potential barrier as a multidimensional Kramers activation process (Hänggi *et al.*, 1990). To determine the activation free energy, Park and Sung computed the free energy of the polymer at the transition state. For a small-curvature barrier, the polymer keeps its random coil conformation during the whole translocation process, giving rise to essentially the same dynamics as that of a Brownian particle. For a large-curvature barrier, on the other hand, a conformational transition (coilstretch transition) occurs at the onset of the barrier crossing, which significantly lowers the activation free energy and so enhances the barrier crossing rate. As the chain length varies, the rate shows a minimum at a certain chain length due to the competition between the potential barrier and the free energy decrease by chain stretching. Synthetic nanopores can thus be used as Coulter counter devices to selectively detect single DNA molecules, resolving their length and diameter.

Spatial asymmetry can rectify translocation through synthetic and biological pores, alike. This is the case, for instance, of a hydrophobic polymer translocating across a curved bilayer membrane. Extensive simulation (Baumgärtner and Skolnick, 1995) showed that the polymer crosses spontaneously and almost irreversibly from the side of lower curvature to the side of higher curvature, so as to maximize its conformational entropy (“entropy” ratchets, Sec. V.A.1). Moreover, at variance with artificial channels, in protein translocation through a biomembrane, the chemical structure of the pores can come into play by helping rectify the thermal fluctuations of the stretched molecule: When specific predetermined segments of the protein cross the membrane, chemicals acting as chaperons bind on the segments to prevent their backward diffusion (Hartl, 1996; Jülicher *et al.*, 1997; Nigg, 1997). The ensuing chemical asymmetry then competes with the entropic asymmetry to determine the translocation current.

D. Toward a next generation of mass rectifiers

1. Zeolites

Zeolites are three dimensional, nanoporous, crystalline solids (either natural or synthetic) with well-defined structures that contain aluminum, silicon, and oxygen in their regular framework. The silicon and aluminum atoms are tetrahedrally connected to each other through shared oxygen atoms; this defines a regular framework of voids and channels of discrete size, which is accessible through nanopores of well-defined molecular dimensions. The negative electric charge of the zeolite framework is compensated by (inorganic or even organic) cations or by protons (in the acidic form of the zeolites). The ions

are not a part of the zeolite framework, and they stand in the channels. The combination of many properties – such as the uniform cross section of their pores, the ion exchange properties, the ability to develop internal acidity, high thermal stability, high internal surface area – makes zeolites unique among inorganic oxides and also leads to unique activity and selectivity. As a result, zeolites can separate molecules based on size, shape, polarity, and degree of unsaturation among others (Kärger, 2008b; Kärger and Ruthven, 1992).

Nuclear magnetic resonance (NMR) provides direct access to the density and the mobility of molecules in zeolites. By implementing a time-dependent NMR technique, termed pulsed field gradient NMR, Kärger and coworkers (see for a review Kärger (2008a)) investigated the problem of particle diffusion in a narrow zeolite nanopore. For instance, they observed that, owing to the constrained pore geometry (0.73 nm across), the mean square displacement of CF_4 molecules (0.47 nm in diameter) diffusing in zeolite $\text{AlPO}_4\text{-5}$, increases linearly with the square root of the observation time rather than with the observation time itself. That was an early experimental demonstration of the single-file diffusion mechanism introduced in Sec. II.A.4. In the meantime, however, real zeolite crystals have been repeatedly found to deviate notably from their ideal textbook structure (Schemmert *et al.*, 1999), so that, their pore cross-sections ought to be regarded as longitudinally corrugated. To what extent this may affect particle diffusion is still matter of ongoing research (Kärger *et al.*, 2005; Taloni and Marchesoni, 2006).

Most zeolite structure types exhibit 3D pore networks. The most studied example are synthetic zeolites of type MFI. Their pore network is formed by mutually intersecting straight (in crystallographic y -direction) and sinusoidal (in crystallographic x -direction) channels. Although there is no corresponding third channel system, molecular propagation has been observed also in z -direction. Experimental data are consistent with a simple law of *correlated* diffusion anisotropy (Fenzke and Kärger, 1993), $a_z^2/D_z = a_x^2/D_x + a_y^2/D_y$, where a_i and D_i , with $i = x, y, z$, denote respectively the lattice and the diffusion constants in the i -direction. This means that the molecular “memory” is shorter than the mean traveling time between two adjacent network intersections.

With the advent of synthetic zeolites and zeolitic membranes, researchers are fascinated by the option that the existence of different channel types within one and the same material may be used for an enhancement of the performance of catalytic chemical reactions. As the diffusion streams of the reactant and product molecules tend to interfere with each other, rerouting them through different channels may notably speed up a catalytic reactor; hence, the idea of reactivity enhancement by “molecular traffic control” (Derouane and Gabelica, 1980; Neugebauer *et al.*, 2000).

2. Nanotubes

Another interesting category of artificial nanopore are carbon nanotubes (Dresselhaus *et al.*, 1996). Single-walled carbon nanotubes are cylindrical molecules of about 1 nm in diameter and 1-100 μm in length. They consist of carbon atoms only, and can essentially be thought of as a layer of graphite rolled-up into a cylinder. Multiple layers of graphite rolled in on themselves are said to form a multi-wall carbon nanotube. The electronic properties of nanotubes depend strongly on the tube diameter as well as on the helicity of the hexagonal carbon lattice along the tube (chirality). For example, a slight change in the pitch of the helicity can transform the tube from a metal into a large-gap semiconductor, hence they potential use as quantum wires in nanocircuits (Collins and Avouris, 2000; Dekker, 1999). An even wider range of geometries and applications became available recently with the synthesis of various oxide nanotubes (R  mskar, 2004). With their hollow cores and large aspect ratios, nanotubes are excellent conduits for nanoscale amounts of material. Depending on the filling material, experimenters have thus realized nanoscale magnets, hydrogen accumulators, thermometers and switches.

Nanotubes also provide an artificial substrate for controllable, reversible atomic scale mass transport. Regan *et al.* (2004) attached indium nanocrystals to a multi-wall carbon nanotube and placed it between electrodes set up in the sample chamber of an electron microscope. Applying a voltage to the tubes, they observed that the metallic particles at one end of the tube gradually disappeared, while those at the other end grew. While the details of the underlying driving mechanisms (thermo- versus electro-migration) remain unclear, they concluded that the voltage dictates the directionality of that nanoscale mass conveyor. Experimenters even succeeded to synthesize carbon nanotubes encapsulating metallic atoms and characterize the electro-mechanical properties of such nanochannels (see e.g., Gao and Bando (2002)). In the next future, carbon nanotubes will also be combined to form molecular “gears”, whose feasibility has been proven so far only by simulation (Drexler, 1992). A conceptual example is provided by a double-walled carbon nanotube consisting of two coaxial single-walled nanotubes with different chirality, immersed in an isothermal bath. In the presence of a varying axial electrical voltage, this system would exhibit a unidirectional ratchet-like rotation as a function of the chirality difference between its constituents (Marchesoni, 1996).

Nanotubes have also been used to realize prototypes of thermal diodes for phonon transport (Chang *et al.*, 2006). With this concept in mind, one can further devise a phonon Brownian motor aimed to ratchet a net heat flux from “cold to hot”, as numerically demonstrated in a recent work by Li *et al.* (2008). This class of devices has the potential to allow an efficient control of heat fluxes at the nanoscales.

In spite of the recent advances in nanotechnology, (inner or outer) transport along nanotubes is still controlled by external gradients. Nevertheless, nanotube based ratchets, though not immediately available, are like to be one of the next frontiers in artificial Brownian motor research. Moreover, synthetic nanotubes are potential building blocks also for nanofluidic devices (Holt *et al.*, 2006), as discussed in Sec. VI.

IV. COLD ATOMS IN OPTICAL LATTICES

Optical lattices are periodic potential for atoms created by the interference of two or more laser fields (Grynberg and Robilliard, 2001; Jessen and Deutsch, 1996). In near resonant optical lattices the laser fields produce simultaneously a periodic potential for the atoms and a cooling mechanism. The optical potential for an atom in an optical lattice is given by the light shift, or ac Stark shift, of the atomic energy level that acts as the ground state of an assigned optical transition. The simplest case is represented by the $J_g = 1/2 \rightarrow J_e = 3/2$ atomic transition in a 1D configuration.

Let us consider two counter-propagating laser fields, detuned below the atomic resonance, with orthogonal linear polarizations and same intensity and wavelength λ . Their interference results into a spatial gradient with polarization ellipticity of period $\lambda/2$. This in turn produces a periodic potential for the atom. For instance, the atomic hyperfine ground states $|g, \pm\rangle = |J_g = 1/2, M = \pm 1/2\rangle$ experience periodic potentials in phase opposition along the direction x of light propagation, namely

$$V_{\pm}(x) = \frac{V_0}{2}(-2 \pm \cos kx), \quad (37)$$

where $k = 2\pi/\lambda$ and the depth of the potential wells V_0 scales as I_L/Δ , with I_L the total laser intensity and Δ the detuning from atomic resonance. As the laser fields are near to resonance with the atomic transition $J_g = 1/2 \rightarrow J_e = 3/2$, the interaction with the light fields also leads to stochastic transitions between the Zeeman sublevels $|g, \pm\rangle$ of the ground state. The rate of this transitions can be quantified by the photon-atom scattering rate Γ' which scales as I_L/Δ^2 . It is therefore possible to vary independently the optical lattice depth V_0 and Γ' by changing simultaneously I_L and Δ .

The stochastic transitions between ground states also lead to damping and fluctuations. The damping mechanism, named Sisyphus cooling, originates from the combined action of light shifts and optical pumping which transfers, through cycles of absorption/spontaneous emission involving the excited state J_e , atoms from one ground state sublevel to the other one. Moreover, the stochastic transitions between the two potentials $V_{\pm}(x)$ also generate fluctuations of the instantaneous force experienced by the atom. In conclusion, the equilibrium between cooling and heating mechanisms determines a stationary diffusive dynamics of the atoms, a process confined to the symmetric ground-state optical lattice $V_{\pm}(x)$.

Random amplitude pulsations of one symmetric potential, Eq. (37), do not suffice to produce rectification. The only missing element to reproduce the rocked set-ups of Secs. II.C and II.D is the additive ac force $F(t)$. In order to generate a time-dependent homogeneous force, one of the lattice beams is phase modulated, and we will indicate by $\phi(t)$ its time-dependent phase. In the laboratory reference frame the phase modulation of one of the lattice beams results into the generation of a moving optical lattice $V_{\pm}(x - \phi(t)/2k)$, reminiscent of the periodic sieves in (Borromeo and Marchesoni, 2007a). In the accelerated reference frame $x \rightarrow x - \phi(t)/2k$, the optical potential would be stationary; however, an atom of mass m experiences also an inertial force in the z -direction proportional to the acceleration of the moving frame, namely $F(t) = (m/2k)\ddot{\phi}(t)$. This is the homogeneous ac drive needed to rock a cold atom ratchet.

The above described harmonic mixing/rocking ratchet set-up was recently used by Renzoni and coworkers (Gommers *et al.*, 2005, 2007, 2006, 2008; Schiavoni *et al.*, 2003) to investigate experimentally the relationship between symmetry and transport in 1D atom traps. We discuss here separately the experimental results for two different cases: (1) a bi-harmonic driving including two harmonics at frequencies Ω_0 and $2\Omega_0$, and (2) a multi-frequency driving obtained by combining signals at three different frequencies.

A. Bi-harmonic driving

These authors (Gommers *et al.*, 2005; Schiavoni *et al.*, 2003) generated a bi-harmonic drive, Eq. (16), with $\Omega_2 = 2\Omega_1$ and $\phi_1 = 0$, and searched for a harmonic mixing current proportional to $\sin(\phi_2 - \phi_0)$. At variance with Eq. 17, a phase lag ϕ_0 was introduced to account for the finite atom dissipation. Indeed, by generalizing our argument of Sec. II.C.1, one can easily prove that increasing the damping makes ϕ_0 drop from 0 down to $-\pi/2$. In the experiment, the atom dissipation could be tuned continuously, without changing the optical potential constant V_0 , by varying simultaneously I_L and Δ at a constant I_L/Δ ratio; thus, harmonic mixing was experimentally accessible in both limiting regimes of zero and infinite damping.

The experimental results of Fig. 13 for cesium atoms cooled in the μK range, clearly demonstrate the mechanism of harmonic mixing at work. In fact, the net atom velocity plotted in panel (a) is well fitted by $v/v_r = A_{\Delta} \sin(\phi_2 - \phi_0)$, where the dependence of ϕ_0 on Γ' is as in panel (b), and A_{Δ} is a characteristic function of the system (Gommers *et al.*, 2005). For the smallest scattering rate examined in the experiment, no current was generated at $\phi_2 = l\pi$, with l integer, as expected from Eq. (17). On the other hand, the magnitude of the phase shift ϕ_0 increases with increasing the scattering rate, thus causing current generation also for $\phi_2 = l\pi$. Besides confirming the notion of harmonic mixing, the experimental

results in Gommers *et al.* (2005); Schiavoni *et al.* (2003) also suggest that symmetry breaking can be controlled by dissipation. Closely related results have been reported by Ustinov *et al.* (2004) in their attempt to control fluxon ratcheting in Josephson junctions by means of harmonic mixing.

B. Multi-frequency driving

Recent experiments with multi-frequency driving (Gommers *et al.*, 2007, 2006) aimed to investigate the transition from periodic to quasi-periodic driving, and to examine how the analysis of Sec. II.C is modified in this transition. The multi-frequency driving was obtained by adding a sinusoidal component to the ac drive employed in the previous Section, i.e.,

$$F(t) = A_1 \cos(\Omega_1 t) + A_2 \cos(2\Omega_1 + \phi_2) + A_3 \cos(\Omega_3 t + \phi_3) \quad (38)$$

For Ω_3/Ω_1 irrational the driving is quasi-periodic. Clearly, in a real experiment Ω_3/Ω_1 is always a rational number, which can be written as p/q , with p, q two coprime positive integers. However, as the duration of the experiment is finite, by choosing p and q sufficiently large it is possible to obtain a driving which is effectively quasi-periodic on the time scale of the experiment.

Let us consider first the case of periodic driving, with Ω_3/Ω_1 rational. Adding a third harmonic with phase constant $\phi_3 \neq 0$ in Eq. (38) breaks the time symmetry of $F(t)$ so that directed transport is allowed also for $\phi_0 = 0$ and $\phi_2 = l\pi$. In other words, for $\phi_3 \neq 0$ the third driving component leads to an additional phase shift of the current as a function of ϕ_2 . As a result, the current will retain its sinusoidal phase dependence $\sin(\phi_2 - \phi_0)$, as above, with the difference that now ϕ_0 accounts for the phase shifts produced both by dissipation and by the added driving component. Following the discussion sketched in Sec. II.D.4, one easily concludes that in the quasi-periodic regime the third harmonic at frequency Ω_3 is not relevant to characterize the time symmetry of the forcing signal, which is entirely determined by the bi-harmonic terms at frequency Ω_1 and $2\Omega_2$.

In later experiments (Gommers *et al.*, 2007, 2006), the transition to quasi-periodicity was investigated by studying the atomic current as a function of ϕ_2 for different p/q . By increasing p and q the driving was made more and more quasi-periodic on the finite duration of the experiment, with the quantity pq an easily accessible measure of the degree of quasi-periodicity. The data for the average atomic current were fitted with the function $v/v_{\max} = \sin(\phi_2 - \phi_0)$ and the resulting value for ϕ_0 were plotted as a function of pq . For small values of pq , i.e., for periodic driving, the added component at frequency Ω_3 lead to a shift which strongly depends on the actual value of pq . For larger values of pq , i.e., approaching quasi-periodicity, the phase shift ϕ_0 tends to a constant value independent of ϕ_3 , which coincides with the purely

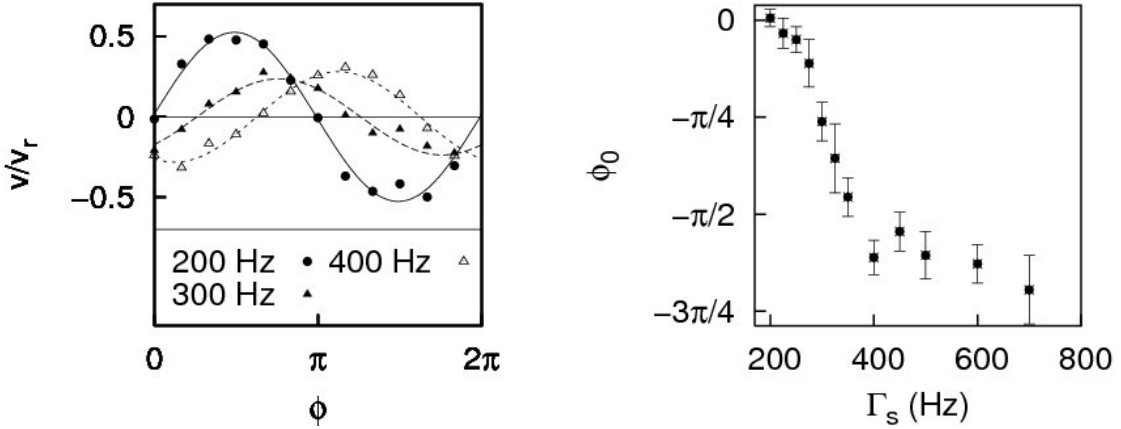


FIG. 13 Cold atoms in an optical lattice. (a) Average atomic velocity as a function of the phase ϕ_2 for different values of $\Gamma_s = [\omega_v/(2\pi)]^2/\Delta$ (a quantity proportional to the scattering rate Γ'). The data are labeled by the lattice detuning Δ , as the vibrational frequency at the bottom of the wells was kept constant, $\omega_v/2\pi = 170\text{kHz}$; the forcing frequency is $\Omega_1/2\pi = 100\text{kHz}$. The lines are the best fit of the data with the function $v/v_r = A_\Delta \sin(\phi - \phi_0)$, where $v_r = \hbar k/m$ is the so-called atom recoil velocity. (b) Experimental results for the phase shift ϕ_0 as a function of Γ_s . After Gommers *et al.* (2005).

dissipative phase-shift measured in the bi-harmonic driving case of Sec. IV.A. The experimental results confirm that in the quasi-periodic limit, the only relevant symmetries are those determined by the periodic bi-harmonic driving and by dissipation.

C. More cold atom devices

Cold atoms in optical traps proved to be a playground for rectification experiments.

(i) *Gating effect.* For instance Gommers *et al.* (2008) modified the experimental set-up described above, to demonstrate experimentally a gating ratchet with cold rubidium atoms in a driven near-resonant optical lattice. As suggested in Sec. II.C.2, a single-harmonic periodic modulation of the optical potential depth with frequency Ω_2 was applied, together with a single-harmonic rocking force with frequency Ω_1 . The modulation of the optical potential depth V_0 was obtained by modulating the intensity I_L of the laser beams. This also resulted in an unavoidable modulation of the optical pumping rate, which affected only the fitting phase shift ϕ_0 . Directed motion was observed for rational values of Ω_2/Ω_1 , a result due to the breaking of the symmetries of the system.

(ii) *Pulsated ratchets.* Although a *bona fide* rocked ratchet for cold atoms in an optical lattice has not been realized (see e.g. Ritt *et al.* (2006)), yet, a clever variation of 1D optical lattice described above allowed an early demonstration of randomly pulsated ratchet (Mennerat-Robilliard *et al.*, 1999). These authors set the polarizations of the laser beams at an angle $\theta \neq \pi/2$ and applied a weak Zeeman magnetic field orthogonal to the optical lattice. The effect of the magnetic field consisted in removing the degeneracy of the ground states by adding a $\lambda/2$ wavelength components to both potentials in Eq. (37), which thus acquired different asymmetric profiles. As a

consequence, the random optical transitions between the modified potentials $V_\pm(x)$ turned out to propel trapped cold rubidium atoms in the vertical direction, with the sign that depended on θ and on the orientation of the magnetic field.

In Sec. II.D.2 we reported that rectification can occur on symmetric 1D substrates that shift *instantaneously* back and forth in space with a fixed amplitude, namely, on substrate that are subjected to a time-discrete phase modulation (periodic or random, alike). In this case, breaking the supersymmetry condition (14) requires appropriate asymmetric space-dependent switching rates (Gorman *et al.*, 1996). Based on this rectification scheme, Sjölund *et al.* (2006) realized an simple flashing ratchet for cold atoms. It consisted again of a μK cold gas of cesium atoms switching between two symmetric ground state optical lattices, coupled via optical pumping. In the presence of induced friction, although small, and for appropriate laser detunings and intensities of the laser beams, the degeneracy of the ground states was removed by making one ground state, say V_+ , long lived and the other one, V_- , short lived. If we further consider that the two optical lattices were shifted one relative to the other, $V_-(x) = V_+(x - x_0)$, then we conclude that the switching rates between potentials were state *and* position dependent with $k_{- \rightarrow +}(x) \gg k_{+ \rightarrow -}(x)$. In this setup, the atoms execute stationary time-asymmetric sequences of random jumps between V_+ and V_- . During the time spent in the short-lived lattice V_- , they experience a potential with an incline that depends on x_0 . Thus, their diffusion is strongly enhanced in one specific direction, and correspondingly reduced in the opposite direction. In the experiment, the spatial shift x_0 and the transition rates between the two optical lattices could be adjusted at will. A directed motion with constant velocity was observed in the absence of additional forcing terms, i.e., for $F(t) = 0$, except for specific system parameters, where

symmetry was restored. Moreover, these authors showed that their device, when operated in 3D (Ellmann *et al.*, 2003), can generate directed motion in any direction.

V. COLLECTIVE TRANSPORT

The studies on rectification mechanisms reviewed in Sec. II, have been conducted mostly for a single particle; however, often systems contain many identical particles, and the collective interactions between them may significantly influence the transport of particle aggregates (Aghababaie *et al.*, 1999). For example, interactions among coupled Brownian motors can give rise to novel cooperative phenomena like anomalous hysteresis and zero-bias absolute negative resistance (Reimann *et al.*, 1999). The role of interactions among individual motors plays a particular important role for the occurrence of unidirectional transport in biological systems, e.g. see Sec. 9 in the review by Reimann (2002).

In this section we shall restrict ourselves to the properties of 1D and 2D systems of point-like interacting particles, although an extension to 3D systems is straightforward. Let the pair interaction potential $\mathcal{W}(r)$ be a function of the pair relative coordinates $\mathbf{r} = (x, y)$, characterized by an appropriate parameter g , quantifying the strength of the repelling ($g > 0$) or attracting force ($g < 0$), and by a constant λ , defining the pair interaction length. An appropriate choice of $\mathcal{W}(r)$, with $g > 0$, can be used to model hardcore particles with diameter λ (Savel'ev *et al.*, 2003, 2004b). We term the pair interaction long-range, if λ is larger than the average interparticle distance, and short-range in the opposite regime. In the absence of perturbations due to the substrate or the external drives, long-range repelling particles rearrange themselves to form a triangular Abrikosov (1957) lattice. When placed on a disordered substrate or forced through a constrained geometry, such an ideal lattice breaks up into lattice fragments punctuated by point-like defects and dislocations and separated by faulty boundaries. In the presence of a drive, such boundaries act like 1D easy-flow paths, or rivers, for the movable particles. This process, often referred to as “plastic” flow, is analyzed numerically in Reichhardt *et al.* (1998).

Rectification of interacting particles occurs as a combined effect of the configuration of the device and the geometry of its microscopic constituents. In this context the dimensionality of the underlying dynamics is also important: (1) Transport in some 2D geometries can often be reduced to the 1D mechanisms illustrated in Sec. II (reducible 2D geometries); (2) Under certain circumstances, however, a *bona-fide* 2D rectification may occur at a non-zero angle with the driving force (irreducible 2D geometries). Finally, we remark that particle interaction can be exploited to rectify particles of one species by acting on particles of another species, alone, either by an appropriate drive or a specially tailored substrate geometry.

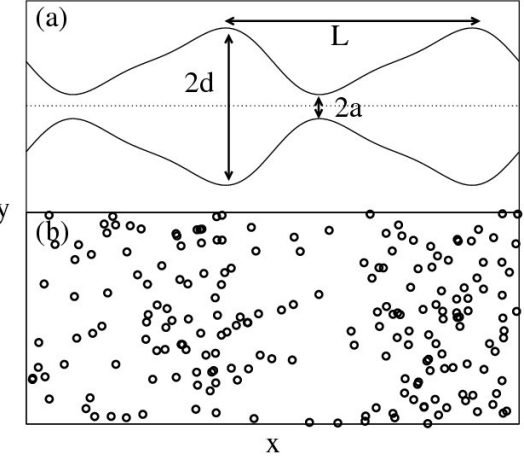


FIG. 14 1D reducible asymmetric geometries: (a) Channel with asymmetric profile $y(x) = y_0 - y_1[\sin(2\pi x/L) + \frac{1}{4}\sin(4\pi x/L)]$; the parameters y_1 and y_0 control the width $2d$ and the bottleneck $2a$; (b) Disordered pattern of circular defects generated with periodic distribution $y(x)$ along the x -axis

A. Asymmetric 1D geometries

We consider now two examples of 2D reducible geometries where the transport of massless repelling particles, subjected to an external ac drive, occurs as a collective effect, namely, under conditions incompatible with the rectification of a single particle. In particular, we show that collective effects make transport of interacting particles even in the absence of an *ad hoc* ratchet substrate.

1. Boundary effects

Let us consider the asymmetric channel sketched in Fig. 14(a) filled with n repelling particles per unit cell. The corresponding particle density is $\rho = n/a_l$, where a_l is the area of the channel unit cell. The walls are rigid and the particle-wall collisions are taken elastic and relatively short-range (interaction length not much larger than λ). The profiles $\pm y(x)$ of the upper (+) and lower (-) walls are modeled by an appropriate double-sine function; $2d$ and $2a$ denote, respectively, the width of the channel and of its bottlenecks. Due to the repulsive interactions, the particles are pressed against the walls which corresponds to an effective asymmetric spatial modulation. As a consequence, when driven by an ac force, the particles are more likely to flow to the left than to the right. The ensuing rectification mechanism is reminiscent of a 1D rocked ratchet with an inverted potential of Eq. (23). Numerical simulations, besides supporting this prediction, clearly indicate an optimal or resonant, temperature regime in which the particle drift is maximized. This observation can be explained by noticing that at low temperatures, the ac drive causes a moving particle to migrate to the

center of the channel where it no longer interacts with the boundaries; while at high temperatures the driving force becomes irrelevant and thus the particle is no longer pushed through the channel bottlenecks periodically in time. The first simulation evidence of this phenomenon was produced by Wambaugh *et al.* (1999). Their results obtained for the special case of magnetic vortex channeling are discussed in Sec. VII.A.

At high enough particle densities, ρ , the net current in the channel is expected to be suppressed, as the repelling particles end up clogging the bottlenecks and thus hampering collective longitudinal oscillations. In the opposite limit of, say, $n = 1$, the arguments above seem to rule out rectification, as a single oscillating particle would be confined in the inner channel of radius a . However, this conclusion holds only in the absence of thermal fluctuations, $T = 0$. At finite T , reducing the diffusion in a 2D channel to a 1D process implies defining an effective diffusion constant (II.A.3), $D(x)/D_0 = [1 + y'(x)^2]^{-1/3}$, equivalent to a periodic asymmetric modulation of the temperature (Reguera *et al.*, 2006) (a Seebeck ratchet in the notation of Reimann (2002)). A particle crossing a channel bottleneck perceives a lower effective temperature on the left, where the wall is steeper, than on the right, so that it gets sucked forwards; the opposite happens in correspondence to the largest channel cross-sections. As long as $\int dx/D(x) \neq 0$, the oscillating motion of a single particle can indeed be rectified, with the sign that depends on the details of the wall profile (Ai and Liu, 2006). No matter how weak, such a mechanism, termed “entropic” ratchet (Slater *et al.*, 1997), supports the conclusion of Wambaugh *et al.* (1999) that rectification in a channel occurs only at finite T , as a certain amount of noise is needed for the particle to explore the asymmetric geometric of the device. Moreover, the argument above hints at the occurrence of an optimal channel density ρ , as detected in real superconducting devices (Sec. VII.A).

2. Asymmetric patterns of symmetric traps

Olson *et al.* (2001) proposed a new type of 2D ratchet system which utilizes gradients of pointlike disorder, rather than a uniformly varying substrate potential. Let us consider a 2D sample containing a periodically graduated density of point defects, as sketched in Fig. 14(b). Each defect is depicted as a circular micro-hole, which acts as a *symmetric* short-range particle trap of finite depth. In real experiments, such defects can actually be created by either controlled irradiation techniques or direct-write electron-beam lithography (Kwok *et al.*, 2002). The defect density $\rho_l(x)$ was chosen to be uniform along the vertical axis, and to follow a typical double-sine asymmetric profile of Eq. (23) along the horizontal axis. Let us now inject into the sample repelling massless particles with average density ρ and interaction length λ . The defect radius controls particle pinning by defects and was taken much smaller than λ . For a sufficiently high

particle-to-defect density ratios, the particles fill most of the pinning sites and create an effective repulsive potential. If we further assume long-range particle pair interactions $\mathcal{W}(r)$, such a 2D potential surely gets insensitive to the details of the defect distribution; it only retains the periodic horizontal modulation of $\rho_l(x)$, thus resulting in a mean-field ratchet potential $V(x)$, like in Eq. (23). The effective amplitude V_0 is a function of at least three length scales: the interaction constant, the average particle distance and the average defect spacing. A certain fraction of the particles does not become pinned at individual defects but, subjected to an applied ac drive, can move in the interstitial regions between pinning sites. Although the moving interstitials do not directly interact with the short-ranged defects, they feel the long-range interaction of the particles trapped at the pinning sites and described by the mean-field potential $V(x)$. As a consequence, a horizontally applied ac drive can induce a longitudinal particle transport, as proven in Olson *et al.* (2001) by means of numerical simulation.

Two conditions are instrumental to the onset of a rectification current: (1) a finite temperature, $T > 0$, and (2) a defect filling fraction close to or larger than one, both conditions being required for interstitial particles to get and stay unpinned. As in Sec. V.A.1, condition (1) implies the existence of an optimal rectification temperature. The dependence on the forcing frequency and amplitude are as discussed in Sec. II.D.1. These ideas have been implemented to control transport of colloids and charge carriers in experimental setups where point defect gradients could be engineered at will (cf. Secs. VI.A, VII.B and VIII.C).

B. 2D lattices of asymmetric traps

Examples of substrates sustaining transverse rectification are asymmetric potential barriers, height $q > 0$, or wells, depth $q < 0$, either isolated or arranged into 1D chains and 2D lattices. Similar lateral displacement devices, also known as bumper arrays, have been proposed to separate particles by exploiting their mass and size dispersion (Heller and Bruus, 2008; Savel'ev *et al.*, 2005). Consider for instance the pyramidal potential barriers/wells with isosceles triangular cross-section. This geometry, sketched in Fig. 15, is a generalization of the experimental setup by Villegas *et al.* (2003).

The substrates discussed here combine two types of asymmetry: the triangular shape of their building blocks and the asymmetry associated with the pyramidal structure of each block. The latter asymmetry affects the motion of the particles only if the drive is strong enough to push them across the barriers/wells. Savel'ev *et al.* (2005) have numerically simulated the dynamics of a gas of *repelling* massive particles driven across 1D or 2D lattices of barriers/wells for different parameters of the substrate lattice (Fig. 15, bottom panel), of the drive $\mathbf{F}(t)$ and of the particle pair potential $\mathcal{W}(r)$. Although

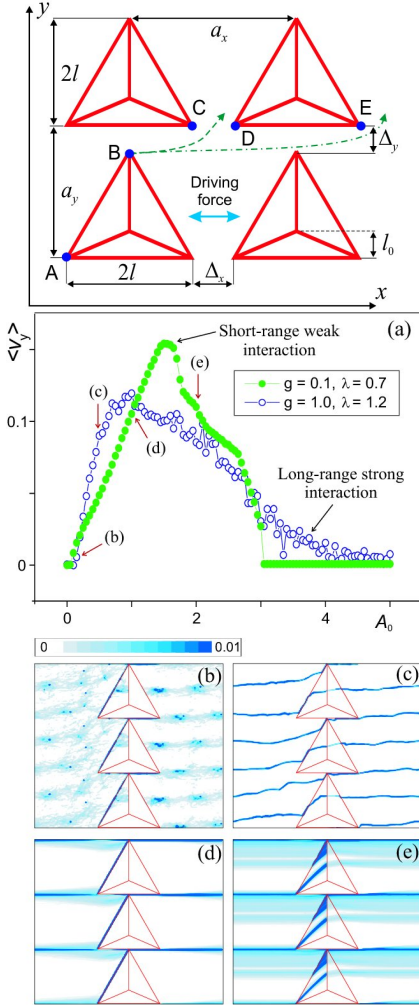


FIG. 15 (Color online) Top panel: asymmetric 2D arrays of potential energy barrier/wells, top view. The parameters l , l_0 , a_x , a_y , Δ_x , Δ_y define the geometry of the array. The dashed and dash-dotted arrows represent trajectories perturbed by thermal noise or particle-particle repulsion. Bottom panel: (a) Transverse net velocity $\langle v_y \rangle$ versus A_1 for *massless* interacting particles ac driven through a gapless triangular chain: $a_y = 2$, $a_x = 6$, $l = 1$, $\Delta_x = 4$, $\Delta_y = 0$, and $T = 0$. The repulsive potential $\mathcal{W}(r)$ is a wedge function with $g = 1$ and half-width $\lambda = 0.05$. Green solid circles are for weak short-range interacting particles, while blue open circles are for strong long-range interacting particles. Particle distributions for strong long-range (b,c) and weak short-range (d,e) interactions for the A_1 values indicated by arrows in (a). See for details Savel'ev *et al.* (2005).

Savel'ev *et al.* (2005) have shown that inertial effects often enhance transverse rectification, we restrict our presentation to the case of massless particles, certainly the most relevant for technological applications. We consider next two distinct operating regimes:

(i) *Deterministic* setups. An ac force applied along the y -axis, i.e., parallel to the symmetry axis of the pyramid cross-section, was known to induce a *longitudinal* particle

drift in the drive direction (see for more details in Zhu *et al.* (2004) and Sec. VII). Indeed, driving a (distorted) lattice of repelling particles along the crystallographic axis of the substrate, oriented parallel to the symmetry axis of the substrate blocks, makes the system reducible to a mean-field 1D dynamics in that direction, along the line of Sec. V.A. Due to the pyramidal shape of its building block, the reduced 1D substrate is spatially asymmetric, which explains the reported *longitudinal* particle flows.

(ii) *Diffusive* setups. Under appropriate conditions, instead, dc or ac forces applied perpendicularly to the symmetry axis may induce a *transverse* particle drift in the y -direction. For all geometries considered, the net velocity of a gas of non-interacting overdamped particles driven perpendicularly to the symmetry axis vanishes for $T \rightarrow 0$. Indeed, sooner or later each particle gets captured in a horizontal lane between two triangle rows and then keeps oscillating back and forth in it forever. At finite temperature, instead, fluctuations tend to push the particle out of its lane, thus inducing the net transverse currents reported in the earlier literature (Bier *et al.*, 2000; Duke and Austin, 1998; Huang *et al.*, 2004). More remarkably, Savel'ev *et al.* (2005) reported that the interaction among particles not only contributes to transverse rectification but actually plays a dominant role if the interaction length λ , or the particle density are large enough. In particular, particle-particle interaction was shown to control transverse rectification for both weak short-range and strong long-range inter-particle forces (see frame (a) of Fig. 15). Therefore, transverse rectification of interacting colloidal particles (short range) and magnetic vortices (long range) are expected to differ appreciably (see Secs. VI.A, and VII).

To illustrate the key mechanism of transverse rectification, we consider only rectification by pyramidal barriers, $q > 0$, subjected to the square ac force $F(t) = A_1 \text{sgn}[\cos(\Omega_1 t)]$. For a fully detailed analysis the reader is referred to Savel'ev *et al.* (2005). Let us consider first the geometry in frames (b)-(e) of Fig. 15 (bottom panel), where the pyramids are stacked up in a close row ($\Delta_y = 0$). The particle interactions have a strong impact on the equilibrium particle distribution; a transition from an ordered lattice-like to a disordered liquid-like phase is displayed in frames (b)-(e). Nevertheless, the transverse currents $\langle v_y \rangle$ show a qualitatively similar A_1 dependence for both weak short-range and strong long-range interactions; only the decaying tail is longer for the latter ones. The region of the linear growth of $\langle v_y \rangle$ for the case of weak short-range interaction corresponds to the regime when a constant fraction of particles (less than 1/2 because of the geometry of the system) is rectified into the y -direction. This regime applies for increasing A_1 until when particles start crossing over the triangles [frames (d) and (e)]. These results can be easily generalized to describe transverse rectification in any 2D lattice of triangular shaped barriers/wells.

Savel'ev *et al.* (2005) also simulated the case of a 2D

array of pyramids, top panel of Fig. 15, where a gap between triangles along the y -axis, $\Delta_y > 0$, turned out to make the net current sensitive to the particle-particle interaction length λ . In the limit of low T , if λ is smaller than a certain threshold value $\lambda^c \sim \Delta_y$, then the net current vanishes; if λ exceeds λ^c then the current rapidly increases. This effect has been advocated to separate particles according to their interaction length. More precisely, particles having an interaction length smaller than λ^c would pass through the array, or sieve of barriers separated by Δ_y . In contrast, particles with a longer interaction length $\lambda > \lambda^c$ would be sifted sidewise. On connecting several such sieves with different gap Δ_y , one can construct a device capable of separating the different fractions of a particle mixture.

The overall conclusions of Savel'ev *et al.* (2005) do not change on replacing barriers with wells of the same shape, nor do so for lattices of asymmetric pins of different aspect-ratio and geometries (Bier *et al.*, 2000; Chepelianskii and Shepelyansky, 2005; Duke and Austin, 1998; Ertas, 1998; Huang *et al.*, 2004; Zhu *et al.*, 2003a, 2004). This effect had been anticipated to some extent by Lorke *et al.* (1998), who investigated the magneto-transport properties of a square lattice of triangular antidots of the type shown in Fig. 15. Antidot lattices are 2D electron gases with appropriately placed sub-micron voids. These authors fabricated their lattices by electron beam lithography on shallow high electron mobility transistor structures, grown on semi-insulating gallium-arsenide substrates. In particular, they reported evidence that under far-infrared irradiation, electron sloshing in-between the antidot rows lead to a net electric current along the symmetry axis of the antidots. Significant transverse effects were observed in the presence of an orthogonal magnetic field. Moreover, in most applications to the electrophoresis of macromolecules, the particles moving through these sieve are suspended in the fluid where they diffuse, thus involving additional microfluidic effects (Sec. VI).

C. Binary mixtures

We address now the problem as how to induce and control the net transport of passive particles (target or A particles), namely, particles that are little sensitive to the applied drives and/or substrates. Savel'ev *et al.* (2003, 2004b) proposed to employ auxiliary B particles that (1) interact with the target species and (2) are easy to drive by means of external forces. By driving the auxiliary particles one can regulate the motion of otherwise passive particles through experimentally accessible means.

Savel'ev and coworkers considered a mixture of two species of pointlike overdamped Brownian particles A and B at temperature T , diffusing on the 1D periodic substrates described by the potentials $V_A(x)$ and $V_B(x)$, respectively. Particles of type A interact pair-wise with one another as well as with the B particles via the po-

tentials \mathcal{W}_{AA} and \mathcal{W}_{AB} ($= \mathcal{W}_{BA}$), while \mathcal{W}_{BB} describes the interaction of the B pairs. The pair interaction is quantified by the tunable strengths g_{ij} , with $i, j = A, B$, whereas the interaction constants λ_{ij} play no significant role as long as they are conveniently small.

To illustrate the rectification mechanisms in a binary mixture, we review in some detail the case of a pulsated device with oscillating temperature, i.e. a temperature ratchet studied originally by Reimann *et al.* (1996), see also Sec. II.D.2). The model can be made even simpler by assuming that (i) One subsystem (say, the auxiliary B particles) is subject to an asymmetric ratchet potential $V_B(x)$, while the other one (the target A particles) is not, $V_A(x) = 0$. This may happen, for instance, in a mixture of neutral and charged particles with the ratchet potential being produced by an electrical field; (ii) The interaction among particles of the same type is repulsive, i.e., $g_{AA} > 0$, $g_{BB} > 0$.

Under these operating conditions, the B particles condense naturally at the minima of the asymmetric substrate potential [see Figs. 16(a) and (b), bottom panels]. In addition, if the B particles repel the A particles, $g_{AB} > 0$, then the latter ones will accumulate in the regions where the density of the B particles is minimum, that is near the maxima of the substrate potential $V_B(x)$. Vice versa, for attractive AB interactions, $g_{AB} < 0$, the B particles concentrate around the minima of $V_B(x)$. Therefore, the target A particles feel an effective potential $V_A^{\text{eff}}(x)$, which has opposite spatial asymmetry with respect to $V_B^{\text{eff}}(x)$ for $g_{AB} > 0$, and has the same asymmetry for $g_{AB} < 0$ [see Figs. 16(a) and (b), top panels]. Note that for low occupation numbers n_A and n_B , the bare potential $V_B(x)$ is only marginally affected by particle interaction, i.e., $V_B^{\text{eff}}(x) \simeq V_B(x)$. During the lower T half cycle, all particles are confined tighter around the minima of the relevant effective potential, while, during the higher T half cycle, the particles of both species diffuse more easily out of the $V_A^{\text{eff}}(x)$, $V_B^{\text{eff}}(x)$ potential wells. As the asymmetry of the ratchet potentials $V_A^{\text{eff}}(x)$ and $V_B^{\text{eff}}(x)$ for repelling A and B particles is opposite, so is the orientation of their currents. On the contrary, two attracting A and B species drift in the same direction. This implies that the transport of both particle species can be effectively and separately controlled by regulating their number n_A and n_B per unit cell, without the need of tuning their substrate.

As $g_{AA}, g_{BB} > 0$, the potential wells of $V_A^{\text{eff}}(x)$ ($V_B^{\text{eff}}(x)$) tend to flatten out when increasing the corresponding density n_B (n_A). This results in the decay of the associated ratchet current $\langle v_B \rangle$ ($\langle v_A \rangle$). In contrast, the ratchet asymmetry and current of one species may be enhanced by increasing the density of the other mixture component. For instance, in the case of AB attractive forces, the A particles tend to concentrate in the regions of higher B densities, that is around the minima of V_B , thus attracting even more B particles and making the $V_B^{\text{eff}}(x)$ potential wells deeper. In short, one can enhance the transport of the target particles by adding a

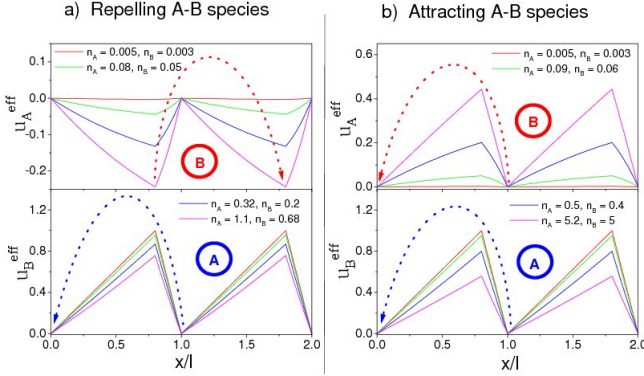


FIG. 16 (Color online) Spatial dependence of the effective potentials $V_A^{\text{eff}}(x), V_B^{\text{eff}}(x)$ at different densities of the A and B particles. In both panels, particles of the same type repel one another; the interaction between particles of different species is repulsive in (a) and attractive in (b). There is no substrate for the A particles, $V_A(x) = 0$, whereas the ratchet potential $V_B(x)$ is piecewise linear: $V_B(0 < x < l_+) = x/l_+$, $V_B(l_+ < x < l) = (1-x)/l_-$, with $l_- = 0.2$ and $l_+ = 0.8$. The other coupling parameters are $g_{AA} = g_{BB} = |g_{AB}| = 1$ and $T = 1$. [After Savel'ev *et al.* (2005)].

certain amount of auxiliary particles. All these properties have been reproduced analytically in the framework of the nonlinear Fokker-Planck formalism (Savel'ev *et al.*, 2003, 2004c).

The influence of the interspecies interaction on the transport of a binary mixture has been investigated further by Savel'ev *et al.* (2004b), where dc and ac external forces were applied at constant temperature, to the particles either of one species, only, or of both, simultaneously. Their main results can be summarized as follows: (1) with increasing the intensity of an applied dc driving force, there is a dynamical phase transition from a “clustered” motion of A and B particles to a regime of weakly coupled motion (Marchesoni *et al.*, 2006b); (2) by applying a time-asymmetric zero-mean drive to the B species only, one can obtain a net current for both the A and B species, even in the absence of a substrate; (3) when two symmetric ac signals act independently on the A and B particles, and only the particles of one species feel an asymmetric substrate, then, the two species can be delivered in the same or opposite direction by tuning the relative signal phase (for both attractive and repulsive AB interactions). Superconducting devices based on these two-species transport mechanisms have been realized experimentally in recent years (Sec. VII.C).

VI. MICROFLUIDICS

Microfluidics (Squires and Quake, 2005) is playing an ever growing role in controlling transport of particles, or even whole extended phases, on the micro- and nanoscales. The ability to manipulate the dynamics of liquids is crucial in various applications such as for a

lab-on-a-chip technology. The Brownian motor concept has recently been invoked in different contexts to face this challenge. In this regard we remark that the inertial forces of small suspended particles are typically quite small (Purcell, 1977). Pointlike particles can then be considered to be advectively transported by the fluid velocity field at the particle's actual position. Then, for an incompressible liquid the particle dynamics is volume conserving and consequently no dynamical attractors emerge (Kostur *et al.*, 2006). However, for extended particles the local velocity of a surface point need not coincide with the fluid velocity which would act at this point in the absence of the particle. Notably, for extended objects with internal degrees of freedom the volume of the state space is no longer conserved by the dynamics, thus giving rise to attractors for stationary flow fields (Kostur *et al.*, 2006). Of course, Brownian diffusion provides an additional transport mechanism that must also be taken into account.

We remark here that in spite of the intrinsic hydrodynamical effects, microfluidic devices do not fall into the category of collective ratchets as defined in Sec. V, because here *transported* objects are not required to interact with one another. The suspension fluid still plays a central role: (a) it powers particle transport, and (b) it determines how the particle dynamics is coupled to the asymmetric geometry of the substrate. Genuine collective ratchets are discussed in Sec. VII.

A. Transporting colloids

Many physical examples and technological applications involve particles or molecules in solution that undergo a directed net motion in response to the action of a ratchet. There, the ratchet does not induce a mean flow of the solvent itself. For instance, colloidal particles or macromolecules, suspended in solution, move when exposed to a sawtooth electric potential that is successively turned on and off (Rousselet *et al.*, 1994). Electrolytic effects can be avoided by shuttling microsized Brownian polystyrene particles by optically trapping them with repeatedly applied on-off cycles in an optical tweezer, thus mimicking a flashing Brownian motor (Faucheux *et al.*, 1995; Faucheux and Libchaber, 1995; Marquet *et al.*, 2002). As a function of the cycle frequency one can even detect flux reversal of diffusing colloidal spheres in an optical three-state thermal Brownian motor (Lee *et al.*, 2004). This modus operandi of a Brownian motor can therefore be put to work to pump or separate charged species such as fragments of DNA. A micromachined silicon-chip device that transports rhodamine-labeled fragments of DNA in water has been demonstrated with a flashing on-off Brownian motor scheme by Bader *et al.* (1999). Yet other devices are based on ideas and experimental realizations of entropic ratchets (Chou *et al.*, 1999; Duke and Austin, 1998; Ertas, 1998; van Oudenaarden and Boxer, 1999; Slater *et al.*, 1997; Tessier and Slater, 2002) which

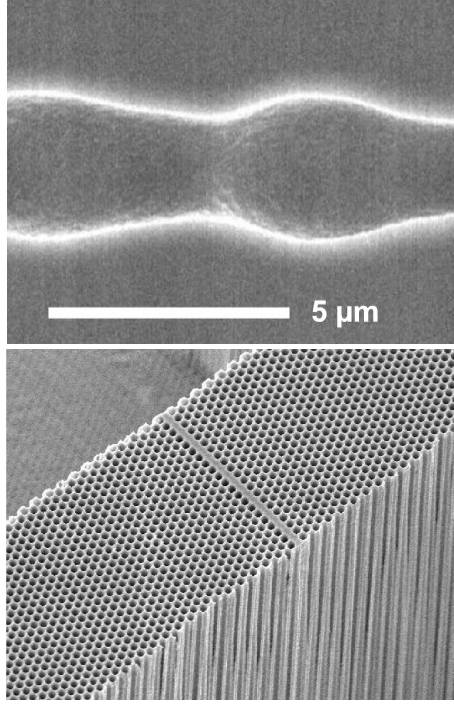


FIG. 17 Top Panel: Scanning-electron-microscope picture of a single pore with ratchet longitudinal profile. The length of one period is $8.4\mu\text{m}$. The maximum pore diameter is $4.8\mu\text{m}$ and the minimum pore diameter is $2.5\mu\text{m}$. Bottom panel: Scanning-electron-microscope picture of a silicon wafer pierced by practically identical pores about 1.5mm apart and 1mm in diameter. This picture illustrates the enormous potential for particle separation of a parallel 3D ratchet architecture. Figure provided by Frank Müller, Max-Planck-Institute of Microstructure Physics, Halle, Germany.

make use of asymmetry within geometric sieve devices to transport and separate polyelectrolytes.

A similar concept is employed to selectively filter mesoscopic particles through a micro-fabricated macro-porous silicon membrane (Fig. 17), containing a parallel array of etched asymmetric bottleneck-like pores (Kettner *et al.*, 2000; Matthias and Müller, 2003; Müller *et al.*, 2000). The working principle and the predicted particle flow for this microfluidic Brownian motor device are shown in Fig. 18. A fluid such as water containing immersed, suspended polystyrene particles is pumped back and forth with no net bias through the 3D array of asymmetric pores of Fig. 17. Such an artificial Brownian motor is thus kept far away from equilibrium by the periodically varying pressure across the membrane. Due to the asymmetry of the pores, the fluid develops asymmetric flow patterns (Kettner *et al.*, 2000), thus providing the ratchet-like 3D force profile in which a Brownian particle of finite size can both: (i) undergo Brownian diffusion into liquid layers of differing speed, and/or (ii) become reflected asymmetrically from the pore walls. Both mechanisms will then result in a driven non-equilibrium net flow of particles. Note that the direction of the net

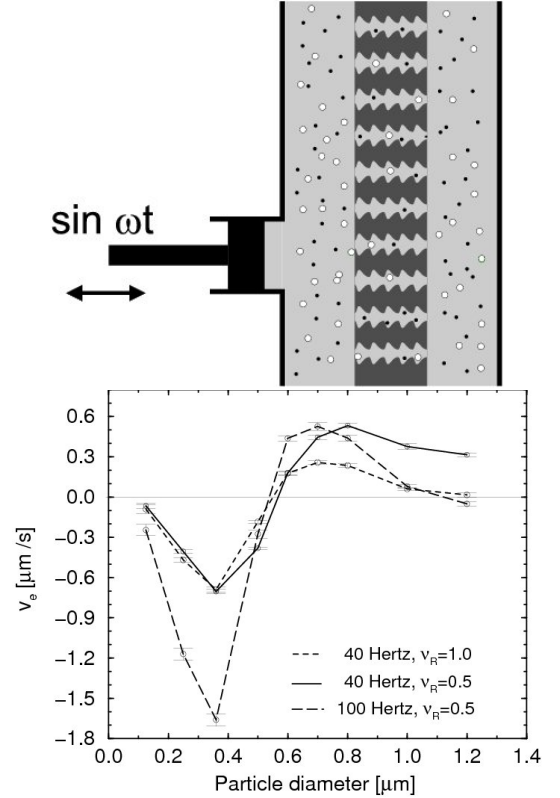


FIG. 18 Microfluidic drift ratchet of Kettner *et al.* (2000). Top panel: A macro-porous silicon wafer is connected at both ends to basins. The pores with their ratchet-shaped profile are sketched in dark grey. The basins and the pores are filled with liquid; microparticles of two different species are represented. The fluid is pumped back and forth by the piston on the left. Figure provided by Christiane Kettner. Bottom panel: theoretically predicted net particle current, v_e , versus the particle diameter for different driving frequencies and viscosities (relative to water) ν_R . Note in particular the very sharp velocity reversal around $0.5\mu\text{m}$. The results are for a pore of infinite length consisting of periodic units with a pore length of $L = 6\mu\text{m}$, a maximum pore diameter of $4\mu\text{m}$ and a minimum pore diameter of $1.6\mu\text{m}$, see Fig. 17 (a). For further details see Kettner *et al.* (2000).

flow cannot be easily guessed *a priori*. Indeed, the direction of the Brownian motor current is determined by the interplay of the Navier-Stokes flow in this engineered geometry and hydrodynamic thermal fluctuations.

A detailed quantitative interpretation of the experimental data is plagued by several complications such as the influence of hydrodynamic interactions and, possibly, electric response effects due to residual charge accumulation near the boundaries. A most striking feature of this setup, however, is the distinct dependence of current reversals on particle size. The sharply peaked current-size characteristics curves of this directed flow, that is, the theoretical flow *vs.* size prediction in Fig. 18 and the experimental current-pressure characteristics in Fig. 19, suggest a highly selective particle separation efficiency

(Kettner *et al.*, 2000). This microfluidic artificial Brownian device has recently been implemented in experiments with suspended polystyrene spheres of well defined diameters (100 nm, 320 nm, 530 nm and 1000 nm) by Matthias and Müller (2003): Their experimental findings are in good qualitative agreement with the theory as shown in Fig. 19.

Remarkably, this device has advantageous 3D scaling properties: A massively parallel architecture composed of about 1.7 million pores illustrated in Fig. 17, is capable to direct and separate suspended microparticles very efficiently. For this reason, such type of devices have clear potential for bio-medical separation applications and therapy use.

The separation and sorting of cellular or colloidal particles is definitely a topic attracting wide interest in different areas of biology, physical chemistry and soft matter physics. The powerful toolbox of optical manipulation (Dholakia *et al.*, 2007; Grier, 2003) uses the optical forces exerted on colloids by focussed laser beams to move and control objects ranging in size from tens of nanometers to micrometers. If the optical forces are sufficiently strong to rule transport, the stochastic Brownian forces play only a minor role, so that transport occurs as a deterministic process with an efficiency close to unity, a circumstance known as (optical) peristalsis (Bleil *et al.*, 2007; Koss and Grier, 2003). Such a scheme can then be implemented also to experimentally realize ratchet cellular automata capable of performing logical operations with interacting objects. All together, in combination with this new optical technology, colloids provides ideal model systems to investigate statistical problems near and far away from thermal equilibrium (Babic and Bechinger, 2005; Babic *et al.*, 2005).

B. Transporting condensed phases

Most present applications use ratchet concepts to transport or filter discrete objects, like colloidal particles or macromolecules. However, ratchets may also serve to induce macroscopic transport of a continuous phase using local gradients, only. One such realization, strongly related to the above cases of particle transport in a “resting” liquid phase, is the Brownian motion of magnetic particles in ferrofluids subjected to an oscillating magnetic field (Engel and Reimann, 2004). In contrast to the cases reported above, here the motion is also transmitted to the solvent by viscous coupling.

Another class of systems does not require colloidal particles to drive the motion of the liquid phase. In a first example, a secondary large scale mean flow is triggered in Marangoni-Bénard convection over a solid substrate with asymmetric grooves (Stroock *et al.*, 2003). The direction and strength of the mean flow can be controlled by changing the thickness of the liquid layer and the temperature gradient across the layer.

Yet another intriguing situation involves self-propelled

Leidenfrost drops placed on a hot surface also with a ratchet-like grooved profile (Fig. 20). The locally asymmetric geometry of the support induces a directed drop motion. This effect has been observed for many liquids and in wide temperature ranges within the film boiling (Leidenfrost) regime (Linke *et al.*, 2006; Quéré and Ajdari, 2006).

Moreover, micro-drops confined to the gap between asymmetrically structured plates, move when drop shape or wetting properties are changed periodically, for instance by vibrating the substrate, applying an on/off electric field across the gap or a low-frequency zero-mean electric field along the gap (Buguin *et al.*, 2002; Gorre *et al.*, 1996). In a related experiment the motion of drops on a global wettability gradient resulted to be strongly enhanced when a periodic force was applied (Daniel *et al.*, 2004). In that work the ratchet aspect was determined by the intrinsically asymmetric shape of the drops and the hysteresis of their contact angle on the gradient substrate.

The theory for particle transport operated by Brownian motors is presently well developed (Astumian, 1997; Astumian and Hänggi, 2002; Hänggi and Bartussek, 1996; Hänggi *et al.*, 2005; Jülicher *et al.*, 1997; Reimann and Hänggi, 2002). In clear contrast, models for ratchet-driven transport of a continuous phase are a rather scarce commodity, although the concept is thought to be important for emerging microfluidic applications (Squires and Quake, 2005).

In recent work, a model for the flow of two immiscible layered liquids confined between two walls and driven by a flashing “wettability ratchet” has been put forward by John and Thiele (2007) and John *et al.* (2008). In doing so, one employs the general concept of wettability comprising all effective interactions between the liquid-liquid free interface and the solid walls. Notably, any interaction that is applicable in a time-periodic, spatially periodic (but locally asymmetric) fashion, is capable to drive a flow, i.e. will result in directed transport. There exist several possibilities for experimental realizations of spatially inhomogeneous and time switching interactions. A practical setup consists of thin films of dielectric liquids in a capacitor with a periodic, locally asymmetric voltage profile, that can be periodically switched on and off. A spatially homogeneous electric field would destabilize the interface between two dielectric liquids. Therefore, an on-off ratchet with a constant lateral force can result in the dewetting-spreading cycle sketched in Fig. 21. The process underlying this motor scheme may be termed “electro-dewetting”.

C. Granular flows

The concept of ratchet physics had found an early application in the field of granular matter (Jaeger *et al.*, 1996). Indeed, to explain the vertical grain size segregation under vibration, the so-called *Brazil-nut* effect

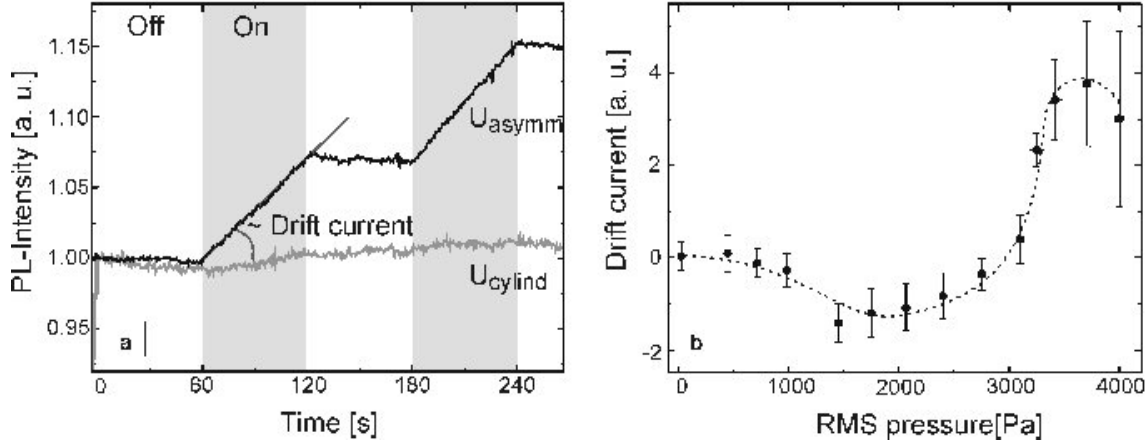


FIG. 19 (Color online) Parallel Brownian motors in a macroporous silicon membrane containing ca. 1.7 million asymmetric pores with 17 etched modulations each (see Fig. 17, top panel). Left panel: When the pressure oscillations of the water are switched on, the measured photoluminescence signal and thus the number of particles in the basin located to the right, see top panel of Fig. 18, increases linearly in time, corresponding to a finite transport velocity. In contrast, for symmetric cylindrical-shaped pores no net drift is observed. Right panel: The experimentally observed net transport behavior strongly depends on the amplitude of the applied pressure and qualitatively shows the theoretically predicted current inversion (Kettner *et al.*, 2000). The pressure oscillations are toggled on and off each 60s. Other experimental parameters are as follows: the suspended luminescent polystyrene spheres in water are $0.32\mu\text{m}$ across, the frequency of the pressure oscillations is 40Hz and the root mean square (RMS) of the applied pressure during the 'on' phase is 2000Pa. A control experiment using straight cylindrical pores with a diameter of $2.4\mu\text{m}$ showed no directed Brownian motor transport. [Image: Max-Planck-Institute of Microstructure Physics, Halle, Germany.]

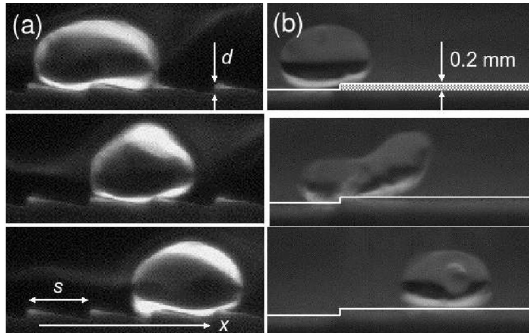


FIG. 20 (a) Video sequence (time interval 32 ms) demonstrating droplet motion perpendicular to a thermal gradient. A droplet of the refrigerant tetrafluoroethane (R134a; boiling point $T_b = 26.1^\circ\text{C}$) was placed on a room-temperature, horizontally leveled brass surface with a ratchet-like grooved profile ($d = 0.3\text{mm}$, $s = 1.5\text{mm}$). See also <http://www.aip.org/pubservs/epaps.html> (b) Droplet of liquid nitrogen on a flat surface moving with a small initial velocity towards a piece of tape (shaded). Figure provided by Heiner Linke.

(Rosato *et al.*, 1987), Bug and Berne (1987) had initially investigated directed diffusion in sawtooth-like inclined grooves. In the meantime, this problem spurred several computer simulations aimed at exploring the wonderful world of granular ratchets. Another unusual phenomenon, observed both experimentally and in computer simulations, is horizontal size segregation. It involves the occurrence of horizontal flows of granular layers that are

vibrated vertically on plates whose surface profile consists of sawtooth-like grooves (Derényi and Vicsek, 1995; Rapaport, 2002).

The spontaneous anelastic clustering of a vibrofluidized granular gas has been employed, for instance, to generate phenomena such as *granular fountains* (convection rolls) and *ratchet transport* in compartmentalized containers, where symmetry breaking flow patterns emerge perpendicular to the direction of the energy input (Brey *et al.*, 2001; Eggers, 1999; Farkas *et al.*, 2002; van der Meer *et al.*, 2004). Granular systems exhibit indeed a rich scenario of intriguing collective transport phenomena, which have been tested and validated both computationally and experimentally (van der Meer *et al.*, 2007).

All these systems are kept away from thermal equilibrium by vertical vibrations, while the presence of random perturbations play a role as a source of complexity, due to the intrinsic chaotic nature of granular dynamics. Closer in spirit of the present review are, however, those devised granular Brownian motors which are truly capable to tame thermal Brownian motion (Cleuren and Van den Broeck, 2007; Costantini *et al.*, 2007, 2008). In those set-ups, an asymmetric object of mass m (Fig. 22), is free to slide, without rotation, in a given direction. Its motion with velocity v is induced by *dissipative* collisions with a dilute gas of surrounding particles of average temperature T . On each collision, only a certain fraction (called restitution coefficient) of the total kinetic energy of the object-particle system is conserved. At variance with the

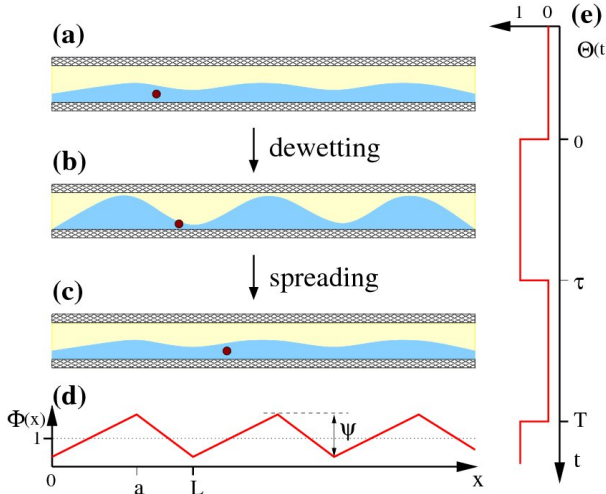


FIG. 21 (Color online) Panels (a) to (c) illustrate the working principle of a fluidic ratchet based on dewetting-spreading cycles. (d) illustrates the spatial asymmetric periodic interaction profile $\Phi(x)$ responsible for the wettability pattern and (e) indicates the time dependence $\Theta(t)$ of the switching in relation to the dewetting and spreading phases (a)-(c). The filled circle indicates a fluid element that gets transported during one ratchet cycle although the evolution of the interface profile is exactly time-periodic. For further details and resulting directed flow pattern see John *et al.* (2008).

case of elastic collisions, here isotropy, implying $\langle v \rangle = 0$, and energy equipartition, implying $\langle v^2 \rangle = kT/m$, do not apply: Dissipation is responsible for breaking the time reversal symmetry. As a result one finds that the asymmetric object undergoes (approximately) a directed random walk with nonzero average velocity, which can be modeled in terms of an effective biased Langevin dynamics for the velocity variable v . Such a Langevin dynamics assumes the form of an Ornstein-Uhlenbeck process (Hänggi and Thomas, 1982; Risken, 1984) governed by an effective Stokesian friction and an effective external force, both depending on the restitution coefficient (Cleuren and Van den Broeck, 2007; Costantini *et al.*, 2007). The directed motion of the object is accompanied by a continuous flow of heat from the gas to the object, in order to balance the dissipation of the collisional processes; as a consequence the average temperature of the asymmetric object is lower than the gas temperature.

Ever since the formulation of the second law of thermodynamics there has been haunting debates about its validity at the small scales. In this context the ratchet gadget invented by Smoluchowski (1912) and later beautifully popularized by Feynman *et al.* (1963) points at the heart of a controversy, which concerns the very working principle of Brownian motors: To be consistent with this law, no rectification of thermal fluctuations can take place at thermal equilibrium for which all dynamics is intrinsically governed by the principle of detailed balance. A steadily working Brownian motors necessarily requires

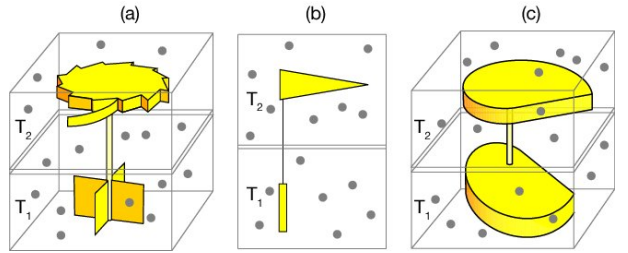


FIG. 22 (Color online) Taming thermal motion. Panel (a) shows a schematic representation of the Smoluchowski-Feynman ratchet device, which is capable to rectify thermal Brownian motion of gases held at two different temperatures (Feynman *et al.*, 1963). An idealized version suitable for computer studies is presented in panel (b) with the ratchet replaced by a triangular unit and the pawl replaced by a rigidly joined blade residing in the lower gas compartment. Panel (c) illustrates a 3D rotational construction. Figure provided by den Broeck and den Broeck (2008).

a combination of asymmetry and non-equilibrium, such as a temperature gradient. This point has been convincingly elucidated in recent molecular dynamic studies by Van den Broeck and his collaborators (Van den Broeck and Kawai, 2006; Van den Broeck *et al.*, 2004, 2005), who variously stylized a Maxwell daemon operating far away from equilibrium (Fig. 22). Several computer versions of Smoluchowski-Feynman ratchets operating in a dilute gas of colliding granular particles, have thus been confirmed to generate directed transport in the presence of a finite temperature difference. With the possibility of today's observation and manipulation of physical, chemical and biological objects at the nano- and meso-scale, such devices no longer represent a theorist's thought experiment, but are rather becoming a physical reality. It is right on these length scales that thermal fluctuations cannot be ignored, as they combine with non-equilibrium forces to yield constructive transport.

VII. SUPERCONDUCTING DEVICES

Magnetic vortices in type-II superconducting devices provide a flexible and experimentally accessible playground for testing our stochastic transport models. In recent years an impressive effort has been directed toward the design and operation of a new generation of vortex devices with potential applications to terahertz (THz) technology (Hecht Fischer *et al.*, 1997; Zitzmann *et al.*, 2002), fluxon circuitry (Shalom and Pastoriza, 2005), and quantum computation (You and Nori, 2005), to mention but a few. We anticipate that magnetic vortices are inherently quantum objects that, under most experimental conditions, behave like (massless, point-like) *classical* particles. Genuine quantum effects in the vortex transport are briefly discussed in Sec. VIII.

A magnetic field applied to a type-II superconduct-

ing film, with intensity H comprised between the critical values H_{c1} and H_{c2} , penetrates into the sample producing supercurrent vortices, termed Abrikosov vortices (Abrikosov, 1957; Blatter *et al.*, 1994). The supercurrent circulates around the normal (i.e. non-superconducting) core of the vortex; the core has a size of the order the superconducting coherence length ξ (parameter of a Ginzburg-Landau theory); the supercurrents decay on a distance λ (London penetration depth) from the core. In the following we assume that $\lambda \gg \xi$. The circulating supercurrents produce magnetic vortices, each characterized by a total flux equal to a single flux quantum $\Phi_0 = hc/2e$ (hence the name fluxon for magnetic vortex) and a radially decaying magnetic field

$$B(r) = B_0 K_0(r/\lambda), \quad (39)$$

where $K_0(x)$ is a modified Bessel function of zero-th order and $B_0 = \Phi_0/(2\pi\lambda^2)$. Far from the vortex core, $r \gg \lambda$, the field decays exponentially, $B(r)/B_0 = \sqrt{\lambda\pi/2r} e^{-r/\lambda}$, whereas, approaching the vortex center, it diverges logarithmically for $\xi < r \ll \lambda$, $B(r)/B_0 = \ln(\lambda/r)$, and then saturates at $B(0) = B_0 \ln(\lambda/\xi)$ inside the core $r < \xi$. As a consequence, the coupling between vortex supercurrents and magnetic fields determines a long range repulsive vortex-vortex interaction.

Due to mutual repulsion, fluxons form a lattice (also called Abrikosov vortex lattice, usually triangular, possibly with defects and dislocations) with average vortex density ρ approximately equal to H/Φ_0 . A local density \mathbf{I} of either a transport current or a magnetization current or both, exerts on each fluxon a Lorentz force $\mathbf{F}_L = \Phi_0 \mathbf{I} \times \mathbf{H}/(cH)$.

The distribution and microscopic properties of pinning centers can qualitatively influence the thermodynamic and vortex transport properties of the superconducting sample. Pinning forces created by isolated defects in the material oppose the motion of the fluxons, thus determining a critical (or threshold) current, below which the vortex motion is suppressed. Many kinds of artificial pinning centers have been proposed and developed to increase the critical current, ranging from the dispersal of small non-superconducting second phases to creation of defects by irradiation (Altshuler and Johansen, 2004). A novel approach to the problem came with advances in lithography, which allowed for regular structuring and modulation of the sample properties over a large surface area (Harada *et al.*, 1996). Long-range correlation in the position of the pinning centers resulted in the interplay between the length scales characterizing the pin lattice and the vortex lattice. Indeed, the magnitude of the commensuration effects is readily controlled by tuning the intensity of the magnetic field H : at the first matching field $H_1 = \Phi_0/a_l$, pin and vortex lattices are exactly commensurate, with one fluxon per pin lattice cell of area a_l ; at the n -th matching field, $H(n) = nH_1$, each pin lattice cell is occupied by $n = \rho a_l$ fluxons; for irrational H/H_1 pin and vortex lattices are incommensurate. Commensuration effects are responsible for a variety of dynamical

superconducting states of great relevance to the problem of vortex rectification (Reichhardt *et al.*, 1998).

As a first attempt to design a vortex ratchet Lee *et al.* (1999) showed that an ac electric current applied to a superconductor patterned with the asymmetric pinning potential shown in Fig. 23, can induce vortex transport whose direction is determined only by the asymmetry of the pattern. The fluxons were treated as zero-mass point-like particles moving on a saw-tooth potential along the x -axis, according to the scheme of Sec. II.D.1. These authors demonstrated theoretically that, for an appropriate choice of the pinning potential, such a rocked ratchet can be used to manipulate single vortices in superconducting samples under realistic conditions. The rectification mechanisms of an extended overdamped string, like a fluxon, on a ratchet potential had been anticipated by Marchesoni and coworkers (Costantini *et al.*, 2002; Marchesoni, 1996). Brownian motor ratcheting of single oscillating fluxons have been observed experimentally in asymmetrically etched Nb strips (Plourde *et al.*, 2000), on planar patterns of columnar defect (Kwok *et al.*, 2002), and in asymmetric linear arrays of underdamped Josephson junctions (Lee, 2003), in an annular Josephson junction (Ustinov *et al.*, 2004), to mention just a few recent experiments.

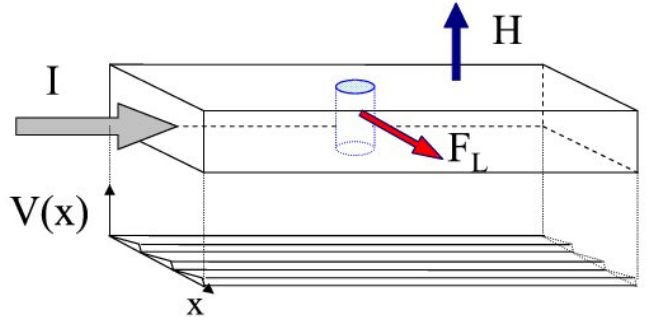


FIG. 23 (Color online) Diagram of a superconductor in the presence of an external magnetic field H . A direct current with density I flowing along the y direction (indicated by the large arrow) induces a Lorentz force \mathbf{F}_L that moves the vortex in the x direction (upper panel). The superconductor is patterned with a pinning potential (lower panel). The potential is periodic and asymmetric along the x direction, and is invariant under translation along y ; the potential $V(x)$ is an effective ratchet potential (see Sec. II.D).

A. Fluxon channels

A more viable approach to achieve controllable stochastic transport of fluxons in superconducting devices consists in exploiting collective boundary effects as suggested Sec. V.A.1. Fluxon rectification in asymmetric channels has been investigated by Wambaugh *et al.* (1999) by means of a molecular dynamics (MD) code, originally developed to study magnetic systems with random and correlated pinning (Reichhardt *et al.*, 1998).

They simulated a thin slice of a zero-field cooled, type-II superconducting slab, taken orthogonally to the magnetic vortex lines generated by a tunable external magnetic field of intensity H . On regarding them as fairly rigid field structures, magnetic vortices formed a confined 2D gas of zero-mass repelling particles with density $\rho = H/\Phi_0$. The simulated sample had very strong, effectively infinite pinning except the “zero pinning” central sawtooth-shaped channel, sketched in the inset of Fig. 24. In the channel fluxons moved subject to fluxon-fluxon repulsions, an externally applied ac driving Lorentz force, forces due to thermal fluctuations, and strong damping. The fluxons outside the channel could not move, thus impeding the movable fluxons in the middle to cross the channel walls. As a consequence, the interaction length of the fluxon-wall collisions was the same as of the fluxon-fluxon collisions. The net fluxon velocity $\langle v \rangle$ versus temperature shown in Fig. 24 is negative and exhibits an apparent resonant behavior, both versus T and H (i.e., the fluxon density ρ), as anticipated in Sec. V.A.1.

These conclusions have been recently corroborated experimentally by Togawa *et al.* (2005) and then by Yu *et al.* (2007). The authors of the more recent work fabricated triangular channels from bilayer films of amorphous niobium-germanium, an extremely weak-pinning superconductor, and niobium nitride (NbN), with relatively strong pinning. A reactive ion etching process removed NbN from regions as narrow as 100 nm, defined with electron-beam lithography, to produce weak-pinning channels for vortices to move through easily. In contrast, vortices trapped in the NbN banks outside of the channels remain strongly pinned. The vortex motion through such asymmetric channels exhibited interesting asymmetries in both the static depinning and the dynamic flux flow. The vortex ratchet effect thus revealed a even richer dependence on magnetic field and driving force amplitude than anticipated by the simplified model simulated by Wambaugh *et al.* (1999).

Devices like that simulated in Fig. 24 serve as excellent fluxon rectifiers. By coupling two or more such devices, one can design fluxon lenses, to regulate the fluxons concentration in chosen regions of a sample, and eventually channel networks or circuits, for fluxons in superconducting films.

Fluxon channeling was observed experimentally for the first time in an effective 1D vortex rectifier by Villegas *et al.* (2003). Their device has the pedagogical merit of showing all collective transport effects summarized in Sec. V at work. A $100\mu\text{m}$ thick Niobium film was grown on an array of nanoscale triangular pinning potentials oriented as in Fig. 25 (top panel), with bases lined up along the x -axis and vertices pointing in the y -direction. Magneto-resistance $R(H)$ experiments were done with a magnetic field H applied perpendicular to the substrate in a liquid Helium system. The dc magneto-resistance curves in the bottom panel of Fig. 25 exhibit commensurability effects in which dissipation minima develop as a consequence of the geometrical matching between the

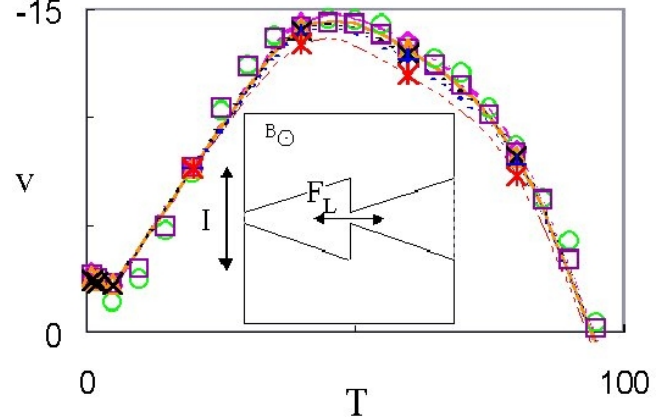


FIG. 24 (Color online) Rectified average fluxon velocity $\langle v \rangle$ (in units of λ/τ) versus T for the sawtooth channel geometry in the inset (width: 7λ , bottleneck: λ). The magnetic field \mathbf{H} is directed out of the figure. A vertically applied alternating current square wave drives the fluxons back and forth horizontally along the channel with period $\tau = 100$ MD steps. The number of fluxons per unit cell is: 1 (circles), 25 (diamonds), 50 (squares), 75 (triangles), 100 (x), 150 (+), 250 (*). [After Wambaugh *et al.* (1999)].

vortex lattice and the underlying periodic structure. At these matching fields, the vortex lattice motion slows down, and $R(H)$ minima appear at the equally spaced values $H(n) = nH_1$, with $H_1 = 32$ Oe. The $R(H)$ minima are sharp at the $n = 1, 2, 3$ matching fields, but shallow and not well-defined for higher n . This effect is a consequence of the appearance of interstitial vortices at increasing H beyond H_3 , three being the maximum number of vortices contained in each triangle.

In order to interpret the experimental results, one separates all vortices in two groups: (i) pinned vortices, which move from one triangular-shaped pinning trap to another one and, thus, are directly affected by an effective 1D rocked ratchet substrate with positive polarity in the y -direction; and (ii) interstitial vortices, which are channeled in-between triangles and do not directly interact with the pinning traps (Savel'ev *et al.*, 2003; Zhu *et al.*, 2003a). However, as apparent in the top panel of Fig. 25 and discussed in Sec. V.C, pinned vortices, being strongly coupled to the substrate potential, determine a weaker mean-field potential that acts on the interstitials with opposite asymmetry (Savel'ev *et al.*, 2003). As a consequence, when all fluxons are subjected to the same ac drive force, the fluxon-fluxon repulsion pushes the interstitials in the direction opposite to the pinned vortices (for an animation see <http://dml.riken.go.jp/vortex>).

The effects of this mechanism are illustrated in Fig. 26. At constant temperature (close to T_c to avoid random pinning) and H multiple of H_1 , an ac current density $I(t) = I_{ac}\sin(\Omega t)$ was injected along the x -axis. This yields a sinusoidal Lorentz force with amplitude F_L acting on the vortices along the y -axis. Despite the zero

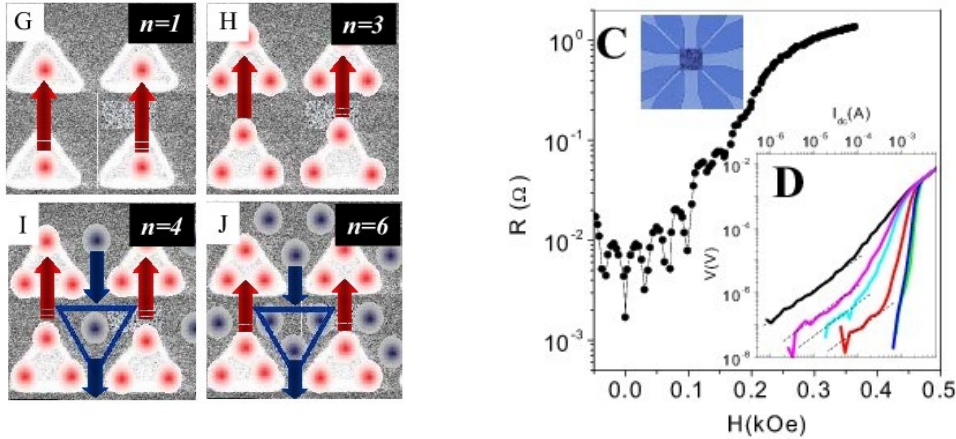


FIG. 25 (Color online) Top panel: Sketch of the positions of the vortices for several matching fields $H(n)$, i.e., for n vortices per unit cell. Vortices pinned on the triangles (no more than 3 per unit cell) are shown in red and interstitial vortices in blue. The pinning substrate is a square lattice with constant 750nm ; the triangular pinning sites have been grown on a Si support, are 40nm thick with side about 600nm long. Bottom panel: dc magneto-resistance $R(H)$ versus H . The temperature is $T = 0.98T_c$ and the injected dc current density is $I_{dc} = 12.5\text{kA}\cdot\text{cm}^{-2}$. The upper inset shows a micrograph of the measuring bridge, which is $40\mu\text{m}$ wide. The darker central area of the inset is the $90 \times 90\mu\text{m}^2$ array of magnetic triangles. The lower inset shows the characteristics curves $V_{dc}-I_{dc}$ at the matching magnetic fields $H(n) = nH_1$ with $H_1 = 32\text{Oe}$ and $n = 1$ (red), 3 (cyan), 4 (blue), 6 (green), 8 (magenta), and 10 (black). The $V(I_{dc})$ curves change abruptly at magnetic fields from $n = 3$ to $n = 4$, because an ohmic regime appears at low currents. This is a clear signature of the presence of interstitial vortices. [After Villegas *et al.* (2003)].

time average of such Lorentz force, a non-zero dc voltage drop V_{dc} in the x -direction was measured, thus proving that the vortices actually drift in the y -direction. Note that, due to the peculiar substrate symmetry, an ac current $I(t)$ oscillating along the y -axis, can rectify the fluxon motion only parallel to it (transverse rectification, Sec. VII.B). The amplitude of the dc voltage signal decreases with increasing H because the effective pinning is suppressed by the inter-vortex repulsion. Moreover, when $n > 3$ (corresponding to more than three vortices per unit cell), a reversed V_{dc} signal begins to develop with a maximum (marked by blue arrows) occurring at a lower Lorentz force F_L than the positive dc maxima (red arrows): The interstitials, which feel a weak inverted ratchet potential with respect to the pinned vortices, dominate the rectification process. This current reversal effect is enhanced when further increasing the magnetic field [panels (c) and (d)] and finally, at very high magnetic fields, close to the normal state, the voltage reversal, although suppressed in magnitude, spans over the entire F_L range [panel (f)].

Moshchalkov and coworkers (Silva *et al.*, 2006; de Vondel *et al.*, 2007) also demonstrated longitudinal fluxon rectification. Silva *et al.* (2006) observed multiple current reversals in regular square lattices of asymmetric double-well traps periodically driven along an “easy” direction, as in the simulations by Zhu *et al.* (2003a,b). More interestingly, de Vondel *et al.* (2007) have detected inverted fluxon currents in large triangular arrays, similar to those reviewed here, but at magnetic fields (or fluxon densities) so high that a collective ratchet mechanism would not be plausible. They attributed their finding to

a new intra-antidot rectification mechanism controlled by the magnetic flux quantization condition synchronously satisfied at the edge of each asymmetric antidot.

B. Fluxon rectification in 2D arrays

The rectification of a fluxon lattice, no matter how distorted or disordered, is an inherently 2D process. Following the theoretical and numerical investigations reviewed in Sec. V.B, a number of experimental groups (Crisan *et al.* (2005); Menghini *et al.* (2007); Van Look *et al.* (2002) to mention a few) prototyped devices aimed at controlling vortex ratcheting both in the direction parallel (longitudinal rectifiers) and perpendicular to an applied ac Lorentz force (transverse rectifiers).

Longitudinal transport in a 2D array of asymmetric pinning traps has been experimentally obtained, for instance, by de Vondel *et al.* (2005), who reported that, under appropriate operating conditions, fluxon rectification can be enhanced for F_L amplitudes comprised between two critical pinning forces of the underlying asymmetric substrate. The shape of the net dc voltage drop V_{dc} as a function of the drive amplitude indicated that their vortex ratchet behaved in a way very different from standard overdamped models. Rather, as the repinning force necessary to stop vortex motion, is considerably smaller than the depinning force, their device resembles the behavior of the inertial ratchets of Sec. II.D.1. More recently, Shalóm and Pastoriza (2005) reported longitudinal fluxon rectification in square arrays of Josephson junctions, where the coupling energies had been period-

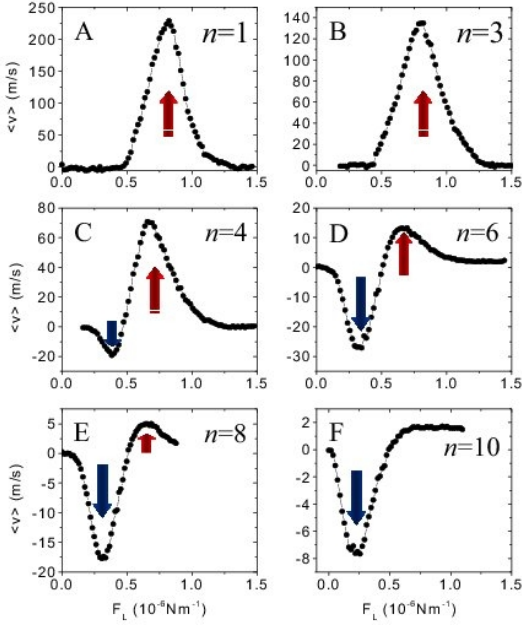


FIG. 26 (Color online) (a)-(f) Net velocity $\langle v \rangle$ of vortices versus the amplitude F_L of the ac Lorentz force for $\Omega = 10\text{kHz}$ and different matching magnetic fields $H(n)$; other parameter values are as in Fig. 25. Red and blue arrows show the direction of the net flow, dominated respectively, by the pinned and the interstitial vortices (see panel (a) of Fig. 25). [After Villegas *et al.* (2003).]

ically modulated along one symmetry axis. Similarly, longitudinal fluxon rectification has been observed also in square arrays of magnetic antidots with size-graded period (Gillijns *et al.*, 2007). Both are nice experimental implementations of the asymmetric patterns of symmetric traps introduced in Sec. V.A.2. Finally, Ooi *et al.* (2007) trapped symmetric fluxon lattices in a triangular dot lattice, they had photo-lithographed on a thin $\text{Bi}_2\text{Sr}_2\text{CaCu}_2\text{O}_{8+\delta}$ (Bi2212) single-crystal film, by setting the applied magnetic field at the lowest multiples of H_1 . By subjecting the fluxon lattice to a bi-harmonic Lorentz force oriented along the crystallographic axes of the dot lattice, they obtained a neat demonstration of harmonic mixing on a symmetric substrate. However, also the results of these experiments can be easily explained in terms of simple 1D models.

Transverse transport, instead, requires genuinely irreducible 2D geometries. When designing and operating a device capable of transverse rectification, experimenters can vary the orientation of the pinning lattice axes, the symmetry axes of the individual traps (if any) and the direction of the injected current (i.e., of the Lorentz force). Many authors explored by numerical simulation the geometries best suitable for the experimental implementation of this concept (Olson Reichhardt and Reichhardt, 2005; Zhu *et al.*, 2001). The most recent realizations of transverse fluxon rectifiers fall into two main categories:

(i) *Symmetric arrays of asymmetric traps.* Gonzalez

et al. (2007) modified the experimental set-up of Villegas *et al.* (2003) to investigate the rectification mechanisms presented in Secs. V.A and V.B. They confirmed the numerical simulations by Savel'ev *et al.* (2005), who had predicted that the same device can exhibit either longitudinal or transverse output current depending on orientation of the ac drive with respect to the pinning lattice axes. In the longitudinal ratchet configuration a sinusoidal driving current $I(t)$ was applied perpendicular to the triangle reflection symmetry axis (x -axis) and the output voltage signal V_{dc} was recorded in the same direction. We recall that the Lorentz force induced vortex motion, parallel to the triangle reflection symmetry axis (y -axis), corresponds to a voltage drop in the direction of the injected current. To observe an optimal transverse rectification effect, the axes of the current injection and the voltage drop were inverted. The asymmetry of the traps with respect to the direction of the Lorentz force is responsible for the observed fluxon drift in the y direction.

The number n of vortices per lattice cell was controlled by varying the intensity of the magnetic field orthogonal to the device, $H = nH_1$. On increasing n , the voltage associated to the longitudinal ratchet current changes sign and gets amplified, as to be expected due to the presence of the $n - 3$ interstitials per unit cell (Sec. VII.A). The H dependence the transverse fluxon rectification is very different: (a) the transverse net current shows no inversions; (b) increasing the number of the interstitials transverse rectification is suppressed.

(ii) *Asymmetric arrays of symmetric traps.* Controlled transport of vortices through rows of antidots was measured by Wördenebber *et al.* (2004) via standard 4-probe Hall-type experiments (Altshuler and Johansen, 2004). 100-150 nm thin $\text{YBa}_2\text{Cu}_3\text{O}_2$ (YBCO) films were deposited on CeO_2 buffered sapphire and then covered with a 50 nm thick Au layer. Asymmetric lattices of symmetric antidots in the shape of circular micro-holes, were patterned via optical lithography and ion beam etching. The inset of Fig. 27 shows a typical antidot lattice. A tunable dc current I_{dc} was then injected so that the corresponding Lorentz force \mathbf{F}_L was at an angle γ with respect to the orientation of the antidot rows.

Reference measurements on samples without antidots as well as temperature-dependent measurements of the Hall resistance R_H for different angles γ clearly indicate that for $T < 83\text{K}$ and low dc drive current, the Hall resistance is dominated by the directed vortex motion along the antidot rows. Under this circumstances, R_H quantifies the fluxon current in the direction of the dc current I_{dc} (with negative Hall voltage), or equivalently, *transverse* to the drive force \mathbf{F}_L . In view of the symmetry of the traps, for currents perpendicular to the antidot rows, no transverse fluxon current was observed; as shown in Fig. 27, changing the sign of γ led to a inversion of the transverse current. Most notably, the detected drift was not restricted by a current threshold, that is, fluxons seemed not to jump from antidot to antidot, like individ-

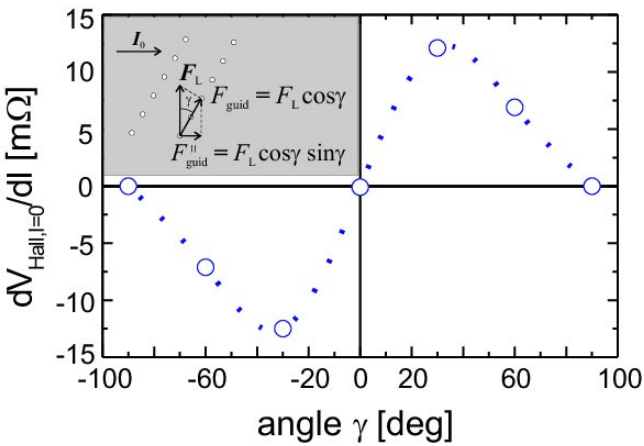


FIG. 27 Angular dependence of R_H measured on a circular shaped 90nm thick sample at $T = 30K$, $H = 143mT$ and with dc current $I_{dc} = 10mA$. Inset: portion of a $20\mu m \times 10\mu m$ rectangular lattice of circular antidots with radius of $1\mu m$; I_{dc} is horizontally oriented from left to right corresponding to a Lorentz force \mathbf{F}_L pointing upwards. The angular dependence is fitted by the sinusoidal law $\sin 2\gamma$, as sketched in the inset. [After Wördenweber *et al.* (2004)].

ual vortices in a defective superconductor sample (Sec. V.A.2), but rather obey an Ohmic behavior. The absence of an activation threshold was explained in Wördenweber *et al.* (2004) by invoking a combination of (i) finite size effects, as the area where vortices can be nucleated is severely restricted by the device geometry; (ii) screening effects, as trapped fluxons induce spatially non-uniform current distributions around neighboring antidots. Due to current screening, the antidot rows serve as easy-flow (i.e., threshold-less) paths for the driven vortices, which thus acquire a transverse velocity proportional to $\sin 2\gamma$ (see Fig. 27, inset and main panel).

At higher temperatures and stronger drives, this effect becomes negligible and no transverse rectification was detected (Wördenweber *et al.*, 2004). Moreover, on replacing I_{dc} with a symmetric ac drive $I_{ac}(t)$, no net current is expected, neither longitudinal nor transversal.

C. Anisotropic fluxon rectifiers

Transport control in a binary mixture can be achieved in samples with no ratchet substrate. As reported in Sec. V.C, when one of the components of the binary mixture is driven, the moving particles drag along the other non-driven component, interacting with it. A time asymmetric ac drive produces rectification of both components of the binary mixture, which can be tuned by means of the ac drive parameters. The device acts like a ratchet, but it has no ratchet substrate.

Savel'ev and Nori (2002) proposed to implement this new ratchet concept in a layered superconductor. In this class of materials, a magnetic field, tilted away from the

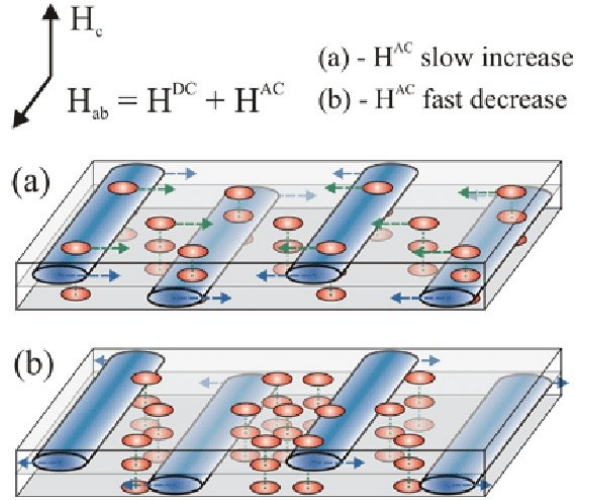


FIG. 28 (Color online) Vortex lens. Subjected to a superposition of dc and time asymmetric ac in-plane magnetic fields, $H_{||}(t) = H_{||}^{dc} + H_{||}^{ac}(t)$, the JV (horizontal cylinders) are asymmetrically pushed in and out of the sample. If the ac component of $H_{||}(t)$ increases slowly, the PV stacks (pancakes) remain trapped on the JV, and both move together towards the center of the lens [panel (a)]. If, on the way back, $H_{||}^{ac}(t)$ decreases rapidly, the JV leave the PV behind them [(panel (b)]. Courtesy of Sergey Savel'ev.

high-symmetry crystalline c -axis, penetrates the sample as two perpendicular vortex arrays (Grigorenko *et al.*, 2001; Matsuda *et al.*, 2001; Ooi *et al.*, 1999), known as “crossing” vortex lattices (Koshelev, 1999). One vortex sublattice consists of stacks of pancake vortices (PV) aligned along the c -axis, whereas the other is formed by Josephson vortices (JV) confined between CuO_2 layers (Fig. 28). A weak attractive PV-JV interaction has been experimentally observed (Grigorenko *et al.*, 2001). The JV are usually very weakly pinned and can be easily driven by changing either the in-plane magnetic field, $H_{||}$, or applying an electrical current, I_z , flowing along the c -axis.

Time-asymmetrically driven JV can drag along the PV, resulting in a net motion of the PV, as in the PV lens device illustrated schematically in Fig. 28. The simplest possible operating mode consists of slowly increasing the in-plane field, $H_{||}$, from 0 to $H_{||}^{\max}$ for a fixed value of the out-of-plane magnetic field, H_z . The increasing in-plane field slowly drives the JV from the edges to the middle of the sample. In turn, the JV drag the PV along with them towards the sample center. As a result, asymmetrically cycling causes either pumping (focusing) or antipumping (defocusing) of the PV at the center of the lens.

Cole *et al.* (2006) actually performed a vortex lensing experiment on an as-grown single Bi2212 crystal. The changes in magnetic induction, arising from PV lensing/anti-lensing, were detected using one centrally placed element of a micro-Hall probe array (Altshuler and Johansen, 2004). In order to realize the asymmetric ac driven mode for the vortex lens, the following steps

sketched in Fig. 29 were carried out: (1) The sample was cooled in fixed H_z at $H_{\parallel} = 0$; (2) A “conditioning” triangular wave was run for 4 min to equilibrate the PV system; (3) A time-asymmetric, zero-mean ac drive, was switched on for 4 min (for an animation see <http://dml.riken.go.jp>). The magnetic induction, B_z , was then monitored in real time starting from step (2) at a centrally located Hall element and then related to the local PV density. The measured efficiency of this vortex lens, displayed in Fig. 29, is quite low. However, the same experiment, when performed on a symmetric substrate, yields a much higher efficiency, as recently proven by Cole *et al.* (2006) for a film of Bi2212 patterned with a square array of circular antidots.

The two main advantages of this class of vortex devices over the earlier proposals reviewed in Secs. VII.A and VII.B are: (1) the possibility to guide particles with no tailored spatial asymmetry; (2) the tuning of the vortex motion by simply changing the parameters of the externally applied drive. The first feature allows to avoid expensive and cumbersome nanofabrication processing; the second property becomes very important if the transport properties of a device must be frequently varied, something which is generally hard to achieve in standard ratchet devices.

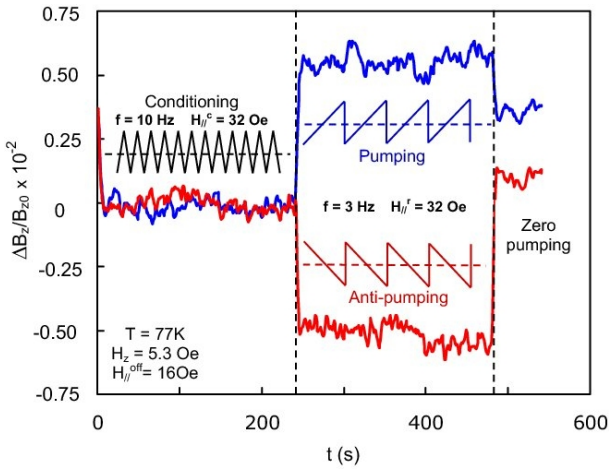


FIG. 29 (Color online) Vortex lens operation. The curves show the measured percentage change of the magnetic induction (PV density) at the samples center, when applying an initial conditioning signal followed by pumping/antipumping time-asymmetric drives. The conditioned PV density increases (decreases) during several cycles of the pumping (antipumping) drive and then saturates. As soon as the drive is switched off, the PV density starts to relax from the non-equilibrium pumping (antipumping) state towards an equilibrium state. Courtesy of Sergey Savel'ev.

VIII. QUANTUM DEVICES

In the foregoing sections, we focused on directed transport within the realm of classical dynamical laws and

classical statistical fluctuations. Totally new scenarios open up when we try to consistently incorporate quantum mechanical laws in the operation of an artificial Brownian motor. The quantum nature of fluctuations and the quantum evolution laws, as governed by quantum statistical mechanics, allow for unexpected transport mechanisms. In particular, quantum mechanics provides the doorway to new features such as under-barrier(-threshold) tunneling, above barrier-reflection and the interplay of coherent (i.e. with oscillatory relaxation) and incoherent (i.e. with overdamped relaxation) quantum transport. Last but not least, quantum mechanics generates the possibility for non-classical correlations, including entanglement among quantum states in presence of coupling.

A. Quantum dissipative Brownian transport

To set the stage and in order to elucidate the complexity involving directed quantum Brownian transport, we consider a 1D quantum particle of coordinate q and mass m , moving in a typically time-dependent ratchet-like potential landscape $V_R(q, t)$. The particle is bi-linearly coupled with strength c_i to a set of N harmonic oscillators x_i , with $i = 1, \dots, N$. The latter set of oscillators models the heat bath, with the oscillators being prepared in a canonical state with density matrix $\hat{\rho}_{\text{bath}}$, corresponding to an isolated, bare bath Hamiltonian and a temperature kT . Accordingly, the total dynamics is governed by the Hamiltonian:

$$H = \frac{p^2}{2m} + V_R(q, t) \quad (40)$$

$$+ \sum_{i=1}^N \left[\frac{p_i^2}{2m_i} + \frac{m_i}{2} \omega_i^2 x_i^2 - q c_i x_i + q^2 \frac{c_i^2}{2m_i \omega_i^2} \right].$$

The last term, which depends only on the system coordinate, represents a potential renormalization term which is needed to ensure that the potential $V_R(q, t)$ coincides with the bare ratchet potential also in presence of coupling to the bath degrees of freedom. This Hamiltonian has been studied since the early Sixties for systems which are weakly coupled to their environment. Only in the Eighties it was realized by Caldeira and Leggett (Caldeira and Leggett, 1983, 1984) that this model is also applicable to strongly damped systems and may be employed to describe, for example, dissipative tunneling in solid state and chemical physics (Hänggi *et al.*, 1990).

One may convince oneself that the Hamiltonian in Eq. (40) models indeed dissipation. Making use of the solution of the Heisenberg equations of motion for the external degrees of freedom, one derives a reduced system operator-valued equation of motion, the so-called inertial *generalized quantum Langevin equation*, that is

$$m\ddot{q}(t) + m \int_{t_0}^t ds \gamma(t-s) \dot{q}(s) + \frac{dV_R(q,t)}{dq} = \eta(t) - m\gamma(t-t_0)q(t_0). \quad (41)$$

The friction kernel is given by

$$\gamma(t) = \gamma(-t) = \frac{1}{m} \sum_{i=1}^N \frac{c_i^2}{m_i \omega_i^2} \cos(\omega_i t), \quad (42)$$

and the quantum Brownian force operator reads

$$\eta(t) = \sum_{i=1}^N c_i \left(x_i(t_0) \cos(\omega_i [t - t_0]) + \frac{p_i(t_0)}{m_i \omega_i} \sin(\omega_i [t - t_0]) \right), \quad (43)$$

The random force $\eta(t)$ is a stationary Gaussian operator noise with correlation functions

$$\langle \eta(t) \rangle_{\hat{\rho}_{\text{bath}}} = 0 \quad (44)$$

$$S_{\eta\eta}(t-s) = \frac{1}{2} \langle \eta(t)\eta(s) + \eta(s)\eta(t) \rangle_{\hat{\rho}_{\text{bath}}} \quad (45)$$

$$= \frac{\hbar}{2} \sum_{i=1}^N \frac{c_i^2}{m_i \omega_i} \cos(\omega_i(t-s)) \coth\left(\frac{\hbar\omega_i}{2kT}\right).$$

Moreover, being an operator-valued noise, the η commutators do not vanish, i.e.,

$$[\eta(t), \eta(s)] = -i\hbar \sum_{i=1}^N \frac{c_i^2}{m_i \omega_i} \sin(\omega_i(t-s)). \quad (46)$$

This complex structure for driven quantum Brownian motion in a potential landscape follows the fact that a consistent description of quantum dissipation necessarily requires the study of the dynamics in the *full* Hilbert space of the system plus environment. This is in clear contrast to the classical models, where the Langevin dynamics is directly formulated in the system state space (Hänggi and Ingold, 2005). Caution applies in making approximations to this structure, even if done semiclassically. The interplay of quantum noise with the commutator structure is necessary to avoid inconsistencies with the thermodynamic laws, such as a spurious finite directed current in an equilibrium quantum ratchet, i.e., even in absence of rocking, i.e., for $V_R(q,t) = V_R(q)$ (Hänggi and Ingold, 2005; Machura *et al.*, 2004a). Simplifications are possible only under specific circumstances like in the case of very strong friction, when quantum corrections can consistently be accounted by a semiclassical quantum Smoluchowski equation operating on the state space of the classical system, only (Ankerhold *et al.*, 2001; Machura *et al.*, 2004a, 2007b). The situation is presently less settled for weakly damped quantum Brownian motors (Carlo *et al.*, 2005; Denisov *et al.*, 2008) and for systems at high temperatures, where reduced descriptions

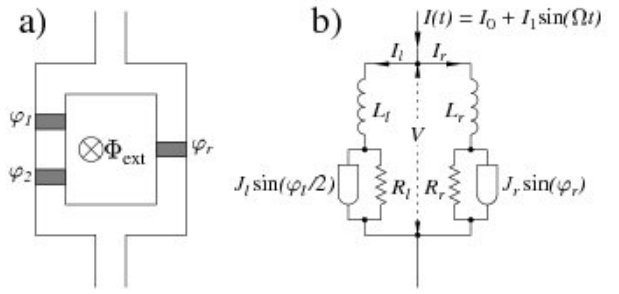


FIG. 30 (a) Schematic picture of an asymmetric SQUID with three junctions threaded by an external magnetic flux. (b) Equivalent electric circuit: the two junctions in series of the left branch behave like a single junction with φ replaced by $\varphi/2$. For further details see Zapata *et al.* (1996).

are often in conflict with the laws of thermodynamics; this is true in particular for the second law, central to this review (Hänggi and Ingold, 2005; Zueco and Garcia-Palacios, 2005).

An alternative approach to the quantum Langevin description, which in addition allows powerful computational methods, is based on the real time path integral technique. Starting from the quantum statistical representation of the density operator evolution of the total dynamics of a system coupled to its environment(s), one traces over the bath degrees of freedom to end up with a path integral representation for the reduced density operator, the so-called influence functional, which consistently incorporates quantum dissipation (see, for instance, (Grifoni and Hänggi, 1998; Hänggi and Ingold, 2005; Hänggi *et al.*, 1990; Kohler *et al.*, 2005)).

B. Josephson Brownian motors

In the following we consider the role of quantum effects on artificial Brownian motors made of coupled Josephson junctions.

1. Classical regime

A first case refers to the limit when quantum coherence and tunneling events, such as photon-assisted tunneling, can safely be neglected, which is often the case at sufficiently high temperatures. In this regime the description of Josephson quantum systems can well be approximated by an effective Fokker-Planck dynamics in the context of the Stewart-McCumber model (Barone and Paternò, 1982), which includes effective parameters containing \hbar . An artificial Brownian motor then can be experimentally realized for instance with the asymmetric superconduct-

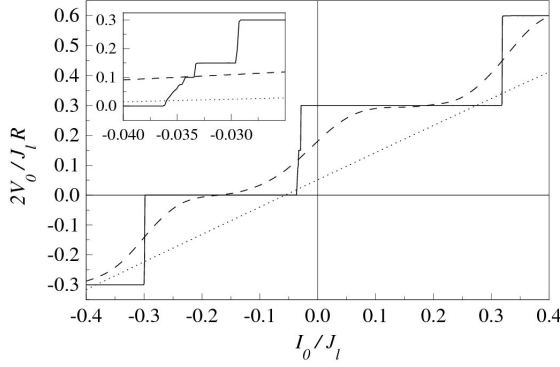


FIG. 31 Theoretically evaluated dc current-voltage (Josephson relation: $V_0 = (\hbar/2e)\langle\dot{\phi}(t)\rangle$) characteristics for the SQUID ratchet of Fig. 30. Simulation parameters: (non-adiabatic) rocking frequency $\omega = 2\hbar\Omega/eRJ_l = 0.3$, ac drive amplitude $A = I_0/J_l = 1.7$, and different noise levels: $D = ek_B T/\hbar J_l = 0$ (solid), 0.01 (dashed), and 0.5 (dotted). Inset: magnified plot showing characteristics steps at fractional values of ω for $D = 0$. Here, R and J_l denote the resistance and the critical current amplitude of the two identical Josephson junctions placed in the left branch of the device, cf. in Fig. 30.

ing quantum interference device (SQUID) illustrated in Fig. 30 (Zapata *et al.*, 1996). In the overdamped regime, where capacitative effects can be ignored, such a device maps precisely onto the rocked ratchet of Sec. II.D.1. Under such operating conditions, the phase of the device is a classical variable which can be adequately described by the aforementioned “resistively shunted junction” model. Thermal Brownian motion at temperature T is included by adding Nyquist noise. The behavior of the so induced ratchet voltage is displayed in Fig. 31 for a non-adiabatically rocked SQUID-ratchet (Zapata *et al.*, 1996).

The results for this ratchet setup have been experimentally validated by use of high temperature superconducting dc SQUID’s by the Tübingen group (Sterck *et al.*, 2005, 2002; Weiss *et al.*, 2000). In the meantime, several variants of this scheme have been studied, both theoretically and experimentally, including fluxon ratchets of various designs (Beck *et al.*, 2005; Berger, 2004; Carapella and Costabile, 2001; Faló *et al.*, 2002; Lee, 2003; Shalóm and Pastoriza, 2005; Zapata *et al.*, 1998); cf. also Sec. VII. Moreover, transport of fluxons in an extended, annular Josephson junction has been demonstrated by Ustinov *et al.* (2004) also as a harmonic mixing effect.

2. Quantum regime

To tackle true quantum effects, including quantum tunneling phenomena, we must resort to the theoretical scheme outlined in Sect. VIII.A. A first theoretical study of quantum ratchets has been pioneered by

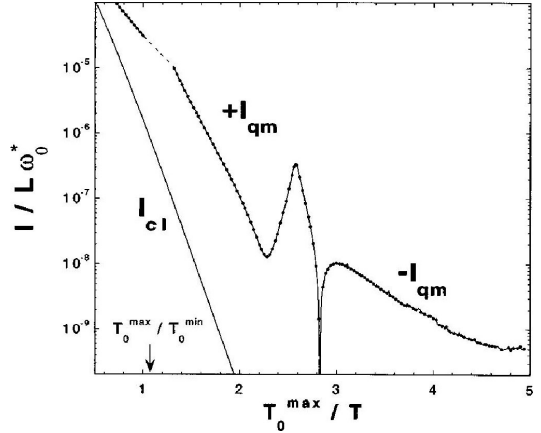


FIG. 32 The classical Brownian motor current I_{cl} occurring in a dichotomously rocked ratchet potential, Eq. (23), of period L , is compared with the corresponding quantum Brownian motor current I_{qm} versus dimensionless inverse temperature T . The current is measured in units of $[L\omega_0^*]$ with $\omega_0^* = [4\pi^2 V_0/(L^2 m)]^{1/2}$ and temperature is measured in units of the (maximal) crossover temperature T_0^{max} occurring in the rocked potential landscape. Notably, in clear contrast to an adiabatically rocked classical Brownian motor, the quantum current changes sign near $T_0^{max}/T = 2.8$ which is a manifestation of true quantum tunneling. For more details we refer to the original work by Reimann and Hänggi (1998).

Reimann *et al.* (1997) (see also (Reimann and Hänggi, 1998)). For a regime with several (quasi)-bound states below a potential barrier one can evaluate the ratchet tunneling dynamics in terms of an effective action for the extremal bounce-solution (in combination with a fluctuation analysis around this bounce solution) to obtain the corresponding tunneling rates. In Fig. 32 the result of such a quantum calculation is compared with the classical result for an adiabatically rocked quantum particle of mass m and coordinate q dwelling in a ratchet potential $V_R(q)$. Note that within a quantum Brownian motor scheme the role of mass m , i.e. the inertia, does enter the analysis explicitly. The most distinctive quantum signature is a striking current reversal which emerges solely as a consequence of quantum tunneling under adiabatic rocking conditions. Moreover, in contrast to the classical result, the directed current no longer vanishes as T tends to zero and additional resonance-like features show up.

Such a dependence of the current versus decreasing temperature in a quantum Brownian motor has been corroborated experimentally for vortices moving in a quasi-1D Josephson junction array with ratchet potential profile specially tailored so as to allow several bands below the barrier (Majer *et al.*, 2003). The experimental setup of this quantum ratchet device is displayed in Fig. 33. The experimental findings are in good agreement with the theoretical analysis reported by Grifoni *et al.* (2002).

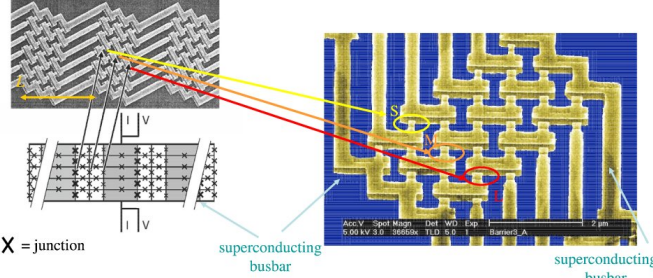


FIG. 33 (Color online) Top left: Scanning electron picture (with enlargement on the right) of a strongly asymmetric array of a long, narrow network of Josephson junctions arranged in a rectangular lattice. This arrangement determines the potential shape felt by vortices. Bottom left: Schematic layout. The Josephson junctions are represented by crosses, each network cell being delimited by four junctions. All arrays have a length of 303 cells and a width of 5 cells, placed between solid superconducting electrodes (busbars). The vortices assume a lower energy in cells with larger area and smaller junctions. Figure provided by Milena Grifoni, University of Regensburg, Germany.

C. Quantum dot ratchets

Another ideal resource to observe the interplay of (i) quantum Brownian motion, (ii) quantum dissipation, and (iii) non-equilibrium driving are semiconductor engineered quantum rectifiers. Composed of arrays of asymmetric quantum rectifiers (Linke *et al.*, 1998), these devices operate on geometric and dynamical length scales ranging between a few nanometers up to micrometers. This class of devices allowed the first experimental validation of the distinctive features of quantum rectifiers, namely, tunneling enhanced ratchet current and tunneling induced current reversals, by Linke and collaborators (Linke *et al.*, 2002, 1999). Their central results are illustrated in Fig. 34.

Their quantum Brownian motor consisted of a 2D gas of electrons moving at the interface of a fabricated, ratchet-tailored GaAs/AlGaAs heterostructure. Its operating regime was achieved by adiabatically switching on and off a square wave source-drain periodic voltage of frequency 190Hz and amplitude of about 1mV. Recalling that for an adiabatically rocked classical ratchet of Sec. II.D.1, noise induced transport exhibits no current reversals, things change drastically when quantum tunnelling enters into the dynamics. A true benchmark for the quantum behavior of an adiabatically rocked Brownian motor is then the occurrence of a tunneling induced reversal at low temperatures (Reimann *et al.*, 1997). This characteristic feature has been first experimentally verified with an electron quantum rocked ratchet by Linke *et al.* (1999). Moreover, the current reversal reported in the top panel of Fig. 34 indicates the existence of parameter configurations where the current of a quantum Brownian motor vanishes. In correspondence to

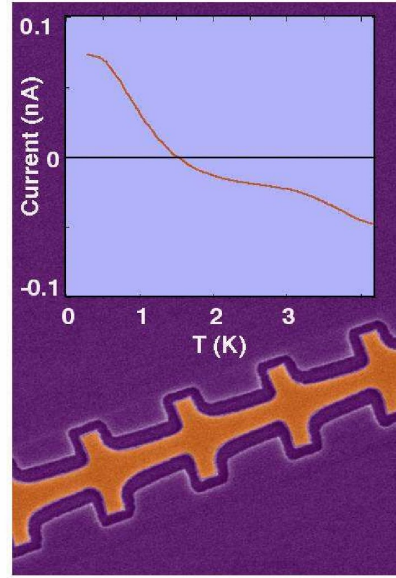


FIG. 34 (Color online) In an experimental *quantum Brownian motor* driven by an adiabatic square-wave zero-mean rocking voltage, quantum tunneling can contribute to the electron current. Due to the underlying asymmetric potential structure, the two opposite components to the time-averaged driven current differ in magnitude, yielding a net quantum ratchet current (Linke *et al.*, 1999; Reimann *et al.*, 1997). The magnitudes can be individually controlled by tuning the temperature. This in turn causes a tunneling induced current reversal (occurring near 1.5K in the top graph) that can be exploited to direct electrons along *a priori* designed routes (Linke *et al.*, 1999). Below the current versus T graph is a scanning electron micrograph of the relevant quantum device. Figure provided by Heiner Linke, University of Oregon.

such configurations, one can imagine to operate the device as a quantum refrigerator to separate “cold” from “hot” electrons in the absence of currents (Linke *et al.*, 2002). At higher temperatures this and other asymmetric quantum-dot arrays, when subjected to unbiased ac drives, exhibit incoherent quantum ratchet currents. Experimental such realizations using two-dimensional electron systems with broken spatial inversion symmetry are reported in Refs. (Lorke *et al.*, 1998; Sassine *et al.*, 2008; Vidan *et al.*, 2004). An even richer behavior of the quantum current, including for example multiple current reversals, emerges when this class of devices is operated in the *non-adiabatic* ac regime, as revealed by recent theoretical studies (Goychuk *et al.*, 1998a,b; Goychuk and Hänggi, 1998; Goychuk and Hänggi, 2005; Grifoni *et al.*, 2002; Kohler *et al.*, 2005).

As a second example of an artificial quantum dot Brownian motor, we consider an experimental double quantum dot device where both dots are independently coupled to a nonequilibrium energy source which is given by a biased quantum point contact. Moreover, both quantum dots are embedded in independent electric circuits via a common central gate, marked by a “C” in the sketch of

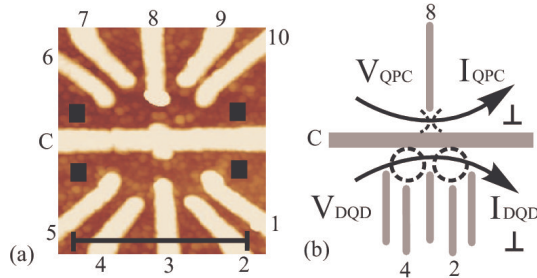


FIG. 35 (Color online) (a) AFM micrograph of a double quantum dot device. Metal surface gates have a light color, black squares mark source and drain regions. The black scale bar marks the length of $1\mu\text{m}$. (b) Schematic diagram: A biased quantum point contact (QPC) provides the nonequilibrium fluctuation source for driving a tunneling current I_{DQD} in the asymmetric double quantum dot (DQD) (dashed two circles) (Khrapai *et al.*, 2006). The asymmetry is induced via gate voltages at the plunger gates 2 and 4. Figure provided by Vadim S. Khrapai, Ludwig-Maximilian University, Munich, Germany.

Fig. 35. On breaking its internal symmetry by tuning the dot gate voltages, this double quantum dot acts as a quantum ratchet device (Khrapai *et al.*, 2006). For weak interdot tunneling, detuning of the quantum dot energy levels results in the localization of an electron in one dot, so that elastic electron transfer to the other dot is energetically forbidden. To operate as a quantum ratchet, the device still requires a nonequilibrium energy source. To this purpose, a strong tunable bias on the quantum point contact induces nonequilibrium energy fluctuations across the dividing central gate, thus promoting inelastic interdot tunneling inside the Coulomb blockaded double quantum dot. This in turn leads to a net quantum ratchet current flow, as plotted in Fig. 36. In the insets of the same figure, the interdot tunneling process is sketched for the right-to-left transition $[m, n+1] \rightarrow [m+1, n]$, with asymmetry energy $\Delta \equiv E_{m+1,n} - E_{m,n+1}$, and for the opposite left-to-right transition with energy $-\Delta$. Notably, a finite ratchet current is only observed if the electron energy states in the dots are detuned asymmetrically, i.e. when $\Delta \neq 0$. In contrast, a likely inelastic ionization of one dot towards its adjacent lead, followed by recharging from the same lead, does not result in a net current. The nonequilibrium energy fluctuations, carried by the quantum point contact electrons and absorbed by the electrons in the double quantum dot, could either consist of acoustic phonons, long wavelength photons or plasmons (Khrapai *et al.*, 2006).

The technology available to generate 2D electron gases can be generalized to ratchet not only charge but also spin carriers. The interplay of spatially periodic potentials, lateral confinement, spin-orbit or Zeeman-type interactions and ac driving then gives rise to directed *spin ratchet* currents, as theoretically proposed in recent studies (Scheid *et al.*, 2007a,b). Of particular experimental relevance is the recent theoretically predicted phe-

nomenon of a spin current which emerges via an unbiased ac charge current driving a dc spin current in a non-magnetic, dissipative spin quantum ratchet which is composed of an asymmetric periodic structure with Rashba spin-orbit interactions (Flatte, 2008; Smirnov *et al.*, 2008). Remarkably, this spin current occurs although *no* magnetic fields are present.

Likewise, substantial rectification of a spin current can also be achieved by coupling impurities to spatially asymmetric Luttinger liquids under ac voltage rocking (Braunecker *et al.*, 2007). The transport mechanism in those schemes is governed by coherent tunneling processes, which will be addressed in more detail in the following subsection.

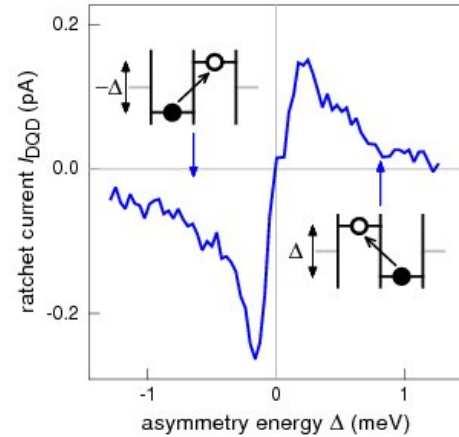


FIG. 36 (Color online) Experimental quantum ratchet current I_{DQD} measured through the double quantum dot as a function of its asymmetry energy Δ . The energy source is a nearby quantum point contact biased with $V_{QPC} = -1.55\text{ mV}$, see in Fig. 35. An elastic contribution to I_{DQD} is subtracted (Khrapai *et al.*, 2006). The two insets sketch the corresponding inelastic tunneling processes which drive the ratchet current. Notably, this quantum ratchet current vanishes when no finite zero asymmetry is present. Figure provided by Stefan Ludwig, Ludwig-Maximilians-University, Munich, Germany.

D. Coherent quantum ratchets

The study of quantum Brownian motors is far from being complete. Actually, there is an urgent need for further developments. In many cases the role of incoherent tunneling and coherent transport channels can not be clearly separated. For quantum devices built bottom-up with engineered molecules or artificial molecules such as quantum dots, the role of coherent quantum transport typically plays a dominant role, as other interactions like electron-phonon processes turn out to be negligible. The key transport process for quantum ratcheting is then driven coherent quantum tunneling (Grifoni and Hänggi, 1998; Kohler *et al.*, 2005).

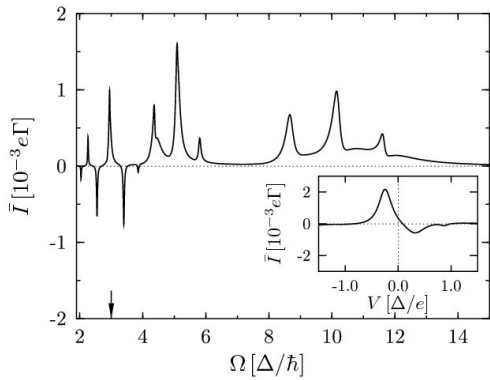


FIG. 37 Time-averaged current \bar{I} (measured in units of the lead coupling strength $e\Gamma$) as a function of the infrared drive angular frequency Ω (measured in units of the tunneling matrix element $\Delta = 0.1\text{eV}$ between sites for a laser amplitude $A = \Delta$ (Lehmann *et al.*, 2002). The inset displays the dependence of \bar{I} on the static voltage drop, V , applied along the molecule. Note that the current at zero voltage is *finite*, thereby indicating a ratchet effect. The driving frequency here corresponds to the vertical arrow in the main panel.

1. Quantum ratchets from molecular wires

This is the case of the quantum Brownian motors consisting of nanowires formed by asymmetric molecular groups and subjected to infrared light sources (Lehmann *et al.*, 2002), or symmetric molecular wires with symmetry breaking now provided by irradiating the wire with harmonic mixing signals (Lehmann *et al.*, 2003). The theoretically predicted quantum ratchet current through an asymmetric molecular wire irradiated by far-infrared light is displayed in Fig. 37.

In these class of quantum ratchets transport proceeds coherently between two or more fermionic leads that ensure the dissipative mechanism for the transported electrons to relax towards equilibrium Fermi distributions. Such a ratchet current can as well be used to sensitively probe the role of the electron correlations in the leads, as it is the case with a ratchet device coupled to Luttinger liquids rather than to Fermi liquids (Feldman *et al.*, 2005; Komnik and Gogolin, 2003).

2. Hamiltonian quantum ratchet for cold atoms

Much to one's surprise, systems governed by strictly Hamiltonian dynamics are able to yield directed transport, as well. Directed transport may then take place even though *no* dissipation mechanisms are present. Trivial such examples are provided by integrable regular dynamics subjected to unbiased ac-drives with *fixed initial phase*, i.e., not to be averaged over (Goychuk and Hänggi, 2001; Yevtushenko *et al.*, 2000). Much more intriguing are time-dependent driven Hamiltonian quantum Brownian motors exhibiting a nontrivial, mixed clas-

sical phase space structure (Denisov and Flach, 2001; Flach *et al.*, 2000; Schanz *et al.*, 2005, 2001). In these systems, the onset of a directed flow requires, apart from the necessity of breaking time reversal symmetry, also an additional dynamical symmetry breaking. As it turns out, in the semi-classical limit, the corresponding directed flow then obeys a remarkable sum rule: Directed currents occurring in regular regimes of the underlying phase space dynamics are counter-balanced by directed flows occurring in chaotic regimes in phase space (Schanz *et al.*, 2005, 2001). As a result, if those individual directed currents are summed up over all disjoint regimes in (semi)-classical mixed phase space, no net transport emerges.

The concept of Hamiltonian quantum Brownian motors extends as well to fully quantum systems governed by a unitary time-evolution (Denisov *et al.*, 2006, 2007; Gong *et al.*, 2007; Goychuk and Hänggi, 2000, 2001; Schanz *et al.*, 2005, 2001). In fact, the issue of pure quantum coherence in the directed transport of chaotic Hamiltonian systems is presently a topic of active research. This in particular holds true for cold atoms loaded in optical lattices: If properly detuned, the intrinsic quantum dynamics is then practically dissipation-free, thus providing a paradigm for Hamiltonian quantum ratchet transport. Various experimental cold atom ratchets have been realized (Sec. IV). Relevant to the topic of this section is also the demonstration of sawtooth-like, asymmetric cold atom potentials by Salger *et al.* (2007). All these systems are currently being employed to effectively shuttle cold matter on a quantum scale.

In the context of quantum ratchets for cold atoms one must distinguish the common case of “rectification of velocity”, implying that the mean position of particles is growing linearly in time, from the case with a “rectification of force”, i.e. with mean momentum growing linearly in time. The latter class is better classified as “quantum ratchet accelerators” (Gong and Brumer, 2004, 2006). In the context of cold atom ratchets the first situation is obtained by rocking a cold atom gas with temporally asymmetric driving forces or temporally asymmetrically flashing, in combination with spatially asymmetric potential kicks (Denisov *et al.*, 2007). The accelerator case originates from the physics of quantum δ -kicked cold atoms displaying quantum chaos features such as the quantum suppression of classical chaotic diffusion (dynamical localization) and the diametrically opposite phenomenon of *quantum resonance* (occurring when the kicking period is commensurate with the inverse recoil frequency). Under quantum resonance condition a linear (quadratic) increase of momentum (kinetic energy) takes place. These ratchet acceleration features, theoretically predicted in suitably modified kicked rotor models (Kenfack *et al.*, 2008; Lundh and Wallin, 2005; Poletti *et al.*, 2007b), requires tuning to *exact* resonance. In contrast, the accelerator models obtained from either a generalization of a quantum kicked rotor or a generalization of a kicked Harper model (Gong and Brumer, 2004, 2006; Wang and

Gong, 2008) are *generic* “rectifiers of force” in the sense that here no need for tuning to exact resonance is necessary. Interestingly, these fully quantum ratchet accelerators display unbounded linear growth of mean momentum, while the underlying classical dynamics is fully chaotic, a situation where classical quantum Brownian motor transport necessarily vanishes according to the above mentioned classical sum rule (Schanz *et al.*, 2005, 2001). Thus, within this full quantum regime, which carries no clear relationship with the dynamics in the semi-classical regime, the quantum accelerator work by Gong and Brumer (2006), see also (Wang and Gong, 2008), presents an intriguing and generic quantum mechanical exception to the classical sum rule.

Early quantum resonance experiments in quantum ratchet have already been successfully carried out: For a δ -kicked rotor model with time-symmetry broken by a 2-period kicking cycle (asymmetric temporal drive), directed growth of momentum has been detected by Jones *et al.* (2007). For a phase-dependent initial preparation of a Bose-Einstein condensate kicked at resonance, a momentum acceleration has been observed by Sadgrove *et al.* (2007) at zero quasimomentum, while for an arbitrary quasimomentum directed quantum Brownian transport has been realized in Dana *et al.* (2008). The latter experiment also evidenced that an intrinsic experimentally non-avoidable finite width in quasimomentum causes a suppression of the acceleration eventually leading to a saturation effect after short times.

This field of Hamiltonian quantum ratchets is presently undergoing a racy development. For example, it is possible to apply control schemes to relative phases for resulting single-particle quantum Brownian motor currents by harvesting Landau-Zener transitions (Morales-Molina *et al.*, 2008). Of particular theoretical and experimental interest is also the study of the role of nonlinearity on the size of directed quantum currents in interacting cold gases, as described within mean field theory by a nonlinear quantum ratchet evolution of the Gross-Pitaevskii-type. There, the interplay of time-dependent driving and *nonlinear* Floquet states yields new features, such as lifting of accidental symmetries (Poletti *et al.*, 2007a) and a resonant enhancement of directed ratchet currents (Morales-Molina and Flach, 2008).

IX. SUNDY TOPICS

In the following we discuss some classes of nanosystems and devices which feature directed transport in the spirit of Brownian motors. In these systems, however, rectification of Brownian motion does not constitute the main element for directed transport. We recall that an artificial Brownian motor is mainly noise-controlled, meaning that such a motor operates in a hardly predictable manner. In contrast, we discuss next systems that exhibit directed transport predominantly as the result of strong coupling schemes. Typical examples are adiabatic pump

scenarios of the peristaltic type, or nanosystems which are driven by unbiased, but asymmetric mechanical or chemical causes that are tightly coupled to resulting motion.

A. Pumping of charge, spin and heat

A first class of physical systems that comes to mind in relation to the working principles of artificial Brownian motors are nanoscale pump devices. Pumping is characterized by the occurrence of a net flux of particles, charges, spins and alike, in response to time dependent external manipulations of an otherwise unbiased system. This mechanism is well studied and peristaltic pumps are being widely exploited in technological applications. These systems do not require a periodic arrangement of components nor is thermal Brownian motion an issue for their operation. In particular, adiabatic turnstiles and pumps for charge and other degrees of freedom have attracted considerable interest both experimentally (Hoherger *et al.*, 2001; Kouwenhoven *et al.*, 1991; Pothier *et al.*, 1992; Switkes *et al.*, 1999) and theoretically (Aono, 2003; Brandes and Vorrath, 2002; Brouwer, 1998; Moskalets and Büttiker, 2004; Shutenko *et al.*, 2000; Sinitsyn and Nemenman, 2007; Spivak *et al.*, 1995; Thouless, 1983; Vavilov *et al.*, 2001; Zhou *et al.*, 1999).

Realizations of artificial pumps on the nanoscale often involve coupled quantum dots or superlattices. Most notably, in such peristaltic devices the number of transferred charges, or more generally, the number of transporting units per cycle is directly linked to the cycle period. As a result the output current thus becomes proportional to the driving frequency. This observation leads to the conclusion that high frequency nonadiabatic pumping might become more effective. Indeed, nonadiabatic pumping of charge, spin (Flatte, 2008; Scheid *et al.*, 2007a; Smirnov *et al.*, 2008) or also heat (Li *et al.*, 2008) does exhibit a rich phenomenology, including resonances (Arrachea *et al.*, 2007; Cota *et al.*, 2005; Kohler *et al.*, 2005; Moskalets and Büttiker, 2002; Platero and Aguado, 2004; Rey *et al.*, 2007; Stafford and Wingreen, 1996) and other potentially useful noise-induced features (Sanchez *et al.*, 2008; Strass *et al.*, 2005); hence yielding a close interrelation between *nonadiabatic* pumping in the presence of noise and the physics of Brownian motors.

B. Synthetic molecular motors and machines

As already emphasized in our introduction, the field of Brownian motors has its roots in the study and applications of intracellular transport in terms of molecular motors (Astumian and Hänggi, 2002; Jülicher *et al.*, 1997; Lipowsky and Klumpp, 2005; Reimann, 2002; Reimann and Hänggi, 2002; Wang and Oster, 2002). These molecular motors function in view of structure and motility by use of specialized proteins in living systems. These

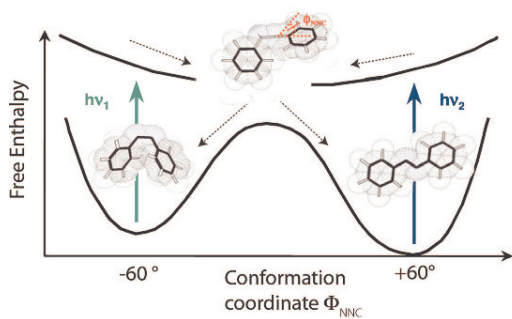


FIG. 38 (Color online) Free energy landscape of a single azobenzene molecule along the reaction coordinate of the conformation coordinate given by the bond angle Φ_{NNC} , which varies from about -60° to $\sim +60^\circ$. Transitions can be induced optically ($\lambda_1 \sim 420$ nm for the short *cis*-form (0.6 nm) and $\lambda_2 \sim 365$ nm for the extended *trans*-form (0.9 nm), respectively) from the singlet ground state S_0 into the excited singlet state S_1 , from which the molecule subsequently relaxes fluctuation-driven into either the *cis*-form or the *trans*-form. Notably, the *trans*-form is thermally favored. The insets depict the corresponding conformations with the transition state located near $\Phi_{NNC} \sim 0^\circ$. Figure provided by Thorsten Hugel from TU-Munich, Germany

biological motor enzymes are fueled by ATP hydrolysis and are able to efficiently perform mechanical work on the nanoscale inside biological cell structures (Howard, 2001; Schliwa, 2002).

Closely related to synthetic motors are the intriguing possibilities of devising DNA-fueled artificial motors: several settings render possible to biologically engineer nanomachines which move along *a priori* designed tracks (Turberfield *et al.*, 2003; Yin *et al.*, 2004; Yorke *et al.*, 2000).

An offspring of this topic is the engineering of nanomachines based on interlocked molecular species. This has spurred a flurry of new investigations within the physical biology and the organic and physical chemistry community, aimed at building bottom-up synthetic molecular systems which carry out such diverse functions as molecular switches, molecular rotors and any other kind of molecular gears.

A beautiful example of this class of molecular motor is the light powered molecular machine developed by Hugel *et al.* (2002). Bistable photosensitive azobenzene molecules can be synthesized into long chains, each containing molecules in either their *trans*- or *cis*-form. The free energy landscape corresponding to different molecule conformational states is sketched in Fig. 38 versus the reaction coordinate. Polymeric chains have the advantage of scaling up the length changes corresponding to the two different conformations of its constituents. The length changes of an azobenzene polymeric chains can then be transformed into mechanical energy by means of the lever arm of a atom force microscope (AFM) which, in combination with the light sources, forms the core of the light driven molecular motor of Fig. 39.

Such a molecular motor can be operated very much according to an idealized thermodynamic cycle of the Stirling type: Individual azobenzene polymers are made stretch and contract by inducing optical *trans*-*cis* transitions of their constituents. This machine thus demonstrates opto-mechanical energy conversion in a single-molecule motor device. The analogy with a thermodynamic cycle should though not be taken too seriously. A thermal Stirling engine operates between baths of differing temperature; here, the “expansion” and “compression” of the molecular motor are performed at a fixed temperature and, most notably, by means of nonequilibrium light sources. This laser operated molecular motor can as well be used as a building block to devise a bioinspired molecular locomotive which can be guided forth and back on a preassigned track via a laser assisted protocol (Wang, 2004).

In the operation of these synthetic nanoscale devices, especially when powered by light or chemical reactive additives, thermal noise does not necessarily play a major role, i.e. the function of these synthetic molecular motors is ruled predominantly by deterministic forces, forces that depend on the mechanical and chemical properties of the molecules (Neuert *et al.*, 2006). Yet, this area of research is fascinating and we therefore encourage the interested reader to read some recent items and tutorials (Astumian, 2007; Balzani *et al.*, 2006; Browne and Feringa, 2006; Porto *et al.*, 2000) and to consult the timely and most comprehensive reviews by Kottas *et al.* (2005) and Kay *et al.* (2007) for more details.

X. CONCLUDING REMARKS

With this review we have taken the reader on a tour of horizon through the many intriguing and multi-faceted applications that Brownian motion can offer in the most diverse areas of nanotechnology, when combined with spatio-temporal symmetry breaking, nonlinearity and, possibly, collective interaction effects.

The physics of classical and quantum Brownian motion is by now well established, also in consideration of the breadth of the theoretical modeling and experimental realizations produced over the last century. Many research activities are still spawning in interdisciplinary fields encompassing chemistry, biological research, information sciences and even are extending into social sciences and economics. The main lesson to be learned from Robert Brown’s and Albert Einstein’s work is therefore: Rather than fighting thermal motion, we should put it to work to our advantage. Brownian motors thrive from these ceaseless noise source to efficiently direct, separate, pump and shuttle degrees of freedom of differing nature reliably and effectively.

In writing this overview we spared no efforts in covering a wide range of interesting developments and potential achievements. In doing so we nevertheless had to make some selective choices of topics and applications, which

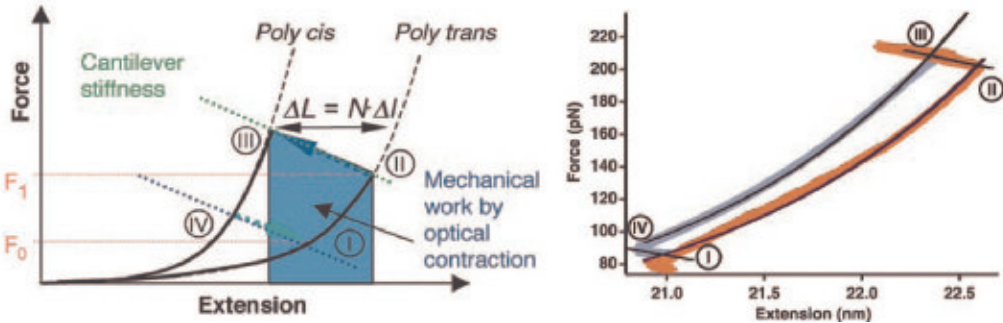


FIG. 39 (Color online) Operation of a light powered molecular motor: The panel on the left depicts the schematic force extension cycle for the opto-mechanical energy conversion cycle of a single poly-azobenzene. In analogy to a thermodynamic Stirling-cycle, the polymer is first stretched by the AFM-tip acting as the piston (I \rightarrow II). Then, the application of the first optical excitation with $\lambda_2 \simeq 365\text{nm}$ shortens the polymer by inducing a (poly)*trans*- (poly)*cis* transition. This yields a first part of work (blue area) in bending the AFM cantilever, which is clearly not as stiff as a piston in a common Stirling motor. In analogy to the Stirling cycle, another amount of work is done during the relaxation of the polymer (III \rightarrow IV). Finally, a second optical excitation with $\lambda_1 \simeq 420\text{nm}$ is needed to reset the molecule into its starting (poly)*trans*-state (IV \rightarrow I). The total work output of the system is the mechanical energy corresponding to the contraction ($\Delta L = N\Delta l$) of the entire polymer chain of N azobenzenes against the external load. The experimental realization of a full single molecule operating cycle (Hugel *et al.*, 2002) is depicted in the panel on the right. Figure provided by Thorsten Hugel from TU-Munich, Germany

to some extent reflect the authors' preferences and prejudices. Closely related topics of ongoing research were not reviewed for space limits. For example, in Sec. IX.B we did not cover in sufficient detail the fascinating topic of ATP-driven molecular motors and DNA-fueled motors, for which we refer to earlier comprehensive reviews and books, like in Jülicher *et al.* (1997), Howard (2001), Schliwa (2002), and Lipowsky and Klumpp (2005). This surely is the case of the bottom-up design and operation of synthetic Brownian molecular devices, extensively covered by the excellent review of Kay *et al.* (2007). Another such topic is the question of the so-called absolute negative mobility, which occurs via quantum tunneling events in quantum systems (Aguado and Platero, 1997; Grifoni and Hänggi, 1998; Keay *et al.*, 1995; Platero and Aguado, 2004) and through mere nonequilibrium driven diffusive dynamics in classical systems (Eichhorn *et al.*, 2002a,b; Kostur *et al.*, 2008; Machura *et al.*, 2007a; Ros *et al.*, 2005).

Our main focus was on noise-assisted directional transport, shuttling and pumping of individual or collective particle-, charge- or matter-degrees of freedom. The concept, however, extends as well to the transport of other degrees of freedom such as energy (heat) and spin modes (see also in Sec.(IX.A)). Both topics are experiencing a surge of interest with new exciting achievements being reported in the current literature. The concept carries potential for yet other applications. Examples that come to mind are the noise-assisted directional transport and transfer of informational degrees of freedom such as probability or entropy and, within a quantum context, the shuttling of entanglement information. These issues immediately relate to the energetics of artificial Brownian motors reviewed in Sec. (II.E), including measures of open and closed loop control scenarios and other opti-

mization schemes.

We have attempted to catch the potential of Brownian motors in nowadays nanotechnology by putting them to work; we discussed how such motors can be constructed and characterized, and how directional, Brownian motion driven transport can be controlled, measured, and optimized. Moreover, we are confident that the interdisciplinary style of this overview shall encourage the readers to bring in new approaches and motivations in this challenging and fast growing research area.

Acknowledgments

This review would not have emerged without continuous support from and insightful discussions with our close collaborators and colleagues. We first express our gratitude to all members of our work groups among which special credit should be given to M. Borromeo, J. Dunkel, I. Goychuk, G.L. Ingold, S. Kohler, G. Schmid, P. Talkner, and U. Thiele for their scientific contributions and personal encouragement. A special thanks goes to our many colleagues and friends who also engaged in the field of Brownian motors and, in particular, to R.D. Astumian, M. Bier, C. Van den Broeck, J. Casado Pascual, D. Hennig, W. Ebeling, J.A. Freund, L. Gammaiton, H.E. Gaub, E. Goldobin, M. Grifoni, P. Jung, J. Kärger, I. Kosinska, J.P. Kotthaus, M. Kostur, H. Linke, B.-W. Li, J. Luczka, S. Ludwig, L. Machura, V.R. Misko, M. Morillo, F. Nori, J. Prost, P. Reimann, F. Renzoni, K. Richter, M. Rubí, S. Savel'ev, L. Schimansky-Geier, Z. Siwy, B. Spagnolo, and A. Vulpiani. In addition, we are indebted to M. Borromeo, M. Grifoni, T. Hugel, H. Linke, S. Ludwig, V.S. Khrapai, F. Müller, S. Savelev, U. Thiele and C. Van den Broeck for providing us with

original figures and unpublished material. Finally, we wish to thank the senior editor of *Reviews of Modern Physics*, Prof. Achim Richter, for the invitation to write the present review and his most efficient handling of our submission.

F.M. wishes to thank Prof. Hunggyu Park for his kind hospitality at the Korea Institute for Advanced Study and, likewise, P.H. for the kind hospitality at the Physics Department of the National University of Singapore: At these two institutions we were both given the opportunity to efficiently continue working on a preliminary version of this review. P.H. acknowledges the financial support by the Deutsche Forschungsgemeinschaft via the Collaborative Research Centre SFB-486, project A10, B 13 and by the German Excellence Cluster *Nanosystems Initiative Munich* (NIM). Both authors thank the Alexander von Humboldt Stiftung, who made this joint project possible by granting to one of us (F.M.) a Research Award to visit the Universität Augsburg, where most of the work was done.

References

Abrikosov, A. A., 1957, "On the magnetic properties of superconductors of the second group," *Soviet Physics JETP* **5**, 1174–1183.

Aghababaie, Y., G. I. Menon, and M. Plischke, 1999, "Universal properties of interacting Brownian motors," *Phys. Rev. E* **59**, 2578–2586.

Aguado, R., and G. Platero, 1997, "Dynamical localization and absolute negative conductance in an ac-driven double quantum well," *Phys. Rev. B* **55**, 12860–12863.

Ai, B.-Q., and L.-G. Liu, 2006, "Current in a three-dimensional periodic tube with unbiased forces," *Phys. Rev. E* **74**, 051114.

Ajdari, A., and J. Prost, 1992, "Drift induced by a spatially periodic potential of low symmetry - Pulsated dielectrophoresis," *C. R. Acad. Sci. Paris (Ser. II)* **315**, 1635–1639.

Aksimentiev, A., J. B. Heng, G. Timp, and K. Schulten, 2004, "Microscopic kinetics of DNA translocation through synthetic nanopores," *Biophys. J.* **87**, 2086–2097.

Altshuler, E., and T. H. Johansen, 2004, "Colloquium: Experiments in vortex avalanches," *Rev. Mod. Phys.* **76**, 471–487.

Ankerhold, J., P. Pechukas, and H. Grabert, 2001, "Strong friction limit in quantum mechanics: The quantum Smoluchowski equation," *Phys. Rev. Lett.* **87**, 086802.

Aono, T., 2003, "Adiabatic spin pumping through a quantum dot with a single orbital level," *Phys. Rev. B* **67**, 155303.

Arrachea, L., M. Moskalets, and L. Martin-Moreno, 2007, "Heat production and energy balance in nanoscale engines driven by time-dependent fields," *Phys. Rev. B* **75**, 245420.

Arvanitidou, E., and D. Hoagland, 1991, "Chain-length dependence of the electrophoretic mobility in random gels," *Phys. Rev. Lett.* **67**, 1464–1466.

Ashkenasy, N., J. Sánchez-Quesada, H. Bayley, and M. R. Ghadiri, 2005, "Recognizing a single base in an individual DNA strand: A step toward DNA sequencing in nanopores," *Angew. Chem. Int. Ed.* **44**, 1401–1404.

Astumian, R. D., 1997, "Thermodynamics and kinetics of a Brownian motor," *Science* **276**, 917–922.

Astumian, R. D., 2007, "Design principles for Brownian molecular machines: how to swim in molasses and walk in a hurricane," *Phys. Chem. Chem. Phys.* **9**, 5067–5083.

Astumian, R. D., and M. Bier, 1994, "Fluctuation driven ratchets: Molecular motors," *Phys. Rev. Lett.* **72**, 1766–1769.

Astumian, R. D., and I. Derényi, 1998, "Fluctuation driven transport and models of molecular motors and pumps," *Eur. Biophys. J.* **27**, 474–489.

Astumian, R. D., and P. Hänggi, 2002, "Brownian motors," *Phys. Today* **55**(11), 33–39.

Babic, D., and C. Bechinger, 2005, "Noise-enhanced performance of ratchet cellular automata," *Phys. Rev. Lett.* **94**.

Babic, D., C. Schmitt, and C. Bechinger, 2005, "Colloids as model systems for problems in statistical physics," *Chaos* **15**, 026114.

Bader, J. S., R. W. Hammond, S. A. Henck, M. W. Deem, G. A. McDermott, J. M. Bustillo, J. W. Simpson, G. T. Mulhern, and J. M. Rothberg, 1999, "DNA transport by a micromachined Brownian ratchet device," *Proc. Natl. Acad. Sci.* **96**, 13165–13169.

Baker, G. L., and J. P. Gollub, 1990, *Chaotic Dynamics* (Cambridge University Press, Cambridge).

Baltanás, J. P., L. López, I. I. Blechman, P. S. Landa, A. Zaikin, J. Kurths, and M. A. F. Sanjuán, 2003, "Experimental evidence, numerics, and theory of vibrational resonance in bistable systems," *Phys. Rev. E* **67**, 066119.

Balzani, V., A. Credi, S. Silvi, and M. Venturi, 2006, "Artificial nanomachines based on interlocked molecular species: Recent advances," *Chem. Soc. Rev.* **35**, 1135–1149.

Bao, J. D., 1999, "Directed current of Brownian ratchet randomly circulating between two thermal sources," *Physica A* **273**, 286–293.

Barone, A., and G. Paternò, 1982, *Physics and Applications of the Josephson Effect* (Wiley, New York).

Bartussek, R., and P. Hänggi, 1995, "Brownsche Motoren: Wie aus Brownscher Bewegung makroskopischer Transport wird," *Phys. Blätter* **51**(6), 506–507.

Bartussek, R., P. Hänggi, and J. G. Kissner, 1994, "Periodically rocked thermal ratchets," *Europhys. Lett.* **28**, 459–464.

Bartussek, R., P. Reimann, and P. Hänggi, 1996, "Precise numerics versus theory for correlation ratchets," *Phys. Rev. Lett.* **76**, 1166–1169.

Baumgärtner, A., and J. Skolnick, 1995, "Spontaneous translocation of a polymer across a curved membrane," *Phys. Rev. Lett.* **74**, 2142–2145.

Beck, M., E. Goldobin, M. Neuhaus, M. Siegel, R. Kleiner, and D. Koelle, 2005, "High-efficiency deterministic Josephson vortex ratchet," *Phys. Rev. Lett.* **95**, 090603.

Berezhkovskii, A. M., M. Pustovoit, and S. M. Bezrukov, 2003, "Channel-facilitated membrane transport: Average lifetimes in the channel," *J. Chem. Phys.* **119**, 3943–3951.

Berger, J., 2004, "Noise rectification by a superconducting loop with two weak links," *Phys. Rev. B* **70**, 024524.

Bier, M., M. Kostur, I. Derényi, and R. D. Astumian, 2000, "Nonlinearly coupled flows," *Phys. Rev. E* **61**, 7184–7187.

Blatter, G., M. V. Feigel'man, V. B. Geshkenbein, A. I. Larkin, and V. M. Vinokur, 1994, "Vortices in high-temperature superconductors," *Rev. Mod. Phys.* **66**, 1125–1388.

Bleckman, I. I., 2000, *Vibrational Mechanics* (World Scien-

tific, Singapore).

Bleil, S., P. Reimann, and C. Bechinger, 2007, "Directing Brownian motion by oscillating barriers," *Phys. Rev. E* **75**, 031117.

Borromeo, M., G. Costantini, and F. Marchesoni, 1999, "Critical hysteresis in a tilted washboard potential," *Phys. Rev. Lett.* **82**, 2820–2823.

Borromeo, M., G. Costantini, and F. Marchesoni, 2002, "Deterministic ratchets: Route to diffusive transport," *Phys. Rev. E* **65**, 041110.

Borromeo, M., S. Giusepponi, and F. Marchesoni, 2006, "Recycled noise rectification: An automated Maxwell's daemon," *Phys. Rev. E* **74**, 031121.

Borromeo, M., and F. Marchesoni, 1998, "Brownian surfers," *Phys. Lett. A* **249**, 199–203.

Borromeo, M., and F. Marchesoni, 2000, "Backward-to-forward jump rates on a tilted periodic substrate," *Phys. Rev. Lett.* **84**, 203–207.

Borromeo, M., and F. Marchesoni, 2004, "Asymmetric confinement in a noisy bistable device," *Europhys. Lett.* **68**, 783–789.

Borromeo, M., and F. Marchesoni, 2005a, "Mobility oscillations in high-frequency modulated devices," *Europhys. Lett.* **72**, 362–368.

Borromeo, M., and F. Marchesoni, 2005b, "Noise-assisted transport on symmetric periodic substrates," *Chaos* **15**, 026110.

Borromeo, M., and F. Marchesoni, 2006, "Vibrational ratchets," *Phys. Rev. E* **73**, 016142.

Borromeo, M., and F. Marchesoni, 2007a, "Artificial sieves for quasimassless particles," *Phys. Rev. Lett.* **99**, 150605.

Borromeo, M., and F. Marchesoni, 2007b, "Stochastic synchronization via noise recycling," *Phys. Rev. E* **75**, 041106.

Brandes, T., and T. Vorrath, 2002, "Adiabatic transfer of electrons in coupled quantum dots," *Phys. Rev. B* **66**, 075341.

Braunecker, B., D. E. Feldman, and F. Li, 2007, "Spin current and rectification in one-dimensional electronic systems," *Phys. Rev. B* **76**, 085119.

Brey, J., F. Moreno, R. García-Rojo, and M. J. Ruiz-Montero, 2001, "Hydrodynamic Maxwell demon in granular systems," *Phys. Rev. E* **65**, 011305.

Breymayer, H. J., and W. Wonneberger, 1981, "Asymptotics of harmonic microwave mixing in a sinusoidal potential," *Z. Phys. B* **43**, 329–334.

Van den Broeck, C., and R. Kawai, 2006, "Brownian refrigerator," *Phys. Rev. Lett.* **96**, 210601.

Van den Broeck, C., R. Kawai, and P. Meurs, 2004, "Microscopic analysis of a thermal Brownian motor," *Phys. Rev. Lett.* **93**, 090601.

Van den Broeck, C., P. Meurs, and R. Kawai, 2005, "From Maxwell demon to Brownian motor," *New J. Phys.* **7**, 10.

den Broeck, C. V., 2005, "Thermodynamic efficiency at maximum power," *Phys. Rev. Lett.* **95**, 190602.

den Broeck, C. V., 2007, "Carnot efficiency revisited," *Adv. Chem. Phys.* **135**, 189–201.

den Broek, M. V., and C. V. den Broeck, 2008, "Chiral Brownian heat pump," *Phys. Rev. Lett.* **100**, 130601.

Brouwer, P. W., 1998, "Scattering approach to parametric pumping," *Phys. Rev. B* **58**, R10135–R10138.

Browne, W. R., and B. L. Feringa, 2006, "Making molecular machines work," *Nature Nanotechnol.* **1**, 25–35.

Bug, A. L. R., and B. J. Berne, 1987, "Shaking-induced transition to a nonequilibrium state," *Phys. Rev. Lett.* **59**, 948.

Buguin, A., L. Talini, and P. Silberzan, 2002, "Ratchet-like topological structures for the control of microdrops," *Appl. Phys. A-Mater.* .

Burada, P. S., P. Hänggi, G. Schmid, and P. Talkner, 2009, "Diffusion in confined geometries," *ChemPhysChem* **yy**, xxxx; arXiv:0808.2345.

Bustamante, C., J. Liphardt, and F. Ritort, 2005, "The nonequilibrium thermodynamics of small systems," *Phys. Today* **58**(7), 43–48.

Caldeira, A. O., and A. J. Leggett, 1983, "Quantum tunneling in a dissipative system," *Ann. Phys.* **149**, 374–456.

Caldeira, A. O., and A. J. Leggett, 1984, "Correction," *Ann. Phys.* **153**, 445–445.

Carapella, G., and G. Costabile, 2001, "Ratchet effect: Demonstration of a relativistic fluxon diode," *Phys. Rev. Lett.* **87**, 077002.

Carlo, G. G., G. Benenti, G. Casati, and D. L. Shepelyansky, 2005, "Quantum ratchets in dissipative chaotic systems," *Phys. Rev. Lett.* **94**, 164101.

Chang, C. W., D. Okawa, A. Majumdar, and A. Zettl, 2006, "Solid-state thermal rectifier," *Science* **314**, 1121–1124.

Chauwin, J. F., A. Ajdari, and J. Prost, 1994, "Force-free motion in asymmetric structures - a mechanism without diffusive steps," *Europhys. Lett.* **27**, 421–426.

Chen, Y.-d., 1997, "Asymmetric cycling and biased movement of Brownian particles in fluctuating symmetric potentials," *Phys. Rev. Lett.* **79**, 3117–3120.

Chepelianskii, A. D., and D. L. Shepelyansky, 2005, "Directing transport by polarized radiation in the presence of chaos and dissipation," *Phys. Rev. B* **71**, 052508.

Chialvo, D., M. Dykman, and M. Millonas, 1997, "Fluctuation-induced transport in a periodic potential: Noise versus chaos," *Phys. Rev. Lett.* **78**, 1605.

Chou, C. F., O. Bakajin, S. W. P. Turner, T. A. J. Duke, S. S. Chan, E. C. Cox, H. G. Craighead, and R. Austin, 1999, "Sorting by diffusion: An asymmetric obstacle course for continuous molecular separation," *Proc. Natl. Acad. Sci.* **96**, 13762–13765.

Chow, W. W., J. Gea-Banacloche, L. M. Pedrotti, V. E. Sanders, W. Schleich, and M. O. Scully, 1985, "The ring laser gyro," *Rev. Mod. Phys.* **57**, 61.

Cleuren, B., and C. Van den Broeck, 2007, "Granular Brownian motor," *EPL* **77**, 50003.

Cole, D., S. Bending, S. Savel'ev, A. Grigorenko, T. Tamegai, and F. Nori, 2006, "Ratchet without spatial asymmetry for controlling the motion of magnetic flux quanta using time-asymmetric drives," *Nature Materials* **5**, 305–311.

Collins, P. G., and P. Avouris, 2000, "Nanotubes for electronics," *Scientific American* **283**, 62–69.

Constantin, D., and Z. S. Siwy, 2007, "Poisson-Nernst-Planck model of ion current rectification through a nanofluidic diode," *Phys. Rev. E* **76**, 041202.

Costantini, G., and F. Marchesoni, 1999, "Threshold diffusion in a tilted washboard potential," *Europhys. Lett.* **48**, 491–497.

Costantini, G., F. Marchesoni, and M. Borromeo, 2002, "String ratchets: ac driven asymmetric kinks," *Phys. Rev. E* **65**, 051103.

Costantini, G., U. M. B. Marconi, and A. Puglisi, 2007, "Granular Brownian ratchet model," *Phys. Rev. E* **75**, 061124.

Costantini, G., U. M. B. Marconi, and A. Puglisi, 2008, "Noise rectification and fluctuations of an asymmetric inelastic pis-

ton.”

Cota, E., R. Aguado, and G. Platero, 2005, “ac-Driven double quantum dots as spin pumps and spin filters,” *Phys. Rev. Lett.* **94**, 107202.

Craig, E. M., N. J. Kuwada, B. J. Lopez, and H. Linke, 2008a, “Feedback control in flashing ratchets,” *Ann. Physik (Berlin)* **17**, 115–129.

Craig, E. M., B. R. L. and J. M. R. Parrondo, and H. Linke, 2008b, “Effect of time delay on feedback control of a flashing ratchet,” *EPL-Europhys. Lett.* **81**, 10002.

Crisan, A., A. Pross, D. Cole, S. J. Bending, R. Wördenweber, P. Lahl, and E. H. Brandt, 2005, “Anisotropic vortex channelling in $\text{YBa}_2\text{Cu}_3\text{O}_{7-\delta}$ thin films with ordered antidot arrays,” *Phys. Rev. B* **71**, 144504.

Crooks, G. E., 1999, “Entropy production fluctuation theorem and the nonequilibrium work relation for free energy differences,” *Phys. Rev. E* **60**, 2721–2726.

Curzon, F. L., and B. Ahlborn, 1975, “Efficiency of a Carnot engine at maximum power output,” *Am. J. Phys.* **43**, 22–24.

Daiguji, H., Y. Oka, and K. Shirono, 2005, “Nanofluidic diode and bipolar transistor,” *Nano Lett.* **5**, 2274–2280.

Dana, I., V. Ramareddy, I. Talukdar, and G. S. Summy, 2008, “Experimental realization of quantum-resonance ratchets at arbitrary quasimomenta,” *Phys. Rev. Lett.* **100**, 024103.

Daniel, S., S. Sircar, J. Gliem, and M. K. Chaudhury, 2004, “Ratcheting motion of liquid drops on gradient surfaces,” *Langmuir* **20**, 4085–4092.

Dekker, C., 1999, “Carbon nanotubes as molecular quantum wires,” *Phys. Today* **52**(5), 22–28.

Dekker, C., 2007, “Solid-state nanopores,” *Nat. Nanotechnol.* **2**, 209–215.

Denisov, S., and S. Flach, 2001, “Dynamical mechanisms of dc current generation in driven Hamiltonian systems,” *Phys. Rev. E* **64**, 056236.

Denisov, S., S. Flach, and P. Hänggi, 2006, “Stationary Hamiltonian transport with dc bias,” *Europhys. Lett.* **74**, 588–594.

Denisov, S., S. Kohler, and P. Hänggi, 2008, “Underdamped quantum ratchets: Attractors and currents.”

Denisov, S., L. Morales-Molina, S. Flach, and P. Hänggi, 2007, “Periodically driven quantum ratchets: Symmetries and resonances,” *Phys. Rev. A* **75**, 063424.

Derényi, I., and A. Ajdari, 1996, “Collective transport of particles in a “flashing” periodic potential,” *Phys. Rev. E* **54**, R5–R8.

Derényi, I., and T. Vicsek, 1995, “Cooperative transport of Brownian particles,” *Phys. Rev. Lett.* **75**, 374–377.

Derouane, E. G., and Z. Gabelica, 1980, “A novel effect of shape selectivity - Molecular traffic control in zeolite ZSM-5,” *J. Catal.* **65**, 486–489.

Dholakia, K., M. P. MacDonald, P. Zemanek, and T. Cizmar, 2007, “Cellular and colloidal separation using optical forces,” *Method Cell. Biol.* **82**, 467–495.

Doering, C. R., W. Horsthemke, and J. Riordan, 1994, “Nonequilibrium fluctuation-induced transport,” *Phys. Rev. Lett.* **72**, 2984–2987.

Dresselhaus, M. S., G. Dresselhaus, and P. C. Eklund, 1996, *The Science of Fullerenes and Carbon Nanotubes* (Academic Press, New York).

Drexler, K. E., 1992, *Nanosystems: Molecular Machinery, Manufacturing and Computation* (Wiley, New York).

Duke, T. A. J., and R. H. Austin, 1998, “Microfabricated sieve for the continuous sorting of macromolecules,” *Phys. Rev. Lett.* **80**, 1552–1555.

Eggers, J., 1999, “Sand as Maxwell’s demon,” *Phys. Rev. Lett.* **83**, 5322–5325.

Eichhorn, R., P. Reimann, and P. Hänggi, 2002a, “Brownian motion exhibiting absolute negative mobility,” *Phys. Rev. Lett.* **98**, 040601.

Eichhorn, R., P. Reimann, and P. Hänggi, 2002b, “Paradoxical motion of a single Brownian particle: Absolute negative mobility,” *Phys. Rev. E* **66**, 066132.

Ellmann, H., J. Jersblad, and A. Kastberg, 2003, “Experiments with a 3D double optical lattice,” *Phys. Rev. Lett.* **90**, 053001.

Engel, A., and P. Reimann, 2004, “Thermal ratchet effects in ferrofluids,” *Phys. Rev. E* **70**, 051107.

Ertas, D., 1998, “Lateral separation of macromolecules and polyelectrolytes in microlithographic arrays,” *Phys. Rev. Lett.* **80**, 1548–1551.

Falo, F., P. J. Martinez, J. J. Mazo, T. P. Orlando, K. Segall, and E. Trias, 2002, “Fluxon ratchet potentials in superconducting circuits,” *Appl. Phys. A-Mater.* **75**, 263–269.

Farkas, Z., F. Szalai, D. E. Wolf, and T. Vicsek, 2002, “Segregation of granular binary mixtures by a ratchet mechanism,” *Phys. Rev. E* **65**, 022301.

Faucheux, L. P., L. S. Bourdieu, P. D. Kaplan, and A. J. Libchaber, 1995, “Optical thermal ratchet,” *Phys. Rev. Lett.* **74**, 1504–1507.

Faucheux, L. P., and A. Libchaber, 1995, “Selection of Brownian particles,” *J. Chem. Soc. - Faraday Trans.* **91**, 3163–3166.

Feito, M., and F. J. Cao, 2007, “Information and maximum power in a feedback controlled Brownian ratchet,” *Eur. Phys. J. B* **59**, 63–68.

Feito, M., and F. J. Cao, 2008, “Transport reversal in a delayed feedback ratchet,” *Physica A* **387**, 4553–4559.

Feldman, D. E., S. Scheidl, and V. M. Vinokur, 2005, “Rectification in Luttinger liquids,” *Phys. Rev. Lett.* **94**, 186809.

Fenzke, D., and J. Kärger, 1993, “On the correlation between the step rates and the diffusivities of guest molecules in microporous crystal,” *Z. Phys. D* **25**, 345–350.

Ferrando, R., R. Spadacini, and G. E. Tommei, 1995, “Retrapping and velocity inversion in jump diffusion,” *Phys. Rev. E* **51**, 126–130.

Festa, R., and E. G. d’Agliano, 1978, “Diffusion coefficient for a Brownian particle in a periodic field of force: I. Large friction limit,” *Physica A* **90**, 229–244.

Feynman, R. P., 1960, *There’s plenty of room at the bottom* (Caltech’s Engineering & Science Magazine, Pasadena).

Feynman, R. P., R. B. Leighton, and M. Sands, 1963, *The Feynman Lectures on Physics*, volume I (Addison-Wesley, Reading, MA).

Flach, S., O. Yevtushenko, and Y. Zolotaryuk, 2000, “Directed current due to broken time-space symmetry,” *Phys. Rev. Lett.* **84**, 2358–2361.

Flatte, M. E., 2008, “Spin ratchets: A one-way street for spin current,” *Nature Physics* **4**, 587–588.

Fleischer, R. L., P. B. Price, and R. M. Walker, 1975, *Nuclear Tracks in Solids. Principles and Applications* (University of California Press, Berkeley).

Freund, J. A., and L. Schimansky-Geier, 1999, “Diffusion in discrete ratchets,” *Phys. Rev. E* **60**, 1304–1309.

Gallavotti, G., and E. G. D. Cohen, 1995, “Dynamical ensembles in nonequilibrium statistical mechanics,” *Phys. Rev. Lett.* **74**, 2694–2697.

Gammaitoni, L., P. Hänggi, P. Jung, and F. Marchesoni, 1998,

"Stochastic resonance," *Rev. Mod. Phys.* **70**, 223–287.

Gao, Y. H., and Y. Bando, 2002, "Carbon nanothermometer containing gallium - Gallium's macroscopic properties are retained on a miniature scale in this nanodevice," *Nature* **415**, 599–599.

Geisel, T., and J. Nierwetberg, 1982, "Onset of diffusion and universal scaling in chaotic systems," *Phys. Rev. Lett.* **48**, 7–10.

Gerland, U., R. Bundschuh, and T. Hwa, 2004, "Translocation of structured polynucleotides through nanopores," *Physical Biology* **1**, 19–26.

Gillijns, W., A. V. Silhanek, V. V. Moshchalkov, C. J. O. Reichhardt, and C. Reichhardt, 2007, "Origin of reversed vortex ratchet motion," *Phys. Rev. Lett.* **99**, 247002.

Gommers, R., S. Bergamini, and F. Renzoni, 2005, "Dissipation-induced symmetry breaking in a driven optical lattice," *Phys. Rev. Lett.* **95**, 073003.

Gommers, R., M. Brown, and F. Renzoni, 2007, "Symmetry and transport in a cold atom ratchet with multifrequency driving," *Phys. Rev. A* **75**, 053406.

Gommers, R., S. Denisov, and F. Renzoni, 2006, "Quasiperiodically driven ratchets for cold atoms," *Phys. Rev. Lett.* **96**, 240604.

Gommers, R., V. Lebedev, M. Brown, and F. Renzoni, 2008, "Gating ratchet for cold atoms," *Phys. Rev. Lett.* **100**, 040603.

Gong, J., and P. Brumer, 2004, "Directed anomalous diffusion without a biased field: A ratchet accelerator," *Phys. Rev. E* **70**, 016202.

Gong, J., and P. Brumer, 2006, "Generic quantum ratchet accelerator with full classical chaos," *Phys. Rev. Lett.* **97**, 240602.

Gong, J., D. Poletti, and P. Hänggi, 2007, "Dissipationless directed transport in rocked single-band quantum dynamics," *Phys. Rev. A* **75**, 033602.

Gonzalez, M., N. O. Nunez, J. V. Anguita, and J. L. Vincent, 2007, "Transverse rectification in superconducting thin films with arrays of asymmetric defects," *Appl. Phys. Lett.* **91**, 062505.

Gorman, M., M. el Hamdi, B. Pearson, and K. A. Robbins, 1996, "Ratcheting motion of concentric rings in cellular flames," *Phys. Rev. Lett.* **76**, 228–231.

Gorre, L., E. Ioannidis, and P. Silberzan, 1996, "Rectified motion of a mercury drop in an asymmetric structure," *Europhys. Lett.* **33**, 267–272.

Goychuk, I., 2006, "Chemically driven electron tunneling pumps," *Molecular Simulation* **32**, 717–725.

Goychuk, I., M. Grifoni, and P. Hänggi, 1998a, "Addendum," *Phys. Rev. Lett.* **81**, 2837–2837.

Goychuk, I., M. Grifoni, and P. Hänggi, 1998b, "Nonadiabatic quantum Brownian rectifiers," *Phys. Rev. Lett.* **81**, 649–652.

Goychuk, I., and P. Hänggi, 1998, "Quantum rectifiers from harmonic mixing," *Europhys. Lett.* **43**, 503–509.

Goychuk, I., and P. Hänggi, 2000, "Directed current without dissipation: reincarnation of a Maxwell-Loschmidt demon," *Lect. Notes Phys.* **557**, 7–20.

Goychuk, I., and P. Hänggi, 2001, "Minimal quantum Brownian rectifiers," *J. Phys. Chem. B* **105**, 6642–6647.

Goychuk, I., and P. Hänggi, 2005, "Quantum dynamics in strong fluctuating fields," *Adv. Phys.* **54**, 525–584.

Grier, D. G., 2003, "A revolution in optical manipulation," *Nature* **424**, 810–816.

Grifoni, M., M. S. Ferreira, J. Peguiron, and J. B. Majer, 2002, "Quantum ratchets with few bands below the barrier," *Phys. Rev. Lett.* **89**, 146801.

Grifoni, M., and P. Hänggi, 1998, "Driven quantum tunneling," *Phys. Rep.* **304**, 229–354.

Grigorenko, A., S. Bending, T. Tamegai, S. Ooi, and M. Henini, 2001, "A one-dimensional chain state of vortex matter," *Nature* **414**, 728–731.

Gross, M., 1999, *Travels To The Nanoworld* (Perseus, New York).

Grossmann, S., and H. Fujisaka, 1982, "Diffusion in discrete nonlinear dynamical systems," *Phys. Rev. A* **26**, 1779–1782.

Grynberg, G., and C. Robilliard, 2001, "Cold atoms in dissipative optical lattices," *Phys. Rep.* **355**, 335–451.

Han, J., and H. G. Craighead, 2000, "Separation of long DNA molecules in a microfabricated entropic trap array," *Science* **288**, 1026–1029.

Han, J., S. W. Turner, and H. G. Craighead, 1999, "Entropic trapping and escape of long DNA molecules at submicron size constriction," *Phys. Rev. Lett.* **83**, 1688–1691.

Hänggi, P., and R. Bartussek, 1996, "Brownian rectifiers: How to convert Brownian motion into directed transport," *Lect. Notes Phys.* **476**, 294–308.

Hänggi, P., R. Bartussek, P. Talkner, and J. Luczka, 1996, "Noise-induced transport in symmetric periodic potentials: White shot noise versus deterministic noise," *Europhys. Lett.* **35**, 315–317.

Hänggi, P., and G.-L. Ingold, 2005, "Fundamental aspects of quantum Brownian motion," *Chaos* **15**, 026105.

Hänggi, P., P. Jung, and F. Marchesoni, 1989, "Escape driven by strongly colored noise," *J. Stat. Phys.* **54**, 1367–1380.

Hänggi, P., F. Marchesoni, and F. Nori, 2005, "Brownian motors," *Ann. Phys. (Leipzig)* **14**, 51–70.

Hänggi, P., M. Ratner, and S. Yaliraki, 2002, "Transport in molecular wires, Preface," *Chem. Phys.* **281**, 111–111.

Hänggi, P., P. Talkner, and M. Borkovec, 1990, "Reaction-rate theory: Fifty years after Kramers," *Rev. Mod. Phys.* **62**, 251–341.

Hänggi, P., and H. Thomas, 1982, "Stochastic processes: Time-evolution, symmetries and linear response," *Phys. Rep.* **88**, 207–319.

Harada, K., O. Kamimura, H. Kasai, T. Matsuda, A. Tonomura, and V. V. Moshchalkov, 1996, "Direct observation of vortex dynamics in superconducting films with regular arrays of defects," *Science* **274**, 1167–1170.

Harms, T., and R. Lipowsky, 1997, "Driven ratchets with disordered tracks," *Phys. Rev. Lett.* **79**, 2895–2898.

Harris, T. E., 1974, "Contact interactions on a lattice," *Ann. Prob.* **2**, 969–988.

Hartl, F. U., 1996, "Molecular chaperones in cellular protein folding," *Nature* **304**, 571–580.

Haw, M., 2007, *Middle World: The Restless Heart of Matter and Life* (Macmillan, New York).

Healy, K., 2007, "Nanopore-based single-molecule DNA analysis," *Nanomedicine* **2**, 459–481.

Healy, K., B. Schiedt, and A. P. Morrison, 2007, "Solid-state nanopore technologies for nanopore-based DNA analysis," *Nanomedicine* **2**, 875–897.

Hechtfischer, G., R. Kleiner, A. V. Ustinov, and P. Müller, 1997, "Non-Josephson emission from intrinsic Junctions in $\text{Bi}_2\text{Sr}_2\text{CaCu}_2\text{O}_{8+y}$: Cherenkov radiation by Josephson vortices," *Phys. Rev. Lett.* **79**, 1365–1368.

Heinsalu, E., M. Patriarca, and F. Marchesoni, 2008, "Dimer diffusion in a washboard potential," *Phys. Rev. Lett.* **77**, 021129.

Heller, M., and H. Bruus, 2008, "A theoretical analysis of the resolution due to diffusion and size dispersion of particles in deterministic lateral displacement devices," *J. Micromech. & Microeng.* **18**, 075030.

van der Heyden, F. H. J., D. Stein, K. Besteman, S. G. Lemay, and C. Dekker, 2004, "Charge inversion at high ionic strength studied by streaming currents," *Phys. Rev. Lett.* **96**, 224502.

Hohberger, E. M., A. Lörke, W. Wegscheider, and M. Bichler, 2001, "Adiabatic pumping of two-dimensional electrons in a ratchet-type lateral superlattice," *Appl. Phys. Lett.* **78**, 2905–2907.

Holt, J. K., H. G. Park, Y. M. Wang, M. Stadermann, A. B. Artyukhin, C. P. Grigoropoulos, A. Noy, and O. Bakajin, 2006, "Fast mass transport through sub-2-nanometer carbon nanotubes," *Science* **312**, 1034–1037.

Howard, J., 2001, *Mechanics of Motor Proteins and the Cytoskeleton* (Sinauer Press, Sunderland MA, USA).

Huang, L. R., E. C. Cox, R. H. Austin, and J. C. Sturm, 2004, "Continuous particle separation through deterministic lateral displacement," *Science* **304**, 987–990.

Huberman, B. A., J. P. Crutchfield, and N. H. Packard, 1980, "Noise phenomena in Josephson junctions," *Appl. Phys. Lett.* **37**, 750–752.

Hugel, T., N. B. Holland, A. Cattani, L. Moroder, M. Seitz, and H. E. Gaub, 2002, "Single-molecule optomechanical cycle," *Science* **296**, 1103–1106.

Im, W., and B. Roux, 2002, "Ion permeation and selectivity of OmpF porin: A theoretical study based on molecular dynamics, Brownian dynamics, and continuum electrodiffusion theory," *J. Mol. Biol.* **322**, 851–869.

Jaeger, H. M., S. R. Nagel, and R. P. Behringer, 1996, "Granular solids, liquids, and gases," *Rev. Mod. Phys.* **68**, 1259–1273.

Jarzynski, C., 1997, "Nonequilibrium equality for free energy differences," *Phys. Rev. Lett.* **78**, 2690–2693.

Jarzynski, C., 2007, "Comparison of far-from-equilibrium work relations," *C. R. Physique* **8**, 495–506.

Jepsen, D. W., 1965, "Dynamics of a simple many-body system of hard rods," *J. Math. Phys.* **6**, 405–413.

Jessen, P. S., and I. H. Deutsch, 1996, "Optical lattices," *Adv. At. Mol. Opt. Phys.* **37**, 95–138.

John, K., P. Hänggi, and U. Thiele, 2008, "Ratched-driven fluid transport in bounded two-layer films of immiscible liquids," *Soft Matter* **4**, 1183–1195.

John, K., and U. Thiele, 2007, "Liquid transport generated by a flashing field-induced wettability ratchet," *Appl. Phys. Lett.* **90**, 264102.

Jones, P. H., M. Goonasekera, D. R. Meacher, T. Jonckheere, and T. S. Monteiro, 2007, "Directed motion for delta-kicked atoms with broken symmetries: Comparison between theory and experiment," *Phys. Rev. Lett.* **98**, 073002.

Jülicher, F., A. Ajdari, and J. Prost, 1997, "Modeling molecular motors," *Rev. Mod. Phys.* **69**, 1269–1281.

Jung, P., and P. Hänggi, 1991, "Amplification of small signals via stochastic resonance," *Phys. Rev. A* **44**, 8032–8041.

Jung, P., J. G. Kissner, and P. Hänggi, 1996, "Regular and chaotic transport in asymmetric periodic potentials: Inertia ratchets," *Phys. Rev. Lett.* **76**, 3436–3439.

Kafri, Y., and D. Nelson, 2005, "Sequence heterogeneity and the dynamics of molecular motors," *J. Phys.-Cond. Mat.* **17**, S3871–S3886.

Kalman, E., K. Healy, and Z. S. Siwy, 2007, "Tuning ion current rectification in asymmetric nanopores by signal mix-

ing," *EPL* **78**, 28002.

Kärger, J., 2008a, "Diffusion measurements by NMR techniques," *Mol. Sieves* **7**, 367–xxx.

Kärger, J., 2008b, "Single-file diffusion in zeolites," *Mol. Sieves* **7**, 329–366.

Kärger, J., and D. M. Ruthven, 1992, *Diffusion in Zeolites and Other Microporous Solids* (Wiley, New York).

Kärger, J., R. Valiullin, and S. Vasenkov, 2005, "Molecular dynamics under confinement to one dimension: Options of measurement and accessible information," *New J. Phys.* **7**, 15.

Karnik, R., C. Duan, K. Castelino, H. Daiguji, and A. Majumdar, 2007, "Rectification of ionic current in a nanofluidic diode," *Nano Lett.* **7**, 547–551.

Kasianowicz, J. J., E. Brandin, D. Branton, and D. W. Deamer, 1996, "Characterization of individual polynucleotide molecules using a membrane channel," *Proc. Natl. Acad. Sci.* **93**, 13770–13773.

Kay, E. R., D. A. Leigh, and F. Zerbetto, 2007, "Synthetic molecular motors and mechanical machines," *Angew. Chem. Int. Ed.* **46**, 72–191.

Keay, B., S. Zeuner, S. Allen, K. Maranowski, A. Gossard, U. Bhattacharya, and M. Rodell, 1995, "Dynamic localization, absolute negative conductance, and stimulated, multi-photon emission in sequential resonant-tunneling semiconductor superlattices," *Phys. Rev. Lett.* **75**, 4102–4105.

Kenfack, A., J. Gong, and A. K. Pattanayak, 2008, "Controlling the ratchet effect for cold atoms," *Phys. Rev. Lett.* **100**, 044104.

Kettner, C., P. Reimann, P. Hänggi, and F. Müller, 2000, "Drift ratchet," *Phys. Rev. E* **61**, 312–323.

Khrapai, V. S., S. Ludwig, J. P. Kotthaus, H. P. Tranitz, and W. Wegscheider, 2006, "Double-dot quantum ratchet driven by an independently biased quantum point contact," *Phys. Rev. Lett.* **97**, 176803.

Kohler, S., J. Lehmann, and P. Hänggi, 2005, "Driven quantum transport on the nanoscale," *Phys. Rep.* **406**, 379–443.

Kolomeisky, A. B., 2007, "Channel-facilitated molecular transport across membranes: Attraction, repulsion, and asymmetry," *Phys. Rev. Lett.* **98**, 048105.

Komnik, A., and A. O. Gogolin, 2003, "Transport, optical properties, and quantum ratchet effects for quantum dots and molecules coupled to Luttinger liquids," *Phys. Rev. B* **68**, 235323.

Koshelev, A. E., 1999, "Crossing lattices, vortex chains, and angular dependence of melting line in layered superconductors," *Phys. Rev. Lett.* **83**, 187–190.

Kosinska, I. D., I. Goychuk, M. Kostur, G. Schmid, and P. Hänggi, 2008, "Rectification in synthetic conical nanopores: A one-dimensional Poisson-Nernst-Planck model," *Phys. Rev. E* **77**, 031131.

Koss, B. A., and D. G. Grier, 2003, "Optical peristalsis," *Appl. Phys. Lett.* **82**, 3985–3987.

Kostur, M., L. Machura, P. Talkner, P. Hänggi, and J. Luczka, 2008, "Anomalous transport in biased ac-driven Josephson junctions: Negative conductances," *Phys. Rev. B* **77**, 104509.

Kostur, M., M. Schindler, P. Talkner, and P. Hänggi, 2006, "Chiral separation in microflows," *Phys. Rev. Lett.* **96**, 014502.

Kosztin, I., and K. Schulten, 2004, "Fluctuation-driven molecular transport through an asymmetric membrane channel," *Phys. Rev. Lett.* **93**, 238102.

Kottas, G. S., L. I. Clarke, D. Horinek, and J. Michl,

2005, "Artificial molecular motors," *Chemical Reviews* **105**, 1281–1376.

Kouwenhoven, L. P., A. T. Johnson, N. C. van der Vaart, C. J. P. M. Harmans, and C. T. Foxon, 1991, "Quantized current in a quantum-dot turnstile using oscillating tunnel barriers," *Phys. Rev. Lett.* **67**, 1626–1629.

Kwok, W. K., R. J. Olsson, G. Karapetrov, U. Welp, V. Vlasko-Vlasov, K. Kadowaki, and G. W. Crabtree, 2002, "Modification of vortex behavior through heavy ion lithography," *Physica C* **382**, 137–141.

Landa, P. S., and P. V. E. McClintock, 2000, "Vibrational resonance," *J. Phys. A* **33**, L433–L438.

Läuger, P., 1991, *Electrogenic Ion pumps Cytoskeleton* (Sinauer Associates, Sunderland MA, USA).

Lebowitz, J. L., and J. K. Percus, 1967, "Kinetic equations and density expansions: Exactly solvable one-dimensional system," *Phys. Rev.* **155**, 122–138.

Lee, C.-S., B. Jankó, I. Derényi, and A.-L. Barabási, 1999, "Reducing vortex density in superconductors using the "ratchet effect"," *Nature* **400**, 337–340.

Lee, K. H., 2003, "Ratchet effect in an ac-current driven Josephson junction array," *Appl. Phys. Lett.* **83**, 117–119.

Lee, S.-H., K. Ladavac, M. Polin, and D. G. Grier, 2004, "Observation of flux reversal in a symmetric optical thermal ratchet," *Phys. Rev. Lett.* **94**, 110601.

Leff, H. S., and A. F. Rex (eds.), 2003, *Maxwell's Daemon 2: Entropy, Classical and Quantum Information, Computing* (Institute of Physics, London), 2nd edition.

Lehmann, J., S. Kohler, P. Hänggi, and A. Nitzan, 2002, "Molecular wires acting as coherent quantum ratchets," *Phys. Rev. Lett.* **88**, 228305.

Lehmann, J., S. Kohler, P. Hänggi, and A. Nitzan, 2003, "Rectification of laser-induced electronic transport through molecules," *J. Chem. Phys.* **118**, 3283–3293.

Levitt, D. G., 1973, "Dynamics of a single-file pore: Non-Fickian behavior," *Phys. Rev. A* **8**, 3050–3054.

Li, J., D. Stein, C. McMullan, D. Branton, M. J. Aziz, and J. A. Golovchenko, 2001, "Ion-beam sculpting at nanometre length scales," *Nature* **412**, 166–169.

Li, N., P. Hänggi, and B. W. Li, 2008, "Ratcheting heat flux against a thermal bias," *EPL-Europhys. Lett.* **82**, arXiv:0804.3630.

Lindner, B., L. Schimansky-Geier, P. Reimann, P. Hänggi, and M. Nagaoka, 1999, "Inertia ratchets: A numerical study versus theory," *Phys. Rev. E* **59**, 1417–1424.

Linke, H., 2002, "Quantum ratchets and quantum heat pumps," *Appl. Phys. A-Mater.* **75**, 167–167.

Linke, H., B. J. Alemán, L. D. Melling, M. J. Taormina, M. J. Francis, C. C. Dow-Hygelund, V. Narayanan, R. P. Taylor, and A. Stout, 2006, "Self-propelled Leidenfrost droplets," *Phys. Rev. Lett.* **96**, 154502.

Linke, H., T. E. Humphrey, P. E. Lindelof, A. Lofgren, R. Newbury, P. Omling, A. O. Sushkov, R. P. Taylor, and H. Xu, 2002, "Quantum ratchets and quantum heat pumps," *Appl. Phys. A-Mater.* **75**, 237–246.

Linke, H., T. E. Humphrey, A. Lofgren, A. O. Sushkov, R. Newbury, R. P. Taylor, and P. Omling, 1999, "Experimental tunneling ratchets," *Science* **286**, 2314–2317.

Linke, H., W. Sheng, A. Löfgren, H. Xu, P. Omling, and P. E. Lindelof, 1998, "A quantum dot ratchet: Experiment and theory," *Europhys. Lett.* **44**, 341–347.

Lipowsky, R., and S. Klumpp, 2005, "Life is motion": Multiscale motility of molecular motors," *Physica A* **352**, 53–112.

Lorke, A., S. Wimmer, B. Jager, J. P. Kotthaus, W. Wegscheider, and M. Bichler, 1998, "Far-infrared and transport properties of antidot arrays with broken symmetry," *Physica B* **249–251**, 312–316.

Luchsinger, R. H., 2000, "Transport in nonequilibrium systems with position-dependent mobility," *Phys. Rev. E* **62**, 272–275.

Luczka, J., R. Bartussek, and P. Hänggi, 1995, "White-noise-induced transport in periodic structures," *Europhys. Lett.* **31**, 431–436.

Lundh, E., and M. Wallin, 2005, "Ratchet effect for cold atoms in an optical lattice," *Phys. Rev. Lett.* **94**, 110603.

Machura, L., M. Kostur, P. Hänggi, P. Talkner, and J. Luczka, 2004a, "Consistent description of quantum Brownian motors operating at strong friction," *Phys. Rev. E* **70**, 031107.

Machura, L., M. Kostur, P. Talkner, J. Luczka, and P. Hänggi, 2007a, "Absolute negative mobility induced by thermal equilibrium fluctuations," *Phys. Rev. Lett.* **98**, 040601.

Machura, L., M. Kostur, P. Talkner, J. Luczka, F. Marchesoni, and P. Hänggi, 2004b, "Brownian motors: Current fluctuations and rectification efficiency," *Phys. Rev. E* **70**, 061105.

Machura, L., J. Luczka, P. Talkner, and P. Hänggi, 2007b, "Transport of forced quantum motors in the strong friction limit," *Acta Phys. Pol. B* **38**, 1855–1863.

Magnasco, M. O., 1993, "Forced thermal ratchets," *Phys. Rev. Lett.* **71**, 1477–1481.

Majer, J. B., J. Peguiron, M. Grifoni, M. Tusveld, and J. E. Mooij, 2003, "Quantum ratchet effect for vortices," *Phys. Rev. Lett.* **90**, 056802.

Marchesoni, F., 1986, "Harmonic mixing signal: Doubly dithered ring laser gyroscope," *Phys. Lett. A* **119**, 221–224.

Marchesoni, F., 1996, "Thermal ratchets in 1+1 dimensions," *Phys. Rev. Lett.* **77**, 2364–2367.

Marchesoni, F., 1997, "Transport properties in disordered ratchet potentials," *Phys. Rev. E* **56**, 2492–2495.

Marchesoni, F., 1998, "Conceptual design of a molecular shuttle," *Phys. Lett. A* **237**, 126–130.

Marchesoni, F., S. Savel'ev, and F. Nori, 2006a, "Achieving optimal rectification using underdamped rocked ratchets," *Phys. Rev. E* **73**, 021102.

Marchesoni, F., S. Savel'ev, and F. Nori, 2006b, "Driven binary mixtures: Clustering and giant diffusion," *Europhys. Lett.* **73**, 513–519.

Marchesoni, F., P. Sodano, and M. Zanetti, 1988, "Supersymmetry and bistable soft potentials," *Phys. Rev. Lett.* **61**, 1143–1146.

Marchesoni, F., and A. Taloni, 2006, "Subdiffusion and long-time anticorrelations in a stochastic single file," *Phys. Rev. Lett.* **97**, 106101.

Marquet, C., A. Buguin, L. Talini, and P. Silberzan, 2002, "Rectified motion of colloids in asymmetrically structured channels," *Phys. Rev. Lett.* **88**, 168301.

Martinez, P. J., and R. Chacon, 2008, "Disorder induced control of discrete soliton ratchets," *Phys. Rev. Lett.* **100**, 144101.

Maruyama, K., F. Nori, and V. Vedral, 2008, "The physics of Maxwell's demon and information," *Rev. Mod. Phys.* **XXX**, yyy.

Mateos, J. L., 2000, "Chaotic transport and current reversal in deterministic ratchets," *Phys. Rev. Lett.* **84**, 258–261.

Mateos, J. L., 2003, "Current reversals in chaotic ratchets: the battle of the attractors," *Physica A* **325**, 92–100.

Matsuda, T., O. Kamimura, H. Kasai, K. Harada, T. Yoshida, T. Akashi, A. Tonomura, Y. Nakayama, J. Shimoyama, K. Kishio, T. Hanaguri, and K. Kitazawa, 2001, "Oscillating rows of vortices in superconductors," *Science* **294**, 2136–2138.

Matthias, S., and F. Müller, 2003, "Asymmetric pores in a silicon membrane acting as massively parallel Brownian ratchets," *Nature* **424**, 53–57.

van der Meer, D., P. Reimann, K. van der Weele, and D. Lohse, 2004, "Spontaneous ratchet effect in a granular gas," *Phys. Rev. Lett.* **92**, 184301.

van der Meer, D., K. van der Weele, P. Reimann, and D. Lohse, 2007, "Compartmentalized granular gases: Flux model results," *J. Stat. Mech.* **2007**, P07021.

Mel'nikov, V. I., 1991, "The Kramers problem: Fifty years of development," *Phys. Rep.* **209**, 1–71.

Menghini, M., J. V. de Vondel, D. G. Gheorghe, R. J. Wijnagaarden, and V. V. Moshchalkov, 2007, "Asymmetry reversal of thermomagnetic avalanches in Pb films with a ratchet pinning potential," *Phys. Rev. B* **76**, 184515.

Mennerat-Robilliard, C., D. Lucas, S. Guibal, J. Tabosa, C. Jurczak, J.-Y. Courtois, and G. Grynberg, 1999, "Ratchet for cold rubidium atoms: The asymmetric optical lattice," *Phys. Rev. Lett.* **82**, 851–854.

Millonas, M. M., and M. I. Dykman, 1994, "Transport and current reversal in stochastically driven ratchets," *Phys. Lett. A* **185**, 65–69.

Morales-Molina, L., and S. Flach, 2008, "Resonant ratcheting of a Bose-Einstein condensate," *New J. Phys.* **10**, 013008.

Morales-Molina, L., J. B. Gong, and S. Flach, 2008, "Quantum ratchet control - Harvesting on Landau-Zener transitions," *Europhys. Lett.-EPL* **83**, 40005.

Moskalets, M., and M. Büttiker, 2002, "Floquet scattering theory of quantum pumps," *Phys. Rev. B* **66**, 205320.

Moskalets, M., and M. Büttiker, 2004, "Floquet scattering theory for current and heat noise in large amplitude adiabatic pumps," *Phys. Rev. B* **70**, 245305.

Movileanu, L., 2008, "Squeezing a single polypeptide through a nanopore," *Soft Matter* **4**, 925–931.

Müller, F., A. Birner, J. Schilling, U. Gösele, C. Kettner, and P. Hänggi, 2000, "Membranes for micropumps from macroporous silicon," *phys. stat. solidi (a)* **182**, 585–590.

Nagel, J., D. Speer, A. Sterck, R. Eichhorn, P. Reimann, K. Illin, M. Siegel, D. Koelle, and R. Kleiner, 2008, "Observation of negative absolute resistance in a Josephson junction," *Phys. Rev. Lett.* **100**, 217001.

Neupert, G., T. Hugel, R. Netz, and H. Gaub, 2006, "Elasticity of polyazobenzene-peptides," *Macromolecules* **39**, 789–797.

Neugebauer, N., P. Bräuer, and J. Kärger, 2000, "Reactivity enhancement by molecular traffic control," *J. Catal.* **194**, 1–3.

Nigg, E. A., 1997, "Nucleocytoplasmic transport: Signals, mechanisms and regulation," *Nature* **386**, 779–787.

Nishiyama, M., H. Higuchi, and T. Yanagida, 2002, "Chemomechanical coupling of the ATPase cycle to the forward and backward movements of single kinesin molecules," *Nature Cell Biology* **4**, 790–797.

Nishiyama, M., E. Muto, Y. Inoue, T. Yanagida, and H. Higuchi, 2001, "Substeps within the 8-nm step of the ATPase cycle of single kinesin molecules," *Nature Cell Biology* **3**, 425–428.

Olson, C. J., C. Reichhardt, B. Jankó, and F. Nori, 2001, "Collective interaction-driven ratchet for transporting flux quanta," *Phys. Rev. Lett.* **87**, 177002.

Olson Reichhardt, C., and C. Reichhardt, 2005, "Rectification and flux reversals for vortices interacting with triangular traps," *Physica C* **432**, 125–132.

Ooi, S., S. Savel'ev, M. B. Gaifullin, T. Mochiku, K. Hirata, and F. Nori, 2007, "Nonlinear nanodevices using magnetic flux quanta," *Phys. Rev. Lett.* **99**, 207003.

Ooi, S., T. Shibauchi, N. Okuda, and T. Tamegai, 1999, "Novel angular scaling of vortex phase transitions in $\text{Bi}_2\text{Sr}_2\text{CaCu}_2\text{O}_{8+y}$," *Phys. Rev. Lett.* **82**, 4308–4311.

van Oudenaarden, A., and S. G. Boxer, 1999, "Brownian ratchets: Molecular separations in lipid bilayers supported on patterned arrays," *Science* **285**, 1046–1048.

Park, P. J., and W. Sung, 1999, "Dynamics of a polymer surmounting a potential barrier: The Kramers problem for polymers," *J. Chem. Phys.* **111**, 5259–5266.

Parrondo, J., and B. de Cisneros, 2002, "Energetics of Brownian motors: A review," *Appl. Phys. A-Mater.* **75**, 179–191.

Parrondo, J. M. R., and P. Espanol, 1996, "Criticism of Feynman's analysis of the ratchet as an engine," *Am. J. Phys.* **64**, 1125–1130.

Platero, G., and R. Aguado, 2004, "Photon-assisted transport in semiconductor nanostructures," *Phys. Rep.* **395**, 1–157.

Plourde, B. L. T., D. J. Van Harlingen, R. Besseling, M. B. S. Hesselberth, and P. H. Kes, 2000, "Vortex dynamics in thin superconducting strips observed by Scanning SQUID microscopy," *Physica C* **341–348**, 1023–1026.

Poletti, D., G. Benenti, G. Casati, and B. Li, 2007a, "Interaction-induced quantum ratchet in a Bose-Einstein condensate," *Phys. Rev. A* **76**, 023421.

Poletti, D., G. G. Carlo, and B. Li, 2007b, "Current behavior of a quantum Hamiltonian ratchet in resonance," *Phys. Rev. E* **75**, 011102.

Pollak, E., J. Bader, B. J. Berne, and P. Talkner, 1993, "Theory of correlated hops in surface diffusion," *Phys. Rev. Lett.* **70**, 3299–3302.

Popescu, M. N., C. M. Arizmendi, A. L. Salas-Brito, and F. Family, 2000, "Disorder induced diffusive transport in ratchets," *Phys. Rev. Lett.* **85**, 3321–3324.

Porto, M., M. Urbakh, and J. Klafter, 2000, "Atomic scale engines: Cars and wheels," *Phys. Rev. Lett.* **84**, 6058–6061.

Pothier, H., P. Lafarge, C. Urbina, D. Esteve, and M. H. Devoret, 1992, "Single-electron pump based on charging effects," *Europhys. Lett.* **17**, 249–254.

Prost, J., J. F. Chauwin, L. Peliti, and A. Ajdari, 1994, "Asymmetric pumping of ratchets," *Phys. Rev. Lett.* **72**, 2652–2655.

Purcell, E. M., 1977, "Life at low Reynolds number," *Am. J. Phys.* **45**, 3–11.

Quéré, D., and A. Ajdari, 2006, "Liquid drops: Surfing the hot spot," *Nat. Mater.* **5**, 429–430.

Rapaport, D. C., 2002, "The wonderful world of granular ratchets," *Comp. Phys. Comm.* **147**, 141–144.

Regan, B. C., S. Aloni, R. O. Ritchie, U. Dahmen, and A. Zettl, 2004, "Carbon nanotubes as nanoscale mass conveyors," *Nature* **428**, 924–927.

Reguera, D., G. Schmid, P. S. Burada, J. M. Rubí, P. Reimann, and P. Hänggi, 2006, "Entropic transport: Kinetics, scaling, and control mechanisms," *Phys. Rev. Lett.* **96**, 130603.

Reichhardt, C., C. J. Olson, and F. Nori, 1998, "Commensurate and incommensurate vortex states in superconductors with periodic pinning arrays," *Phys. Rev. B* **57**, 7937–7943.

Reimann, P., 2001, "Supersymmetric ratchets," *Phys. Rev.*

Lett. **86**, 4992–4995.

Reimann, P., 2002, “Brownian motors: Noisy transport far from equilibrium,” Phys. Rep. **361**, 57–265.

Reimann, P., R. Bartussek, R. Häussler, and P. Hänggi, 1996, “Brownian motors driven by temperature oscillations,” Phys. Lett. A **215**, 26–31.

Reimann, P., C. Van den Broeck, H. Linke, P. Hänggi, J. M. Rubí, and A. Pérez-Madrid, 2001, “Giant acceleration of free diffusion by use of tilted periodic potentials,” Phys. Rev. Lett. **87**, 010602.

Reimann, P., C. V. den Broeck, H. Linke, P. Hänggi, J. M. Rubí, and A. Perez-Madrid, 2002, “Diffusion in tilted periodic potentials: Enhancement, universality, and scaling,” Phys. Rev. E **65**, 031104.

Reimann, P., M. Grifoni, and P. Hänggi, 1997, “Quantum ratchets,” Phys. Rev. Lett. **79**, 10–13.

Reimann, P., and P. Hänggi, 1998, “Quantum features of Brownian motors and stochastic resonance,” Chaos **8**, 629–642.

Reimann, P., and P. Hänggi, 2002, “Introduction to the physics of Brownian motors,” Appl. Phys. A-Mater. **75**, 169–178.

Reimann, P., R. Kawai, C. V. den Broeck, and P. Hänggi, 1999, “Coupled Brownian motors: Anomalous hysteresis and zero-bias negative conductance,” Europhys. Lett. **45**, 545–551.

Rey, M., M. Strass, S. Kohler, P. Hänggi, and F. Sols, 2007, “Nonadiabatic electron heat pump,” Phys. Rev. B **76**, 085337.

Risken, H., 1984, *The Fokker-Planck Equation* (Springer, Berlin).

Ritt, G., C. Geckeler, T. Salger, G. Cennini, and M. Weitz, 2006, “Fourier synthesis of optical potentials for atomic quantum gases,” Phys. Rev. A **74**, 063622.

Ros, A., R. Eichhorn, J. Regtmeier, T. Duong, P. Reimann, and D. Anselmetti, 2005, “Brownian motion - Absolute negative particle mobility,” Nature **436**, 928.

Rosato, A., K. J. Strandburg, F. Prinz, and R. H. Swendsen, 1987, “Why the Brazil nuts are on top: Size segregation of particulate matter by shaking,” Phys. Rev. Lett. **58**, 1038–1040.

Rousselet, J., L. Salome, A. Ajdari, and J. Prost, 1994, “Directional motion of Brownian particles induced by a periodic asymmetric potential,” Nature **370**, 446–448.

Rozenbaum, V., D. Yang, S. Lin, and T. Tsong, 2004, “Catalytic wheel as a Brownian motor,” J. Phys. Chem. B **108**, 15880–15889.

Rēmskar, M., 2004, “Inorganic nanotubes,” Adv. Mater. **16**, 1497–1504.

Sadgrove, M., M. Horikoshi, T. Sekimura, and K. Nakagawa, 2007, “Rectified momentum transport for a kicked Bose-Einstein condensate,” Phys. Rev. Lett. **99**, 043002.

Salger, T., C. Geckeler, S. Kling, and M. Weitz, 2007, “Atomic Landau-Zener tunneling in Fourier-synthesized optical lattices,” Phys. Rev. Lett. **99**, 190405.

Sanchez, R., F. J. Kaiser, S. Kohler, P. Hänggi, and G. Platero, 2008, “Shot noise in spin pumps,” Physica E **40**, 1276–1278.

Sassine, S., Y. Krupko, J. C. Portal, Z. D. Kvon, R. Murali, K. P. Martin, G. Hill, and A. D. Wieck, 2008, “Experimental investigation of the ratchet effect in a two-dimensional electron system with broken spatial inversion symmetry,” Phys. Rev. B **78**, 045431.

Savel’ev, S., F. Marchesoni, P. Hänggi, and F. Nori, 2004a, “Transport via nonlinear signal mixing in ratchet devices,” Phys. Rev. E **70**, 066109.

Savel’ev, S., F. Marchesoni, and F. Nori, 2003, “Controlling transport in mixtures of interacting particles using Brownian motors,” Phys. Rev. Lett. **91**, 010601.

Savel’ev, S., F. Marchesoni, and F. Nori, 2004b, “Manipulating small particles in mixtures far from equilibrium,” Phys. Rev. Lett. **92**, 160602.

Savel’ev, S., F. Marchesoni, and F. Nori, 2004c, “Stochastic transport of interacting particles in periodically driven ratchets,” Phys. Rev. E **70**, 061107.

Savel’ev, S., F. Marchesoni, P. Hänggi, and F. Nori, 2004, “Nonlinear signal mixing in a ratchet device,” Europhys. Lett. **67**, 179–185.

Savel’ev, S., V. Misko, F. Marchesoni, and F. Nori, 2005, “Separating particles according to their physical properties: Transverse drift of underdamped and overdamped interacting particles diffusing through two-dimensional ratchets,” Phys. Rev. B **71**, 214303.

Savel’ev, S., and F. Nori, 2002, “Experimentally realizable devices for controlling the motion of magnetic flux quanta in anisotropic superconductors,” Nature Materials **1**, 179–184.

Schanz, H., T. Dittrich, and R. Ketzmerick, 2005, “Directed chaotic transport in Hamiltonian ratchets,” Phys. Rev. E **71**, 026228.

Schanz, H., M.-F. Otto, R. Ketzmerick, and T. Dittrich, 2001, “Classical and quantum Hamiltonian ratchets,” Phys. Rev. Lett. **87**, 070601.

Scheid, M., D. Bercioux, and K. Richter, 2007a, “Zeeman ratchets: pure spin current generation in mesoscopic conductors with non-uniform magnetic fields,” New J. Phys. **9**, 401.

Scheid, M., A. Pfund, D. Bercioux, and K. Richter, 2007b, “Coherent spin ratchets: A spin-orbit based quantum ratchet mechanism for spin-polarized currents in ballistic conductors,” Phys. Rev. B **76**, 195303.

Schemmert, U., J. Kärger, C. Krause, R. A. Rákoczy, and J. Weitkamp, 1999, “Monitoring the evolution of intracrystalline concentration,” Europhys. Lett. **46**, 204–210.

Schiavoni, M., L. Sanchez-Palencia, F. Renzoni, and G. Gryngberg, 2003, “Phase control of directed diffusion in a symmetric optical lattice,” Phys. Rev. Lett. **90**, 094101.

Schliwa, M., 2002, *Molecular Motors* (Wiley-VCH, Weinheim, Germany).

Schneider, W., and K. Seeger, 1966, “Harmonic mixing of microwaves by warm electrons in germanium,” Appl. Phys. Lett. **8**, 133–135.

Sekimoto, K., 1998, “Langevin equation and thermodynamics,” Prog. Theor. Phys. Suppl. **130**, 17–27.

Shalóm, D. E., and H. Pastoriza, 2005, “Vortex motion rectification in Josephson junction arrays with a ratchet potential,” Phys. Rev. Lett. **94**, 177001.

Shushin, A. I., 2002, “Specific features of threshold diffusion in a tilted periodic potential. Simple model and analytical results in the underdamped regime,” Europhys. Lett. **60**, 525–531.

Shutenko, T. A., I. L. Aleiner, and B. L. Altshuler, 2000, “Mesoscopic fluctuations of adiabatic charge pumping in quantum dots,” Phys. Rev. B **61**(15), 10366–10375.

Silva, C. C. D., J. V. de Vondel, M. Morelle, and V. V. Moshchalkov, 2006, “Controlled multiple reversals of a ratchet effect,” Nature **440**, 651–654.

Simon, S. M., C. S. Peskin, and G. F. Oster, 1992, “What

drives the translocation of proteins," Proc. Natl. Acad. Sci. **89**, 3770–3774.

Sinitsyn, N. A., and I. Nemenman, 2007, "Universal geometric theory of mesoscopic stochastic pumps and reversible ratchets," Phys. Rev. Lett. **99**, 220408.

Siwy, Z., and A. Fuliński, 2004, "A nanodevice for rectification and pumping ions," Am. J. Phys. **72**, 567–574.

Siwy, Z., I. D. Kosińska, A. Fuliński, and C. R. Martin, 2005, "Asymmetric diffusion through synthetic nanopores," Phys. Rev. Lett. **94**, 048102.

Siwy, Z., and A. Fuliński, 2002, "Fabrication of a synthetic nanopore ion pump," Phys. Rev. Lett. **89**, 198103.

Sjölund, P., S. J. H. Petra, C. M. Dion, S. Jonsell, M. Nylén, L. Sanchez-Palencia, and A. Kastberg, 2006, "Demonstration of a controllable three-dimensional Brownian motor in symmetric potentials," Phys. Rev. Lett. **96**, 190602.

Slater, G. W., H. L. Guo, and G. I. Nixon, 1997, "Bidirectional transport of polyelectrolytes using self-modulating entropic ratchets," Phys. Rev. Lett. **78**, 1170–1173.

Smirnov, S., D. Bercioux, M. Grifoni, and K. Richter, 2008, "Quantum dissipative Rashba spin ratchets," Phys. Rev. Lett. **100**, 230601.

Smoluchowski, M., 1912, "Experimentell nachweisbare, der üblichen Thermodynamik widersprechende Molekularphänomene," Physik. Zeitschr. **13**, 1069–1080.

Son, W. S., J. W. Ryu, D. U. Hwang, S. Y. Lee, Y. J. Park, and C. M. Kim, 2008, "Transport control in a deterministic ratchet system," Phys. Rev. E **77**, 066213.

Speer, D., R. Eichhorn, and P. Reimann, 2007, "Transient chaos induces anomalous transport properties of an under-damped Brownian particle," Phys. Rev. E **76**, 051110.

Spivak, B., F. Zhou, and M. T. Beal Monod, 1995, "Mesoscopic mechanisms of the photovoltaic effect and microwave absorption in granular metals," Phys. Rev. B **51**, 13226–13230.

Squires, T. M., and S. R. Quake, 2005, "Microfluidics: Fluid physics at the nanoliter scale," Rev. Mod. Phys. **77**, 977–1026.

Stafford, C. A., and N. S. Wingreen, 1996, "Resonant photon-assisted tunneling through a double quantum dot: An electron pump from spatial Rabi oscillations," Phys. Rev. Lett. **76**, 1916–1919.

Stein, D., M. Kruithof, and C. Dekker, 2004, "Surface-charge-governed ion transport in nanofluidic channels," Phys. Rev. Lett. **93**, 035901.

Sterck, A., R. Kleiner, and D. Koelle, 2005, "Three-junction SQUID rocking ratchet," Phys. Rev. Lett. **95**, 177006.

Sterck, A., S. Weiss, and D. Koelle, 2002, "SQUID ratchets: basics and experiments," Appl. Phys. A-Mater. **75**, 253–262.

Storm, A. J., J. H. Chen, X. S. Ling, H. W. Zandbergen, and C. Dekker, 2003, "Fabrication of solid-state nanopores with single-nanometre precision," Nat. Mater. **2**, 537–540.

Strass, M., P. Hänggi, and S. Kohler, 2005, "Nonadiabatic electron pumping: Maximal current with minimal noise," Phys. Rev. Lett. **95**, 130601.

Stroock, A. D., R. F. Ismagilov, H. A. Stone, and G. M. Whitesides, 2003, "Fluidic ratchet based on Marangoni–Benard convection," Langmuir **19**, 4358–4362.

Suzuki, D., and T. Munakata, 2003, "Rectification efficiency of a Brownian motor," Phys. Rev. E **68**, 021906.

Switkes, M., C. M. Marcus, K. Campman, and A. C. Gossard, 1999, "An adiabatic quantum electron pump," Science **283**, 1905–1908.

Talkner, P., P. Hänggi, and M. Morillo, 2008, "Microcanonical quantum fluctuation theorems," Phys. Rev. E **77**, 051131.

Talkner, P., E. Lutz, and P. Hänggi, 2007, "Fluctuation theorems: Work is not an observable," Phys. Rev. E **75**, 050102.

Taloni, A., and F. Marchesoni, 2006, "Single-file diffusion on a periodic substrate," Phys. Rev. Lett. **96**, 020601.

Tessier, F., and G. W. Slater, 2002, "Strategies for the separation of polyelectrolytes based on non-linear dynamics and entropic ratchets in a simple microfluidic device," Appl. Phys. A-Mater. **75**, 285–291.

Thouless, D. J., 1983, "Quantization of particle transport," Phys. Rev. B **27**, 6083–6087.

Togawa, Y., K. Harada, T. Akashi, H. Kasai, T. Matsuda, F. Nori, A. Maeda, and A. Tonomura, 2005, "Direct observation of rectified motion of vortices in a niobium superconductor," Phys. Rev. Lett. **95**, 087002.

Tsang, T. Y., 2002, "Na,K-ATPase as a Brownian motor: Electric field-induced conformational fluctuation leads to uphill pumping of cation in the absence of ATP," J. Biol. Phys. **28**, 309–325.

Tu, Z. C., 2008, "Efficiency at maximum power of Feynman's ratchet as a heat engine," J. Phys. A **41**, 312003.

Turberfield, A. J., J. C. Mitchell, B. Yurke, A. P. Mills, M. I. Blakey, and F. C. Simmel, 2003, "DNA fuel for free-running nanomachines," Phys. Rev. Lett. **90**, 118102.

Ustinov, A. V., C. Coqui, A. Kemp, Y. Zolotaryuk, and M. Salerno, 2004, "Ratchetlike dynamics of fluxons in annular Josephson junctions driven by biharmonic microwave fields," Phys. Rev. Lett. **93**, 087001.

Van Look, L., B. Y. Zhu, R. Jonckheere, B. R. Zhao, Z. X. Zhao, and V. V. Moshchalkov, 2002, "Anisotropic vortex pinning in superconductors with a square array of rectangular submicron holes," Phys. Rev. B **66**, 214511.

Vavilov, M. G., V. Ambegaokar, and I. L. Aleiner, 2001, "Charge pumping and photovoltaic effect in open quantum dots," Phys. Rev. B **63**, 195313.

Vercoutere, W. A., S. Winters-Hilt, V. S. DeGuzman, D. Deamer, S. E. Ridinoa, J. T. Rodgers, H. E. Olsen, A. Marziali, and M. Akeson, 2003, "Discrimination among individual Watson-Crick base pairs at the termini of single DNA hairpin molecules," Nucleic Acids Res. **31**, 1311–1318.

Vidan, A., R. M. Westervelt, M. Stopa, M. Hanson, and A. C. Gossard, 2004, "Triple quantum dot charging rectifier," Appl. Phys. Lett. **85**, 3602–3604.

Villegas, J. E., S. Savel'ev, F. Nori, E. M. Gonzalez, J. V. Anguita, R. Garcia, and J. L. Vicent, 2003, "A superconducting reversible rectifier that controls the motion of magnetic flux quanta," Science **302**, 1188–1191.

Vlassioux, I., and Z. S. Siwy, 2007, "Nanofluidic diode," Nano Lett. **7**, 552–556.

de Vondel, J. V., C. C. de Souza Silva, and V. V. Moshchalkov, 2007, "Diode effects in the surface superconductivity regime," EPL **80**, 17006.

de Vondel, J. V., C. C. de Souza Silva, B. Y. Zhu, M. Morelle, and V. V. Moshchalkov, 2005, "Vortex-rectification effects in films with periodic asymmetric pinning," Phys. Rev. Lett. **94**, 057003.

Wambaugh, J. F., C. Reichhardt, C. J. Olson, F. Marchesoni, and F. Nori, 1999, "Superconducting fluxon pumps and lenses," Phys. Rev. Lett. **83**, 5106–5109.

Wang, H., and G. Oster, 2002, "Ratchets, power strokes, and molecular motors," Appl. Phys. A **75**, 315–323.

Wang, J., and J. Gong, 2008, "Quantum ratchet accelerator

without a bichromatic lattice potential," *Phys. Rev. E* **78**, 036219.

Wang, Z. S., 2004, "Bioinspired laser-operated molecular locomotive," *Phys. Rev. E* **70**, 031903.

Weiss, S., D. Koelle, J. Müller, R. Gross, and K. Barthel, 2000, "Ratchet effect in dc SQUIDs," *Europhys. Lett.* **51**, 499–505.

Wördenweber, R., P. Dymashevski, and V. R. Misko, 2004, "Guidance of vortices and the vortex ratchet effect in high- T_c superconducting thin films obtained by arrangement of antidots," *Phys. Rev. B* **69**, 184504.

Xie, T. D., P. Marszalek, Y. D. Chen, and T. Y. Tsong, 1994, "Recognition and processing of randomly fluctuating electric signals by Na, K-ATPase," *Biophys. J.* **67**, 1247–1251.

Xu, C., W. Rice, W. He, and D. Stokes, 2002, "A structural model for the catalytic cycle of Ca²⁺-ATPase," *J. Mol. Biol.* **316**, 201–211.

Yevtushenko, O., S. Flach, and K. Richter, 2000, "ac-driven phase-dependent directed diffusion," *Phys. Rev. E* **61**, 7215–7218.

Yevtushenko, O., S. Flach, Y. Zolotaryuk, and A. A. Ovchinnikov, 2001, "Rectification of current in ac-driven non-linear systems and symmetry properties of the Boltzmann equation," *Europhys. Lett.* **54**, 141–147.

Yin, P., H. Yan, X. G. Daniell, A. J. Turberfield, and J. H. Reif, 2004, "A unidirectional DNA walker that moves autonomously along a track," *Ang. Chemie-Int. Ed.* **43**, 4906–4911.

Yorke, B., A. J. Turberfield, A. P. Mills, F. C. Simmel, and J. L. Neumann, 2000, "A DNA-fuelled molecular machine made of DNA," *Nature* **406**, 605–608.

You, J. Q., and F. Nori, 2005, "Superconducting circuits and quantum information," *Physics Today* **58**(11), 42–47.

Yu, K., T. W. Heitmann, C. Song, M. P. DeFeo, B. L. T. Plourde, M. B. S. Hesselberth, and P. H. Kes, 2007, "Asymmetric weak-pinning superconducting channels: Vortex ratchets," *Phys. Rev. B* **76**, 220507.

Zapata, I., R. Bartussek, F. Sols, and P. Hänggi, 1996, "Voltage rectification by a SQUID ratchet," *Phys. Rev. Lett.* **77**, 2292–2295.

Zapata, I., J. Luczka, F. Sols, and P. Hänggi, 1998, "Tunneling center as a source of voltage rectification in Josephson junctions," *Phys. Rev. Lett.* **80**, 829–832.

Zhou, F., B. Spivak, and B. Altshuler, 1999, "Mesoscopic mechanism of adiabatic charge transport," *Phys. Rev. Lett.* **82**, 608–611.

Zhu, B. Y., L. V. Look, V. V. Moshchalkov, B. R. Zhao, and Z. X. Zhao, 2001, "Vortex dynamics in regular arrays of asymmetric pinning centers," *Phys. Rev. B* **64**, 012504.

Zhu, B. Y., F. Marchesoni, V. V. Moshchalkov, and F. Nori, 2003a, "Controllable step motors and rectifiers of magnetic flux quanta using periodic arrays of asymmetric pinning defects," *Phys. Rev. B* **68**, 014514.

Zhu, B. Y., F. Marchesoni, and F. Nori, 2003b, "Biologically inspired devices for easily controlling the motion of magnetic flux quanta," *Physica E* **18**, 318–319.

Zhu, B. Y., F. Marchesoni, and F. Nori, 2004, "Controlling the motion of magnetic flux quanta," *Phys. Rev. Lett.* **92**, 180602.

Zitzmann, J., A. V. Ustinov, M. Levitchev, and S. Sakai, 2002, "Super-relativistic fluxon in a Josephson multilayer: Experiment and simulation," *Phys. Rev. B* **66**, 064527.

Zueco, D., and J. L. García-Palacios, 2005, "Quantum ratchets at high temperatures," *Physica E* **29**, 435–441.

Zwolak, M., and M. Di Ventra, 2008, "Physical approaches to DNA sequencing and detection," *Rev. Mod. Phys.* **80**, 141–165.